# Experimental Analysis of Oil Based Cavitation Peening in Air

A Thesis
Presented to
The Academic Faculty

by

Richard Marsh

In Partial Fulfillment
of the Requirements for the Degree
Master of Science in the
School of Mechanical Engineering

Georgia Institute of Technology
May 2011

# Experimental Analysis of Oil Based Cavitation Peening in Air

Approved by:

Dr. Shreyes Melkote, Advisor
School of Mechanical Engineering
*Georgia Institute of Technology*

Dr. Steven Danyluk
School of Mechanical Engineering
*Georgia Institute of Technology*

Dr. Minami Yoda
School of Mechanical Engineering
*Georgia Institute of Technology*

Date Approved: January 19, 2011

## Acknowledgements

This project and all the associated efforts would not have been possible without The Boeing Company and their Manufacturing Research Initiative and all those who are associated with making sure the initiative operated smoothly. I would specifically like to thank James Castle from The Boeing Company and his willingness to provide insight and help whenever called upon. I would also like to thank the faculty members and staff of the Precision Machining Research Consortium who provide a research environment that encourages innovation. In particular I would like to thank my advisor, Dr. Shreyes Melkote, for not only encouraging this innovative spirit, but for also being patient when the innovation didn't occur quite on schedule. Also, I would like to thank Steven Sheffield for his help in fabricating and operating the prototype peening system (and allowing me to use the machine tools for purposes well outside their design). Additionally I would like to thank my fellow lab-mates for acting as a sounding board for my crazy ideas and never complaining when things blew up. Finally I would like to thank my wife, Avalon, for never doubting and always encouraging.

# Table of Contents

# List of Tables

# List of Figures

## Summary

Mechanical surface enhancement techniques are utilized to improve the fatigue life of formed and machined components by inducing a compressive residual stress in the workpiece surface and subsurface. Shot peening is the primary technique utilized in most applications today. However, the physical size and cost of the equipment as well as its inability to process small features has led to the development of newer processes aimed at addressing these concerns.

Liquid cavitation peening is a newer surface enhancement technique that utilizes a cavitating stream to induce compressive residual stresses in the workpiece surface and subsurface. As the cavitation bubble collapses in the vicinity of the workpiece, a large pressure wave is generated at the workpiece surface, which interacts with the workpiece to create a compressive residual stress field. Current research has focused primarily on water based cavitation peening systems and its effect on the surface properties of the workpiece. The available research suggests oil as a preferred fluid as it erodes less of the surface during impact by impeding lateral fluid jetting. However, only a single attempt at oil cavitation peening has been reported. This system requires the part to be completely submerged in an oil bath, limiting the part size to the size of the oil tank. New research needs to be conducted to address the lack of knowledge of oil cavitation peening, specifically a better understanding of how process parameters affect mass loss, surface roughness, residual stress, and other process results. Also, the process should be operated in a free environment and not limited to a tank while being integrated into a standard machine tool.

This thesis presents a new process, oil jet cavitation in air, and evaluates its effectiveness by investigating how changes in the process parameters affect physical and mechanical properties of the workpiece surface. This is accomplished through the design and fabrication of an experimental prototype system for the process that can be integrated into

a standard machine tool environment. In addition a detailed experimental study is carried out to determine the effects of the process parameters (stand-off distance, traverse speed, pass to pass overlap) on the workpiece surface characteristics as well as the through-thickness residual stress. The workpiece material utilized throughout is a 2024-T3 Almen strip. With the stresses relieved throughout the entire thickness, Almen strips are flat, thin workpieces that are often used to determine shot peening parameters. As the strips are peened, a residual stress field is created. As the residual stress varies with the thickness, the part deflects. This allows for a quick comparison to be made between process settings utilizing strip deflection as an indicator for induced compressive residual stress.

The results of this study demonstrate that all three process parameters, standoff distance, traverse speed, and pass to pass overlap, are statistically significant with respect to deflection, microhardness, and mass loss. The process was able to induce -155 MPa compressive residual stress, improve micro hardness by 21%, limit mass loss to 1.3 µg/s, and cause a 0.010 inch (0.254 mm) deflection in the strip. The process did not create a change in the surface area roughness (Sa) of the part over the range of parameters tested. The acoustic emission magnitude is suggested as a good indicator of deflection, micro hardness, and mass loss for Al 2024-T3 over the range of the values tested in the experiment. An explanation of how each process parameter affects the surface characterstics is discussed, with a complete analysis of variance provided for each. This thesis concludes by describing future research areas, including different fluids that may be used as well as how the system may be scaled for industrial use.

# 1 Introduction

Improving fatigue performance in aerospace components is a long researched area. By changing the material, heat treatments, or by applying a mechanical surface enhancement technique to induce compressive residual stresses, the aerospace community has been able to improve the fatigue life. The research presented in this thesis focuses on improvements and modifications to existing mechanical surface enhancement techniques in order to generate compressive residual stresses in aerospace grade aluminum.

Due to imperfections in the part from machining, casting, or other forming processes, surface and sub-surface cracks are present. Under cyclic and/or continual tensile loading of the surface, the cracks may propagate and ultimately cause part failure. Forming processes can also generate surface tensile stresses that adversely affect fatigue life. To mitigate the problems of surface imperfection and surface tensile stresses, the critical areas are typically peened using one of a select few processes. The peening process can induce compressive residual stresses and prevent the surface cracks from propagating or in the case of surface tensile stresses, it can relieve the tensile stress [1].

The critical surface then will not develop tensile stresses necessary for part failure until after the enhanced area's compressive stresses are overcome. This result allows for a longer fatigue life in the part or higher operating stresses at the initial fatigue life as shown in Figure 1.

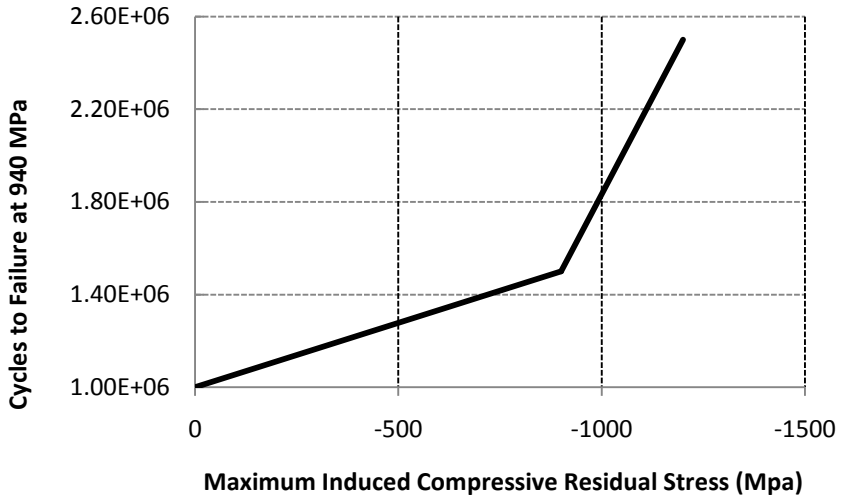


**Figure 1:** Effect of Induced Stress on Fatigue Life [2]

Shot peening, the most prevalent mechanical surface enhancement techniques, requires large dedicated equipment. Due to this, the workpiece must be removed from the fabrication/machining area and transported to the peening area where it is re-fixtured and then shot peened. While the shot-workpiece surface interaction has been modeled, the process itself is controlled utilizing predetermined exposure times and shot intensities with no control capabilities *in situ.* Shot peening systems offer high throughput rates. However, under normal operating conditions, shot peening is only able to induce compressive residual stress levels to approximately 50% of the yield strength of the material. Shot peening also significantly roughens the surface [3] and requires a chemical wash to remove any deposited shot material [1].

Newer techniques have been developed to address some of the issues of shot peening, mainly the size requirement of the equipment and the lack of *in situ* process control. In laser shock peening, a laser is focused on the workpiece and then pulsed to irradiate the top most ablative layer (Figure 2). The ablative layer vaporizes, and with the additional energy of the laser becomes a plasma. With the plasma's rapid expansion, a large shock wave is generated that is driven into the workpiece surface.

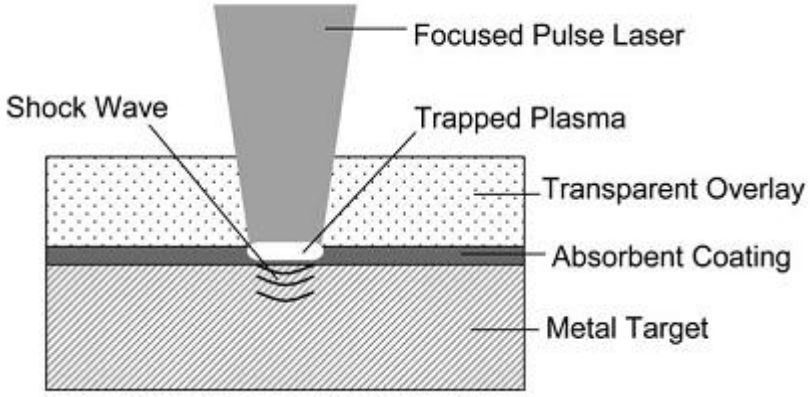


**Figure 2:** Laser Shock Peening Schematic [4]

Laser shock peening offers similar compressive residual stresses to higher depths than shot peening, but initial efforts were limited by the high cost of laser systems [5]. Unlike shot peening, laser shock peening can be controlled *in situ* by varying the pulse energy. The process, including both the laser-ablative layer interaction as well as the plasma shock wave – surface interaction has seen considerably more process modeling in an effort to better control the process. Laser peening systems still require large support equipment (water chillers, transformers) as well as requiring extra precautions due to the use of lasers. Laser shock peening with an ablative layer does not roughen the surface of the workpiece material, but does require the ablative layer (typically paint) to be removed after the process is complete. Compared to shot peening, laser peening is slow process, with spot sizes around 4 mm, and pulse rates of approximately 5 spots/second [6].

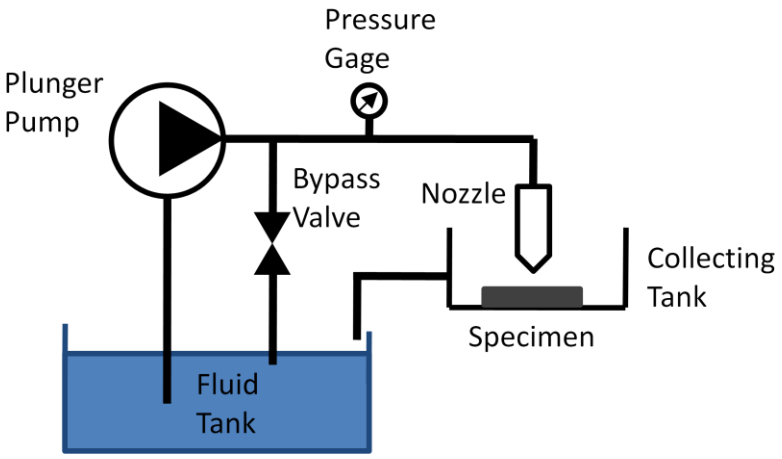


**Figure 3**: Standard Liquid Peening Schematic

Utilizing a high pressure, typically above 10,000 psi (70 MPa), fluid stream impinging directly on the workpiece surface, liquid based jet peening systems (Figure 3) can generate similar residual stress to those of shot peening [7, 8]. Water based fluid peening systems suffer from high material erosion rates, which impacts both the surface finish and the fatigue life of the workpiece. In order to lessen the erosion rates, oil based fluid peening has been developed [9], as certain hydraulic oils have been found to lessen the amount of surface erosion in impinging streams. Both water based [10, 11, 12] and oil based [9] fluid jet peening have been numerically modeled, which have aided in further process optimization.

Fluid based cavitation peening utilizes a high pressure fluid jet, typically at or above 10,000 psi (70 MPa), surrounded by a lower pressure fluid jet, typically around 15 to 30 psi (100 to 200 kPa). The low pressure fluid may either be in the form of stagnant fluid in which the part is submerged, or a flowing stream completely encompassing the high pressure fluid. With the part submerged in the low pressure fluid, problems arise in creating holding tanks large enough to fixture the part while capturing the entering fluid stream. By providing the low pressure as an additional pumped stream, this need to fixture the part in a tank is removed. As the high pressure fluid moves past the lower pressure fluid, low-pressure areas are formed, which create cavitation bubbles upon

reaching the vapor pressure of the fluid. These bubbles, upon reaching and collapsing on the workpiece surface, generate higher amplitude pressure waves than the surrounding impinging fluid [13]. The interaction of the pressure wave and the workpiece material leads to inhomogeneous plastic deformation leading to the formation of residual stresses in the workpiece. This process is able to induce higher residual stress than shot peening while providing a less rough surface [14, 15, 16]. Water has been primarily used as the peening fluid, but as was the case with standard water jet peening, high erosion rates were observed [13]. A single attempt at cavitation peening with oil has been reported [16]. This attempt was done with the workpiece completely submerged in a stagnant oil bath. The initial effort in oil jet cavitation peening produced promising compressive residual stress and mass loss results, but no further work has been reported.

Oil jet cavitation peening addressed the issue of mass loss that was present in water based cavitation peening in water and air. The system utilized still required the workpiece to be completely submerged in oil, and was built as a standalone system, not integrated into a machine tool. Finally, the oil based cavitation peening in oil results are limited to addressing one of the process parameters impacts on the workpiece characteristics, with no clear understanding how the process responds to other changes in the process parameters.

In order to determine the efficacy of oil jet cavitation peening, all the process parameters (standoff distance, pass to pass overlap, traverse speed) need to be explored. Prior work in oil jet cavitation peening was limited to a single process parameter (traverse speed) with the workpiece characterization limited to the surface roughness, micro hardness, and induced compressive residual stress. A better understanding is needed of all three process parameters (traverse speed, standoff distance, and pass to pass overlap) and their effects on the workpiece characteristics. Verification of the occurrence of cavitation during the peening process is needed, as this has not been accomplished with current research.

## 1.1 Research Objectives

The objectives of this thesis are as follows:

1. To understand the effect of oil based cavitation peening in air on micro hardness, residual stress, surface roughness, and mass loss.
2. To determine if cavitation can be induced in the oil jet cavitation peening in air process.
3. To determine if acoustic emission information can be used to monitor the process *in situ*.
4. To determine the feasibility of integrating an oil jet cavitation peening system in a standard machine tool.

Objective 1 is accomplished through the use of an experimental study, utilizing a $3^{k-1}$ fractional factorial with three replicates to determine the effects of the process parameters on the workpiece surface characteristics as well as the through-thickness residual stress. The workpiece material utilized throughout is a 2024-T3 Almen strip. Objective 2 is achieved by investigating the acoustic emission signal characteristics obtained from the process. Objective 3 is accomplished by comparing the acoustic emission data with the material responses (mass loss, micro hardness, and deflection) and identifying any correlations that exist. Objective 4 is evaluated throughout the design, build and testing phases, and will be based on the prototype system built and the machine tool into which it is integrated.

## 1.2 Outline

Chapter 2 provides an overview of prior research in mechanical surface enhancement techniques and their associated process results. It finally discusses areas that are not addressed or inadequately addressed and then presents the proposed process, oil jet cavitation peening in air, for study. Chapter 3 focuses on how the oil cavitation peening in air system is designed to create the necessary cavitation phenomenon to peen the surface. Additional information on the limitations imposed by the lab environment as well as how the process may be scaled and utilized in a production environment is presented. Chapter 4 presents the results of an experimental study designed to understand

the effects of the oil cavitation peening in air process on residual stress, surface roughness, surface finish and other process responses. The chapter also presents statistical analysis corresponding to the design of experiment results. Chapter 5 presents a discussion of each process parameter and its effect on the measured response variables. Additional recommendations are made as to further research potential as well as potential applications within a production environment.

# 2 Literature Review

This chapter reviews past as well as current methodologies that are utilized for mechanical surface enhancement, specifically compressive residual stress and surface roughness. This chapter begins by providing an overview of general peening and its applications to metal enhancement. Newer methods with their associated process capabilities are then presented. Each technique is presented with key operating principles. The limitations as well as research areas for each method are discussed. This chapter concludes by summarizing the limitations of the current methods, and emphasizing the need for additional research in the chosen field.

## 2.1 Shot Peening

### 2.1.1 Operating Principles

In shot peening, the shot media is blasted through a controlled nozzle, directly impinging on the workpiece surface. The media typically consists of small round metal or ceramic shot, but can also utilize conditioned cut metal wire shot that is more cylindrical in shape. As the each shot impacts the workpiece surface, a small depression is created, as seen in Figure 4. The area surrounding the depression, typically around 0.13 – 1.02 mm in depth, is in a compressive residual state. Below the compressive area a tensile stress layer will develop to achieve equilibrium in the workpiece [1].

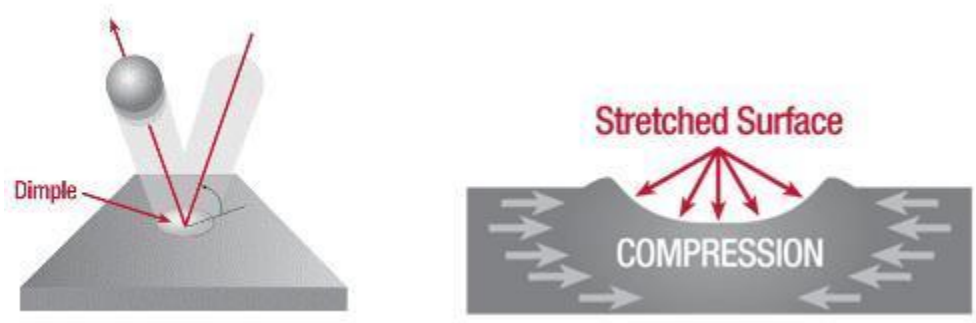


**Figure 4:** Shot Peening (http://www.metalimprovement.com/shot_peening.php)

### 2.1.2 Capabilities

Peyre et al [5] conducted studies on AL7075-T7531 to determine the through-thickness residual stresses. As seen in Figure 5, the surface residual compressive stress induced is -325 MPa, or 75% of the yield strength of the material. The maximum compressive residual stress is approximately -350 MPa, which is 80% of the yield strength of the material and is seen at a depth of approximately 75 µm. The shot peening process is able to induce a compressive residual stress to a depth of approximately 200 µm.

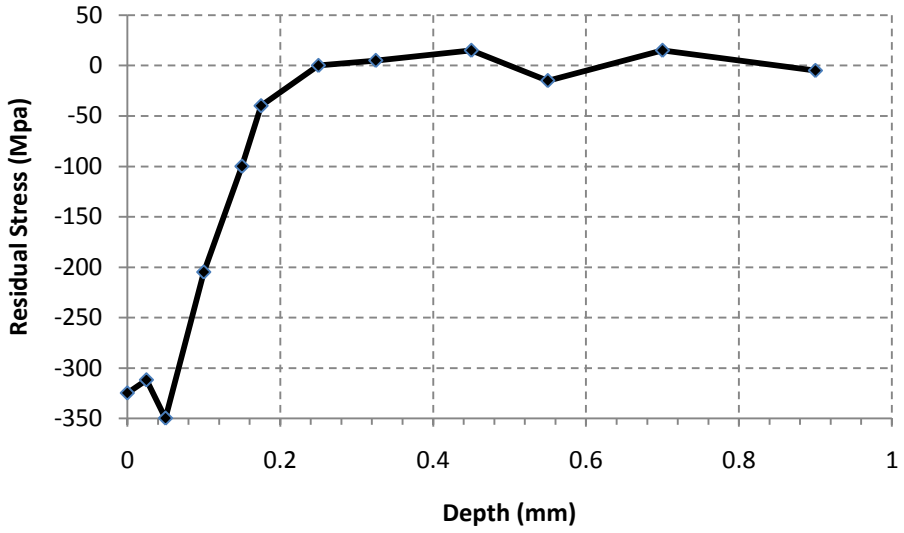


**Figure 5:** Compressive Residual Stress of Shot Peened Al7075-T7351 [5]

Hammond, et al. [3] conducted similar studies on Al7075-T7351. As seen in Figure 6, the sample was first peened to 100% coverage and was then found to have an induced surface residual compressive stress of -129 MPa, or 28% of the yield strength of the material. The maximum compressive residual stress is approximately -208 MPa, or 47% of the yield strength of the material and is seen at a depth of approximately 100 µm.

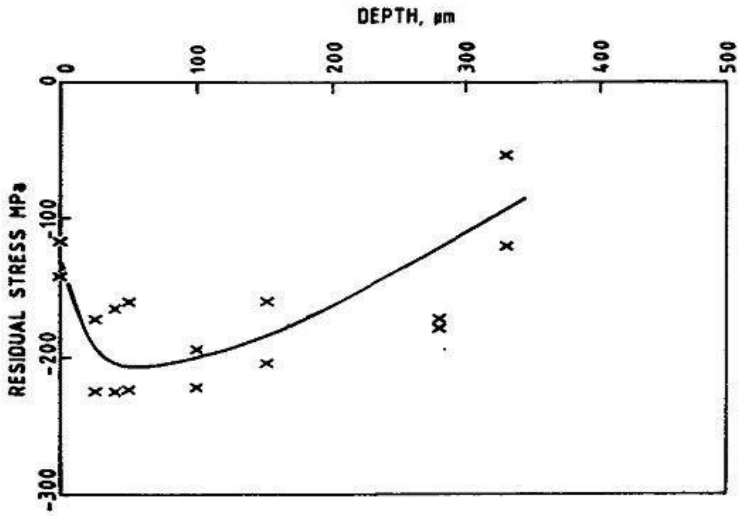


**Figure 6:** Compressive Residual Stress of Shot Peened Al7075-T7351 [3]

Peyre et al. [5] found the surface roughness of their shot peened samples to be 5.7 μm (Ra), which is considerably worse than the base material roughness of 0.6 μm. The surface roughening of shot peening is one of the process's key limitations. While deeper and larger compressive residual stresses are the goal of any of the peening processes, in shot peening, increasing the shot size is able to accomplish this, but, as Peyre, et al found, the resulting surface roughness falls well outside of most machined part surface roughness specifications.

## 2.2 Low Plasticity Burnishing

### 2.2.1 Operating Principles

Low plasticity burnishing involves a tool with a hydraulically supported burnishing ball that is brought into contact with the workpiece surface, shown in Figure 7. The burnishing tool is designed to be mounted and operated in conventional lathes and vertical mills. Once the burnishing tool is mounted and the workpiece is properly secured, the ball is brought into contact with the workpiece and rolled over its surface. Fluid is pumped in to create a layer between the tool and the ball, preventing metal-to-

metal contact between the two. As the ball passes over the workpiece, compressive stresses are induced due to the plastic deformation, improving the surface finish and increasing its high cycle fatigue resistance [17]. The level of cold work produced by low plasticity burnishing is significantly lower than that of other surface enhancement techniques [18]. This is important for high temperature applications as cold working could be annealed out of the material.

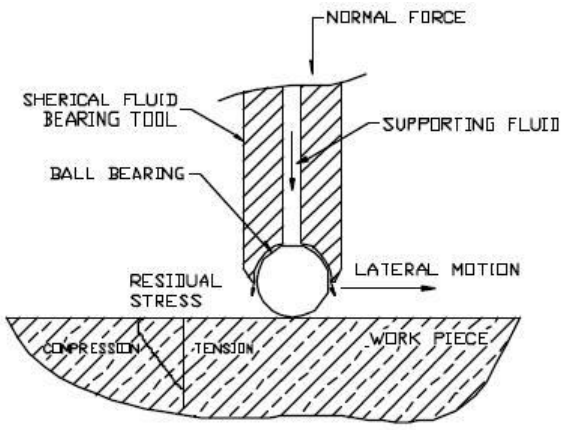


**Figure 7:** Operating Schematic for Low Plasticity Burnishing [17]

### 2.2.2 Capabilities

Low plasticity burnishing has been found to be capable of inducing compressive residual stresses of approximately 70% of the yield strength of IN718 [19], and 80% of the yield stress in Aluminum 7075-T6 [20].

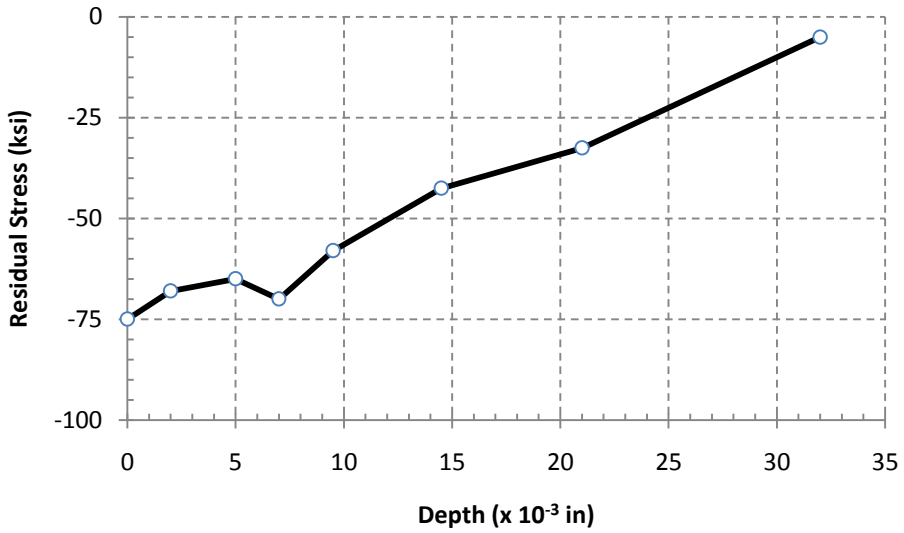


**Figure 8:** Induced Residual stress on burnished 7075-T6 [20]

As seen in Figure 8, low plasticity burnishing is capable of creating compressive residual stresses to significant depths (>100 μm), which allows for considerable gains in fatigue life, reportedly as high as 100 times greater than untreated specimens when tested in a salt fog [20]. Burnishing also offers the potential benefit of creating a smoother surface. As seen in Table 1, low plasticity burnishing reduced the surface roughness of a machined surface by as much as 79%. Burnishing has been tested and found to be effective in stainless steels [18], steel [17,19], titanium alloys [21], and aluminum alloys [20,22,23,24].

**Table 1:** Surface Roughness values for low plasticity burnishing [20]

| | Surface Roughness (µin, Ra) | | |
|---|---|---|---|
| **Surface Condition** | *Baseline* | *Corrosion Fatigue* | *100 hour Pitting* |
| Machined | 39±7 | 36±2 | 139±34 |
| LPB | 8±3 | 11±3 | 31±33 |

While burnishing can reach high levels of residual stress in the workpiece and potentially produce smoother surfaces, it has significant geometric limitations. As the process requires direct interaction between the burnishing ball and the workpiece surface, any sharp edges or discontinuities in the workpiece surface prevent the ball from burnishing the complete surface, as illustrated in Figure 9.

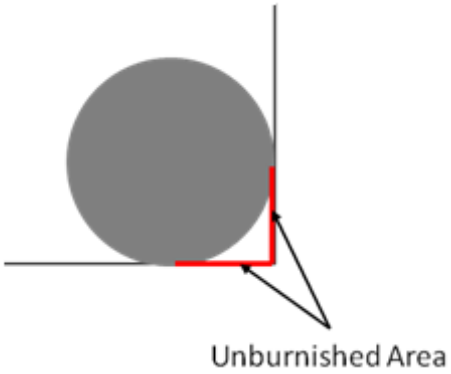


**Figure 9:** Unaffected region due to geometric limitations of burnishing

## 2.3 Laser Peening

### 2.3.1 Operating Principles

Most laser peening is comprised of two different steps, the initial application of an ablative layer and the focused pulse of a layer at the desired spot of peening. The ablative layer is painted on and then cured or applied through the use of an adhesive, similar to a black tape. The ablative layer acts as a sacrificial layer, preventing any burning of the surface. As the layer prevents the laser from attacking the workpiece surface, no additional surface roughening is seen during laser shock peening [25].

A laser is focused on the workpiece and then pulsed to irradiate the top most ablative layer. The workpiece is completely submerged in a tamping layer, typically water, which helps to confine the shock waves that occur due to ablation, as illustrated in Figure 10. The pulsed laser vaporizes the ablative layer creating a high-density vapor. The water confines the vapor, which is then ionized to form a plasma. Subsequent laser energy absorption into the plasma generates a heat-sustained shock wave that then impinges on the workpiece surface, typically with an intensity of several GPa [5,26].

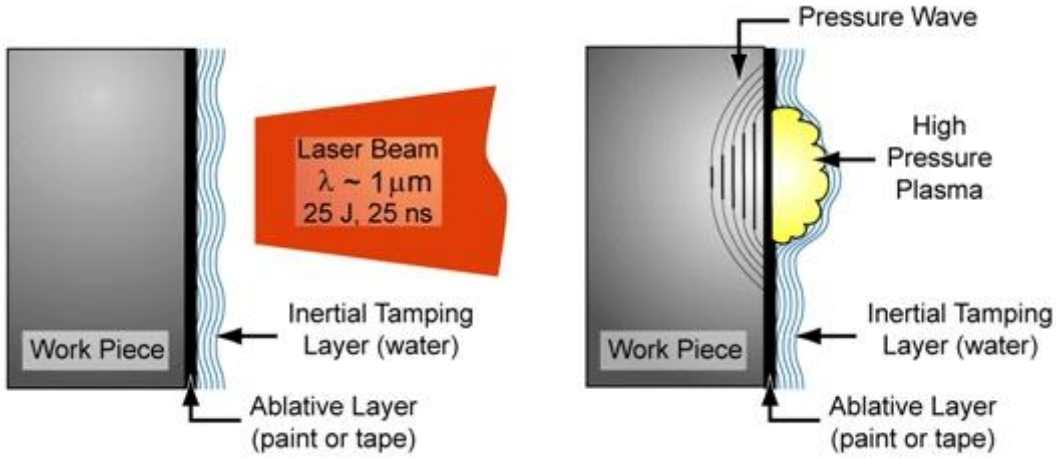


**Figure 10**: Laser shock peening (www.metalimprovement.com)

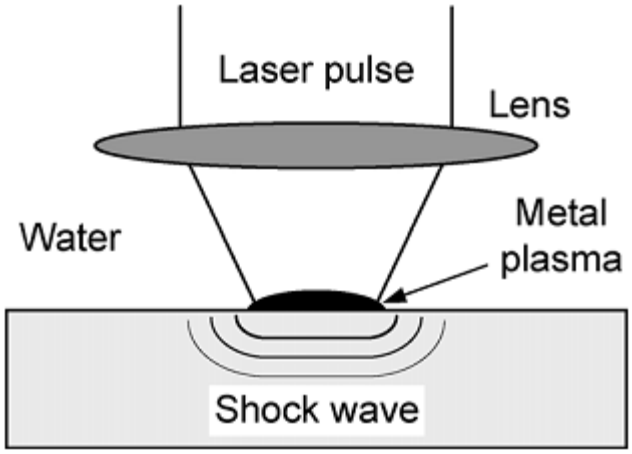


**Figure 11:** Laser shock peening without protective coating [26]

In laser shock processing without coating, Figure 11, the ablative layer is not applied, instead allowing the top most layer of the workpiece to be ablated away creating the plasma. Other than this change, the operating principles are similar to those of laser shock processing with coating [26]. Laser shock processing without coating has the main benefit of being usable in areas that are inaccessible to normal machinery such as nuclear reactors and underwater pressure vessel [26,27] where it would impossible or impractical to apply the ablative layer coating.

### 2.3.2 Ablative Layer Capabilities

As seen in Figure 12, laser shock peening is able to generate high compressive residual stresses up to 67% of yield, to relatively large depths, greater than 1 mm. In comparison, standard shot peening generates compressive residual stresses to depths around 250 μm. As the excess ablative layer is removed after peening, no workpiece material is removed, yielding no mass loss. Laser shock peening with ablative layer has been tested and found effective on a variety of materials, namely aluminum alloys [5,28,29,30], stainless steels [25,26], and titanium alloys [31].

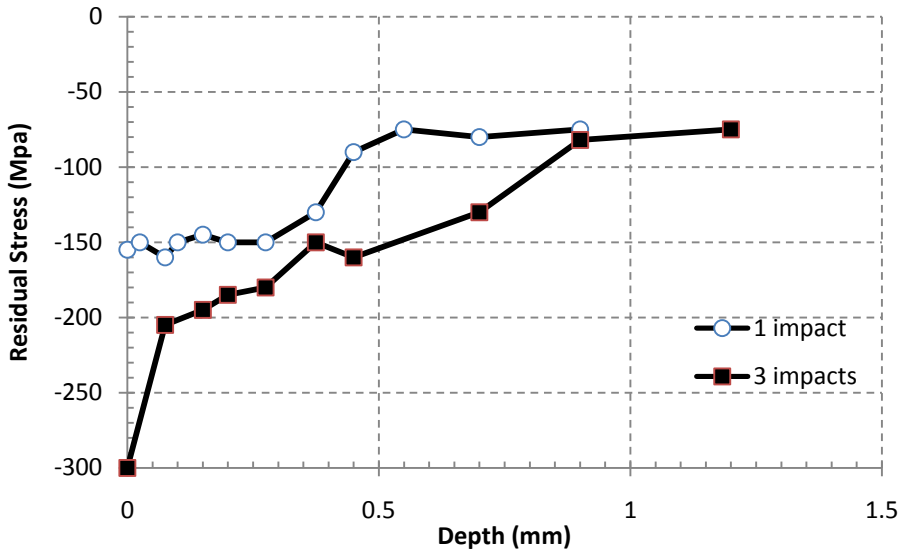


**Figure 12:** Laser shock peening on Al7075 [5]

However, laser shock peening is a relatively slow process with each spot requiring at least one complete laser pulse and as many as three to reach the highest induced compressive residual stress [5]. Due to the slow processing speeds of laser shock peening, it has seen more use in small surface area, critical stress regions where the slow process time is offset by the increase in fatigue performance [29]. The largest limitation of laser shock peening from a practical stand point is the cost, both of the lasing system as well as the environmental control necessary to provide a safe working area.

### 2.3.3 Non-Ablative Layer Capabilities

As seen in Figure 13, laser shock peening without ablative layer is able to induce high compressive residual stresses at comparable depths to laser shock peening with ablative layer [27]. Due to the laser-surface interaction in laser shock peening without ablative layer, surface roughening occurs. The surface roughness, Ra, after laser shock peening without ablative layer was reported to have increased to 1.3 μm from 0.3 μm [32]. Laser shock peening without ablative layer has been utilized on both 304 stainless steel [26,27,32], and 316 stainless steel [26,27].

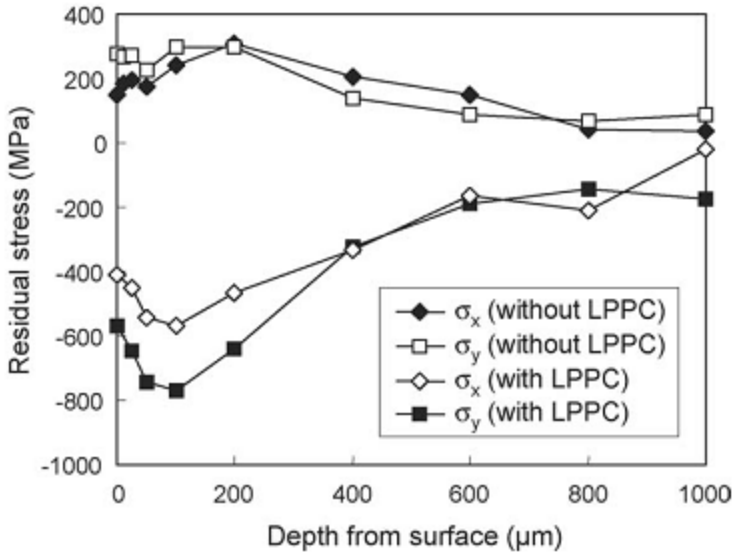


**Figure 13**: Residual stress depth profile of laser shock peened with no ablative layer on SUS316L [26]

## 2.4 Liquid Peening

### 2.4.1 Jet Peening

#### 2.4.1.1 Operating Principles

Jet peening requires a base fluid, typically purified water, to be pumped at high pressures. The high pressure fluid passes through a restricting nozzle, creating high pressures, typically 15,000 psi or more [33]. The stream is then directed towards the desired workpiece region and scanned in order to induce compressive residual stresses. Alternatively, air or fluid can be injected into the exiting stream to aid in the atomization of the stream resulting in a better surface finish [34].

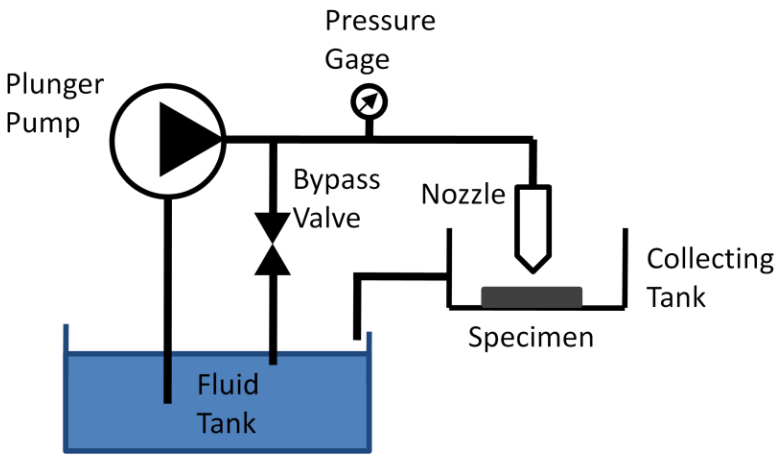


**Figure 14:** Fluid Jet Peening Schematic

The viscosity of the fluid used for the peening greatly affects the mass loss rates of the process. Early erosion experiments indicated that more viscous hydraulic oils would prevent erosion, leading to better surface finishes [35] and in the case of peening systems, remove less of the peened surface, thus increasing fatigue life [9].

#### 2.4.1.2 Jet Peening Capabilities

As seen in Figure 15 and Figure 16, liquid jet peening is capable of inducing compressive residual stresses of approximately 70% of the yield strength of the material [7,8]. Regardless of the fluid utilized, either oil or water, the process was able to generate a compressive residual stress to a depth of 200-250 μm.

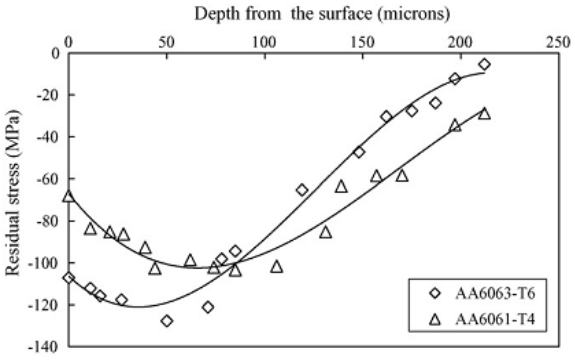


**Figure 15:** Residual stress profile of Al 6063 of oil jet peening process [7]

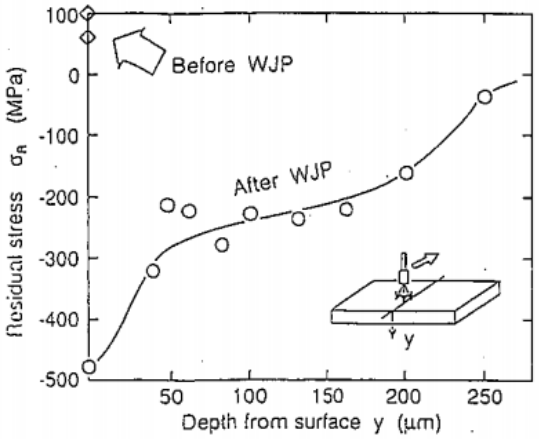


**Figure 16:** Residual stress profile on 304 stainless steel of water jet peening process [8]

The surface roughness, Ra, of liquid jet peening processes has been reported to increase from 0.05 μm to 3 μm [34] for water peening on tool steel and from a base roughness of 0.62 μm to 1.5 μm for oil [36]. The mass loss rates for oil, ($1x10^{-6}$ g/s [36]) were considerably lower than water jet peening ($8.3x10^{-5}$ g/s [37]) for similar materials.

### 2.4.2 Cavitation Peening

#### 2.4.2.1 Operating Principles

The fluid that is used for the cavitation peening process is setup in a closed loop system. Pumps send a high pressure fluid through the nozzle where it then interacts with a lower pressure fluid, as shown in Figure 17.

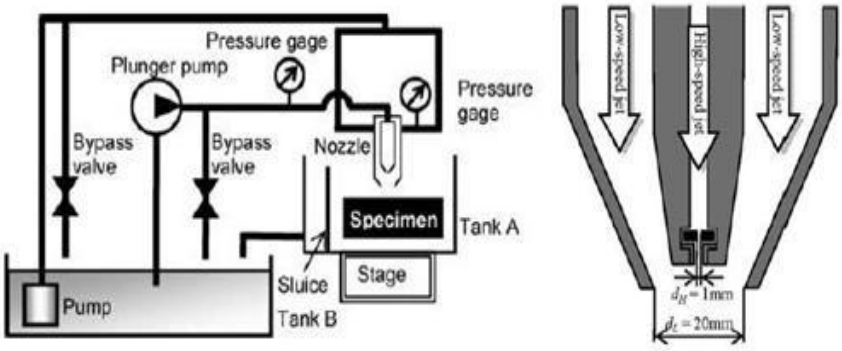


**Figure 17:** Cavitation Jet Peening Schematic [13]

The shearing action created from the high velocity and low velocity fluid interaction induces cavitation bubbles, which are then used to directly impinge on the workpiece surface. The likelihood of the system to cavitate is defined by the cavitation number, $\sigma_c$. and is defined in equation 1, where $P_2$ is the pressure of the low pressure fluid and $P_1$ is the pressure of the high pressure fluid. The lower the cavitation number, the higher the likelihood for cavitation.

$$\sigma_c = \frac{P_2}{P_1} \tag{2.1}$$

Utilizing this relationship, the systems studied all drove the $P_1$ as high as possible with $P_2$ generally held at or as close to $P_{atm}$ as possible [6, 7, 9, 13, 30].

The workpiece is located exposed to the environment, known as cavitating jet in air (CJA) or submerged in water, which is known as cavitating jet in water (CJW). As the bubbles impact and subsequently collapse on the workpiece surface, compressive stresses are induced on the surface. As the bubble collapses, Figure 18, the fluid is channeled into the collapsing region. The channeled fluid increases in velocity, creating microjets of higher pressure and higher velocity fluid. This microjet then impinges on the workpiece surface, inducing a compressive residual stress due to surface deformation [13].

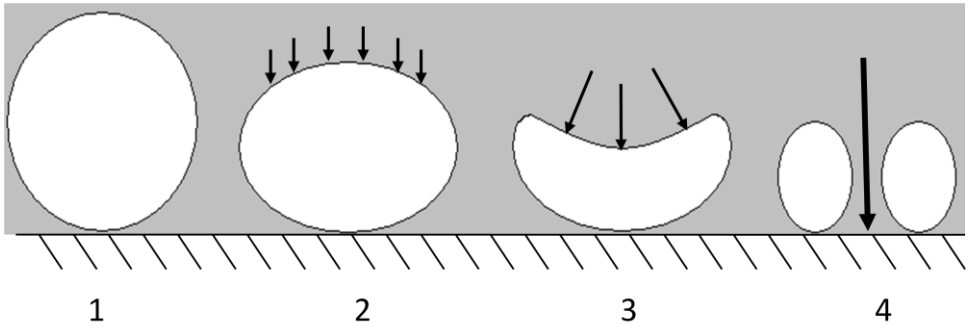


**Figure 18:** Cavitation Bubble Collapse [13]

2.4.2.2 Cavitating Jet in Air Capabilities

Cavitation peening in air is reported to be able to produce compressive residual stresses of approximately 80% of the material yield strength in Ti-6Al-4V [14] and 80% in SKD61 [13] tool steel with the maximum occurring at the surface of both materials. In the reported literature, for all materials the induced compressive residual stress was measured to a maximum depth of 150 µm in 1045 steel [38] ( see Figure 19), but was often found to only affect much shallower depths in Ti-6Al-4V, around 80 µm-100 µm [13, 14, 15], as seen in Figure 20.

Significant surface erosion has been reported, with cavitating jet in air having a mass loss of 18.5 mg/min [13], which is 3.9 times higher than a standard water jet peening system [14]. With this increase in mass loss, the surface undergoes some roughening with surface roughness (Ra) increasing from as little as 0.06 µm [14] to as high 5.4 µm [34].

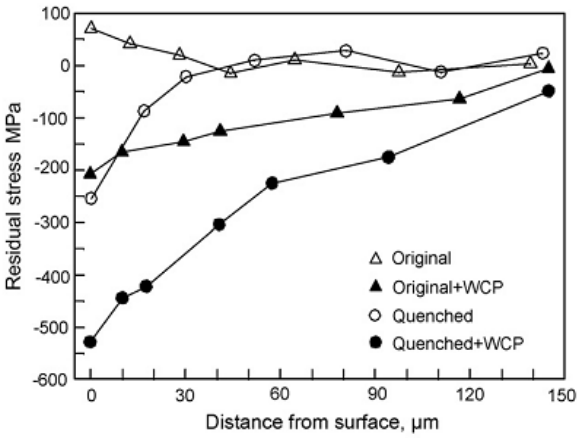


**Figure 19:** Induced compressive residual stress in 1045 steel [38]

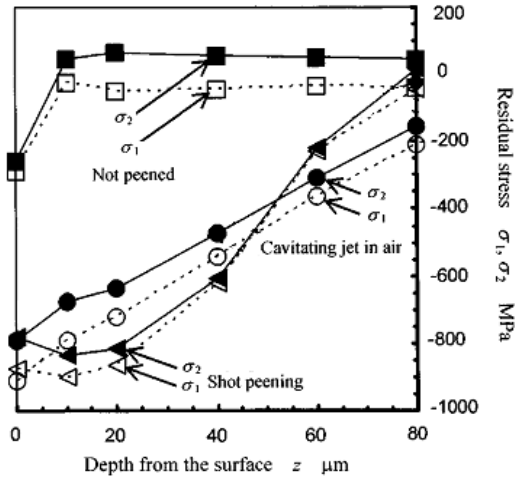


**Figure 20:** Induced compressive residual stress comparison of various methods on Ti-6Al-4V [14]

#### 2.4.2.3 Cavitating Jet In Liquid Capabilities

Cavitation peening in liquid, which is carried out with the workpiece submerged in liquid, is able to induce compressive residual stresses of up to 70% [14] to 80% [15] of the yield strength of the workpiece material. As noted in Figure 21, the maximum induced compressive residual stress for cavitation peening in liquid samples occurs at the workpiece surface, then quickly diminishes within 100 µm to 150µm depth [13, 14, 15, 16].

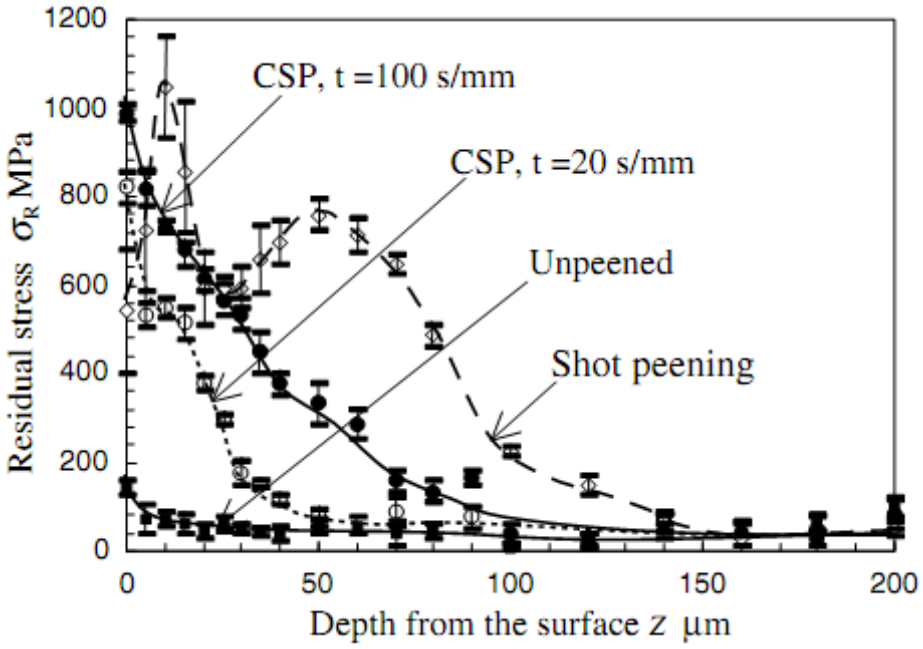


**Figure 21:** Residual stress profile of cavitation peening in water on Ti-6Al-4V [15]

As with cavitation peening in air, erosion and surface roughening of the workpiece material is a concern with cavitation peening in liquid. For water based peening, mass loss was measured to be around 1.2 mg/min to 5 mg/min depending on the distance from the nozzle to the workpiece surface [13].

When the fluid was changed from water to oil, there was no measurable or visible surface erosion [16]. For cavitation peening in oil, the surface roughness, Ra, was found to

increase less than 1.6% over the unpeened value. The promising result from oil based peening follows from previous work by Pai and Hargreaves [35] which indicates that oil is more suitable to minimize both mass loss and surface roughening in areas where cavitation may occur.

## 2.5 Deficiencies and Process Selection

After reviewing the current methods utilized for mechanical surface enhancement, there appears to be a need for a system that produces as small a change in surface roughness and workpiece mass while still generating deep compressive residual stresses. Depending on the material, both low plasticity burnishing [23, 20] and laser peening [5, 26, 27] are able to induce compressive residual stresses to depths in excess of 750 µm, which is much deeper than what can typically be achieved by shot peening (250 µm [3]). However, both low plasticity burnishing and laser peening suffer from process limitations that do not allow for their use in as wide a range of applications as shot peening. Low plasticity burnishing, as mentioned in section 2.2.2, cannot process sharp corners or areas with any significant surface discontinuity. This limits low plasticity to smooth flat or rounded surfaces, with no part features creating interruptions in the surface. Due to the geometric limitations of low plasticity burnishing, it was not chosen for further research.

Laser peening requires the laser to completely scan the entire treated surface. As the peened area must be submerged in water, corrosion and/or oxidation of part surface becomes a concern. In order to provide sufficient process speed, larger pulsed lasers are utilized [28, 29, 21]. Laser systems require additional support equipment, most notably water chillers, to keep the laser at proper operating temperature and water pumps to keep the peened surface submerged during the lasing process. With the speed and cost limitations of laser peening, it was not chosen for further research.

Liquid peening is able to produce compressive residual stresses, typically around 200 µm – 300 µm [7, 10, 14] comparable to those of shot peening. Unlike burnishing, it does not

suffer from geometric constraints, as the stream can be directed at any surface. While liquid peening does require extra equipment, low and high pressure pumps are relatively common items that do not require a large capital investment as is the case with laser peening. When compared to the other methods presented, liquid peening, specifically liquid cavitation peening, has seen limited reported research. A better understanding of how the process responds to various parameter changes as well as material responses to the process are needed. Due to these benefits, liquid peening was chosen as the field for further research.

While liquid peening by itself can induce up to 70% of the yield strength in compressive residual stresses [7, 8], when combined with a cavitating stream, the process can induce up to 80% of the yield strength in compressive residual stresses [13, 14]. As the system would most likely be utilized in a standard machine tool, the need to keep the workpiece in the free environment arises. Submerging the workpiece is not possible, so the research has to focus on creating a cavitating stream being created internal to the system. Also, the process must be flexible to allow for easy adaption into the same machine where the parts are machined. Following prior work in cavitation peening systems, most notably Soyama et al [13,14], and Grinspan et al [16], a cavitation peening system could be designed so as to be utilized in a machine tool. This is a far departure from current shot peening systems that require significant amounts of dedicated tooling and fixturing, as well as a large amount of dedicated floor space.

Pai and Hargreaves [35] indicate specific oils are able to reduce the amount of mass loss and surface roughening in simple jet impingement and cavitating environments. Grinspan et al [9,36] utilized Pai and Hargreaves results and applied it to standard water peening practices to produce an oil based process that is capable of similar compressive residual stress states while mitigating the large erosion rates seen in water jet peening. They then followed with a brief study of cavitation peening in oil, with the workpiece completely

submerged, but found the process was incapable of producing stress states similar to those in standard oil jet peening [16]. No further work after this initial study in oil cavitation peening in oil has been reported.

Soyama has shown that water cavitation in air is able to produce significantly higher compressive residual stresses when compared to water cavitation in water or even standard water jet peening [13, 14]. With Soyama indicating an increase in compressive residual stress in a cavitating stream in air versus a cavitating stream in water, applying Pai and Hargreaves findings would indicate that oil cavitation peening in air would produce higher compressive residual stresses while decreasing the amount of surface erosion caused by the process. Due to this, the process selected for design, testing, and evaluation was oil jet cavitation in air, which has never been reported in literature.

# 3 System Design and Fabrication

As there are no commercially available oil jet cavitation in air systems, a complete unit had to be designed and built for this research. In the following sections the complete design as well as decision justifications are presented. Section 1 introduces and explains the basic system schematic. Section 2 indentifies and addresses the different constraints the system must meet in order to be practical and useable in the available operating environment. Section 3 discusses the components chosen for the initial system. Section 4 addresses the assembly and its associated issues. Section 5 deals with the limitations of the system and section 6 finishes with how the system may be scaled for both an industrial setting as well as for future research.

## 3.1 System Schematic

The first step was to develop a schematic of a system that would induce cavitation through the use of two interacting oil jet streams and then capture and re-circulate the oil. The system schematic, shown in Figure 22, illustrates the operating principles that the final design had to meet.

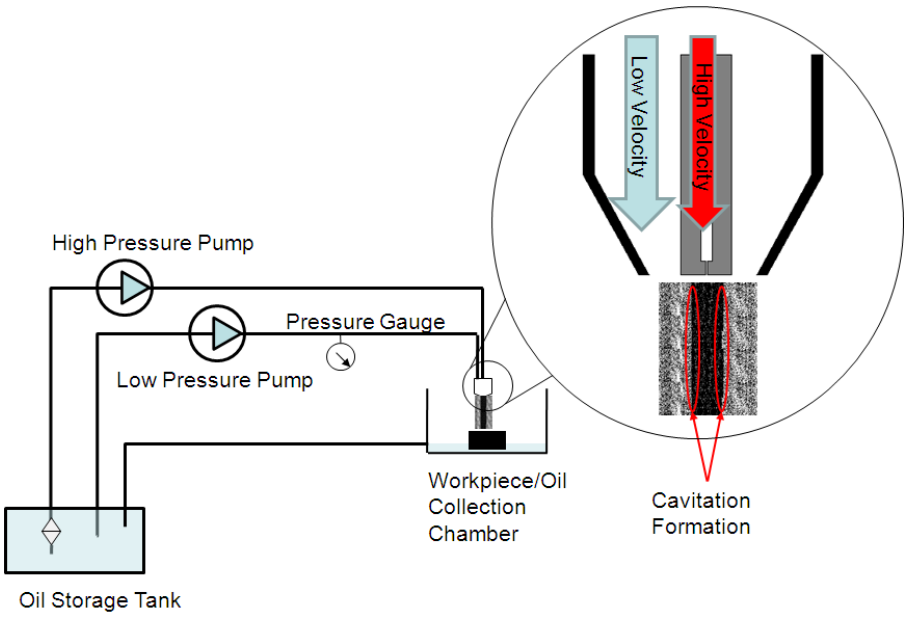


**Figure 22:** Oil Jet Peening in Air Schematic

Oil is to be pumped from the oil storage tank through the high pressure pump directly into the high pressure section of the combining nozzle. Oil would also be pumped from the oil storage tank through the low pressure supply pump directly into the low pressure section of the combining nozzle. Once in the combining nozzle, the two streams interact immediately at the nozzle exit, forming a single stream with cavitation bubbles, which is directed at the workpiece. The workpiece is to be placed in an oil collection chamber that has a drain back into the oil storage tank. The draining must be done through the use of a low pressure pump to ensure the oil collection chamber does not overflow.

As the system is intended to be used in a machining environment, the system must also be easily and quickly integrated into a standard machine tool. This requirement produces additional physical constraints on the system, and will be discussed in further detail in the following sections.

## 3.2 Geometric Constraints

### 3.2.1 External Constraints

In order to begin the initial design of the oil jet cavitation system, an acceptable footprint had to be determined. The footprint of the oil jet cavitation peening in air system is dictated by the size, layout, and design of the machine tool in which it is to be installed. In the current work, the machine tool chosen is the Okuma Millac-44V Vertical


**Figure 23:** Front-Left View of Okuma Millac-44V Vertical Machining Center

Machining Center located in the Precision Machining Research Laboratory at Georgia Tech. As seen in Figure 23, there is a transformer located directly beneath the left side access panel on the Okuma Millac-44V Vertical Machining Center. Due to safety

requirements, the hydraulic fluid could not be placed in the immediate vicinity of the transformer.

With this limitation in mind, the opposite side of the machine was surveyed. The right side has no such obstructions, has an access panel that can be removed without circumventing any safety systems, and there is a 6 ft X 6 ft open space directly next to the machine that allows for unobstructed access while still allowing for access to the other machines in the area.


**Figure 24:** Right Side View of Okuma Millac-44V Vertical Machining Center

### 3.2.2 Internal Constraints

In order to prevent backflow of the fluid from the reservoir tank into the machine tool, the reservoir must be placed at a lower height than the machine's work table. Okuma lists the height of the table top from the floor as 33 ½ inches [39]. With the machine installed on leveling feet, the distance from the table to the floor was measured to be 41".

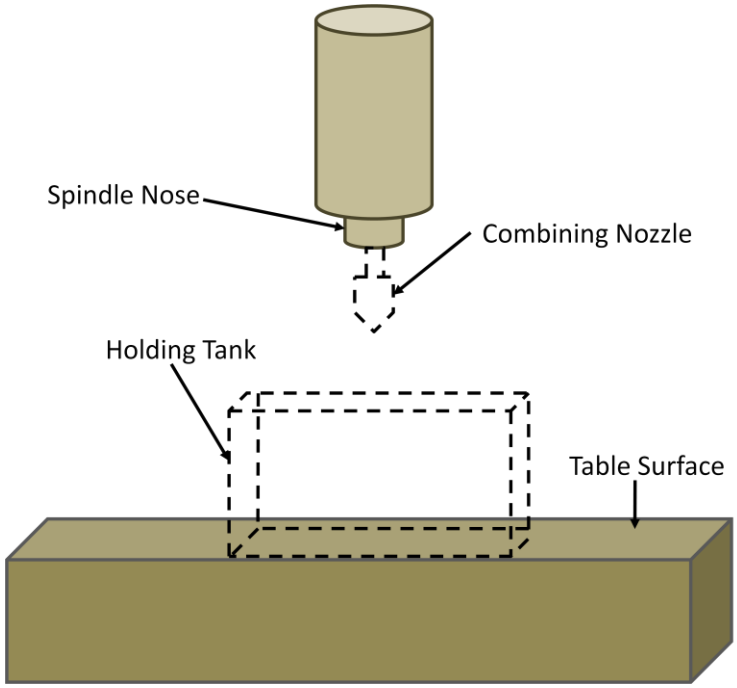


**Figure 25:** Internal schematic of machine tool

The spindle imposes 2 different constraints. The maximum distance from the spindle nose to the table surface is 22". Accounting for the additional 2 ½" the tool holder requires below the spindle, only 19 ½" are available for use. This constrains both the fixture holding tank overall height as well as the nozzle-tool holder height.

## 3.3 Part Selection and Design

### 3.3.1 Hydraulic Fluid

Pai and Hargreaves [35] indicate hydraulic fluid represents the best improvement with regards to mass loss in a cavitating environment. Their research found the higher the viscosity of the hydraulic oil, the lower the measured mass loss in the part. As the system would be operated under a variety of conditions, a robust, general purpose oil was desired. ISO Grade 68 fluid was chosen for its high relative viscosity and its low corrosiveness to metallic materials.

One of the key parameters in choosing an appropriate ISO Grade 68 oils was viscosity index. Viscosity index is an empirical number indicating the rate of change in viscosity within a given temperature change. The lower the index, the larger the change in viscosity, while the higher the index, the smaller the change in viscosity with temperature. Of the ISO Grade 68 oils available, this was a differentiating factor as large changes in viscosity due to temperature could potentially negatively affect the mass loss rate.

Hydro Safe produces a vegetable based, biodegradable hydraulic fluid that meets the ISO Grade 68 standard and, as indicated in Table 2, has a viscosity index sufficiently high to prevent large changes in viscosity.

**Table 2:** HydroSafe ISO VG-68FR Properties

| | |
|---|---|
| Viscosity, cSt@212$^{o}$F (100 $^{o}$C) | 12.5 |
| Viscosity Index | 214 |
| ASTM Flash Point ($^{o}$F) | 580 |
| Specific Gravity | 0.92 |
| Surface Tension (mN/m) | 35 |
| Vapor Pressure at 25$^{o}$C (kPa) | .1 |

Produced from canola oil, the VG68FR oil requires no special handling or storage requirements as it is 90% biodegradable within 120 days of exposure to a ground environment [40]. Hydro Safe has also added a fire resistant chemical that prevents flame propagation throughout the fluid and provides self-extinguishing capability when any flame is present.

### 3.3.2 High Pressure Pump

A piston driven positive displacement pump was the only style pump that could both generate pressures of at least 5,000 psi (35 MPa) while handling oils with a SUS viscosity

of at least 68. Standard vane style pumps cannot generate sufficient pressures and are generally not recommended for higher viscosity fluids. While they can typically generate much higher flow rates, the foregoing limitations prevented their use in the oil jet cavitation system.

The positive displacement pump needed to meet a few key requirements. First, it needed to utilize standard inlet and outlet port threads. Second, positive displacement high pressure pumps are available in two different configurations: 1) Intensifier style pumps, and 2) Crank drive style pumps. It was necessary to evaluate which pump configuration would be best suited for the application.

#### 3.3.2.1 Intensifier Pumps

Intensifier pumps work well when electric power at the pump may not be available. They are typically either pneumatically or hydraulically driven and deliver specific intensification ratios (Output Pressure/Inlet Pressure). The pneumatic/hydraulic side pushes on a large piston to generate a high force on a small diameter plunger. This plunger in turn pressurizes the liquid of interest (in this case the peening fluid) to a level directly proportional to the relative cross sectional areas of the large piston to the small plunger. The issue with intensifier pumps is the fluctuation in pressure that is experienced between strokes. Various methods have been developed to attenuate the fluctuation, but even these methods are only able to minimize the fluctuations to a few thousand psi per stroke.

#### 3.3.2.2 Crank Style Pumps

Crank style pumps have typically been relegated to lower pressure realms relative to intensifier pumps. When run at similar pressures to early intensifier pumps, crank style pumps had a shorter seal and check valve life [41]. With the advent of newer, stronger materials, crank style pumps are able to achieve up to 60 ksi (413 MPa), with easily

obtained commercially-available units capable of producing around 10-15 ksi (68-103 MPa) (Dynex, CAT, General). Crank style pumps are typically more energy efficient due to the lack of a secondary liquid being pumped, and do not suffer from the wide pressure fluctuations between strokes. The pressure fluctuations in crank style pumps are minimized due to the pumps multiple cylinders, their associated layout, and the cycle frequency at which the pump is run.

#### 3.3.2.3 Selection

Taking both positive displacement style pumps into consideration, the pulsing frequency and duration caused by the intensifier pumps could have added additional research variability and for this reason were excluded from the final design.

Crank style pumps were selected due to their efficiency and lack of pulsation when utilized under recommended rpm ranges. Dynex offers a small, compact pump that operates at 15,000 psi (103.4 MPa) at 1800 rpm and can handle a variety of hydraulic fluids. The unit is compact but only provides 0.2 gpm (0.75 lpm) in the recommended rpm range. This relatively low flow rate affects other design decisions, specifically the inner diameter of the high pressure nozzle, which will be discussed further below. The pump is also not self-priming, which necessitates that the pump is placed at a lower height than the fluid reservoir.

### 3.3.3 Low Pressure Pump

The low pressure pump posed fewer problems as oil transfer pumps are commonly used in a variety of applications and are readily available. In order to maximize the cavitation number, the low pressure fluid needs to be pumped at as low a pressure as possible. Most oil transfer pumps operate around 30 psi (206 kPa) with minimal pulsations. Due to the space limitations for the pumping unit, the oil transfer pump needed to be placed on top of the reservoir since the high pressure pump required a positive fluid head to maintain

prime. This positioning requirement necessitates the pump be self-priming with no positive fluid head.

Graco manufactures a positive displacement pump that meets both the pressure and self-priming requirement. The Graco 260102 pumps 25 psi (171 kPa) at 3.5 gpm (13.25 lpm). As the pump is a self priming system, the fluid level only needs to be within 25 feet of the pump. The pump requires a 2" threaded male port to mount the pump onto the tank. Graco requires the internal suction pipe to be approximately 2" (50.8 mm) from the bottom of the tank as well as an air vent on the top of the reservoir to prevent loss of suction. These requirements affected the design of the reservoir tank, the positioning of the low pressure pump, and the necessary fittings.

### 3.3.4 Nozzle Assembly

In order to combine the high pressure and low pressure streams, and consequently induce cavitation, a nozzle assembly was designed and built. The assembly consisted of two nozzles, the high pressure nozzle and the low pressure nozzle. The high pressure nozzle was further divided into two sections, the upper section and the constricting nozzle.

#### 3.3.4.1 High Pressure Nozzle

The high pressure nozzle was designed to fit into the small envelope created by the machine environment, and to minimize the total number of connections necessary. The nozzle assembly, both the upper section and the constricting nozzle, were machined from 304 stainless steel due to its strength, machinability, and chemical inertness to the oil.

##### *3.3.4.1.1 Upper Section*

The upper section needed to provide a connection for the high pressure hose as well as turning 90° and passing through the combining nozzle cap. In order to connect to the high pressure hose to the upper section, the necessary threads were machined directly into the upper section, as seen in Figure 26.

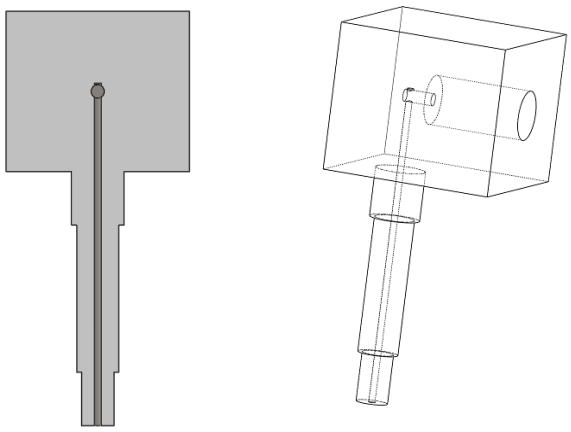

**Figure 26:** A) Cross sectional view of upper section of the high pressure nozzle B) Line drawing view of upper section of the high pressure nozzle

To pass through the cap, the exterior of the upper section required threads to attach it to the cap. The threads were machined into the upper half of the pass through section. At the end of this section, additional threads were machined to attach the constricting nozzle to the upper section.

*3.3.4.1.2 Constricting Nozzle*

The constricting nozzle was designed to restrict the high pressure flow sufficiently to generate the full 15,000 psi (103 MPa) the pump is capable of producing. Due to the low flow rates of the pump, a hole with a diameter of .010” (0.254 mm) was required.

**Figure 27**: a) Schematic of the high pressure constricting nozzle b) High pressure constricting nozzle used on system

The hole was created using a micro-drilling process to a depth of 0.2" (5.08 mm). This depth allowed for enough surrounding material to prevent the nozzle from blowing out at the constricted area. The upstream side of the nozzle was threaded to the same dimensions as the lower half of the upper section, creating a direct connection between the two. As seen in Figure 27a, the exterior of the nozzle was tapered. This taper was necessary due to the internal geometries of the combining nozzle. The taper prevented the combining nozzle and the constricting nozzle from interfering with each other while also allowing low pressure fluid to fully surround the constricting nozzle for the cavitation process. After 1 hour of peening, the restricting orifice was measured and found to have retained the original 0.010" diameter. The nozzle was then checked approximately every 5 hours, and was always found to have retained the original 0.010" nozzle diameter, with none of the material eroding away.

#### 3.3.4.2 Combining Nozzle

The combining nozzle was designed to combine the high and low pressure fluids at the outlet of the nozzle. The low pressure fluid hose attaches to the combining nozzle cap**.**

Allowing the low pressure flow to initially release into the inside of the combining nozzle permits the low pressure flow to fully encompass the high pressure nozzle which ensures no voids in the initial low pressure-high pressure fluid interaction. With the low pressure completely encompassing the high pressure, very little misting action occurs due to the high pressure-workpiece impingement.

### 3.3.5 High Pressure Hose

In order to deliver the pressurized fluid to the nozzle, a high pressure tube or hose was needed. Inspecting various high pressure water jet machines, there are no plastic or rubber hoses used in the high pressure fluid delivery, instead they utilize stainless steel tubing. At the prototype stage, flexibility was important, especially with regards to the various components and their respective positions. Given the amount of unknowns, flexible hose is the only viable option. Standard rubber hydraulic hose has a maximum working pressure of approximately 5000 psi (34.3 MPa), which is insufficient for the selected pump. In order to handle the full 15,000 psi (103 MPa) of the Dynex pump, reinforced thermoplastic hose was selected. Thermoplastic hose is chemically inert to oil and can handle elevated temperatures.

Parker manufactures a thermoplastic hose that meets the pressure, flexibility, and connection requirements of the system. The Polyflex 2440N series hose was selected. The hose has a maximum working pressure of 23,780 psi (164 MPa) and a minimum bend radius of 6.1” (155 mm) allowing for the nozzle to move relative to the pump with no issues. The hose was fitted with NPT male fittings, rated at 15,000 psi (103 MPa), allowing for the hose to thread directly into the upper section of the high pressure nozzle without the use of additional fittings.

### 3.3.6 High Pressure Fittings

As mentioned in the high pressure hose section, standard hydraulic fittings did not meet the 15,000 psi (103 MPa) working pressure requirements of the system, with most fittings rated for approximately 5,000 psi (34.3 MPa). This limitation is due to a combination of the fitting material as well as the fitting wall thickness. To prevent hydraulic blow-outs of the fittings and connections, only NPT and Autoclave male fittings were used to build the system.

Due to the design of the nozzle assembly, only two high pressure connections needed to be made in the nozzle assembly. As seen in Figure 29, the high pressure hose threads directly into the upper section of the high pressure nozzle.

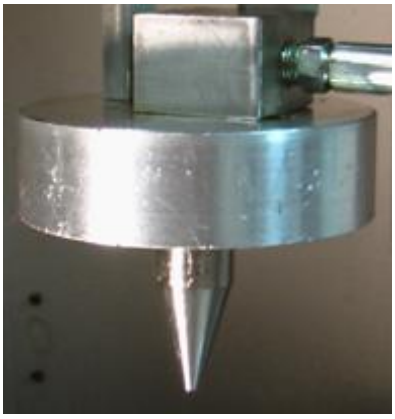

**Figure 29:** Hose threading into the upper section of the high pressure nozzle

This direct connection helped to simplify the system while also reducing the number of possible failure points. The second connection in the nozzle assembly occurs between the upper section and the constricting nozzle. As seen in Figure 28, the two sections thread directly into each other, once again simplifying the system.

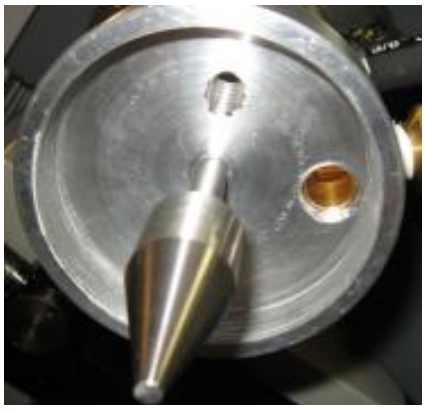

**Figure 28:** Constricting nozzle threaded onto the upper section

At the pump, three connections needed to be made: one adapter from the pump to a standard NPT connection, one from the adapter to a 90° fitting, and one from the 90° fitting to the hose. From the outlet of the pump to the 90° fitting, an Autoclave-NPT fitting was used as seen in Figure 30. The 90° adapter was fabricated from 304 stainless steel with sufficiently thick wall sections to prevent part failure at 15,000 psi. As seen in Figure 30, it was connected directly to the Autoclave-NPT fitting with the high pressure hose connected into the downstream side.

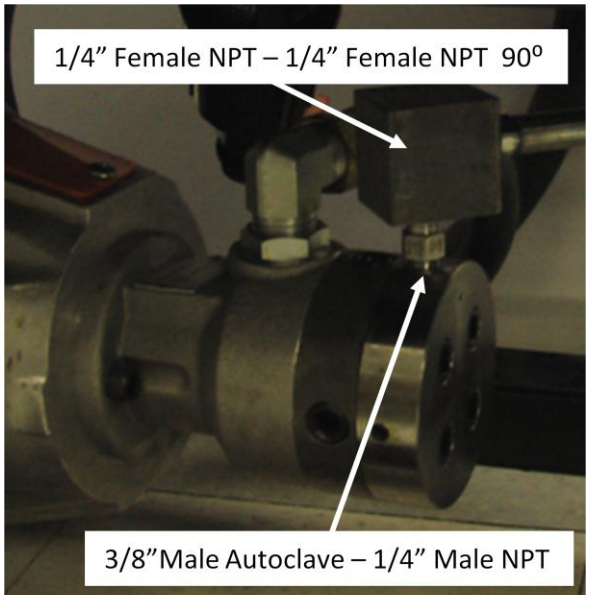


**Figure 30:** High pressure fittings

### 3.3.7 Reservoir Tank and Frame

With all the various components selected and/or designed, the reservoir tank and frame could then be designed. The reservoir tank was sized at 5 times the pumping capability of the system. With a pumping capability of 4 gpm (15 lpm), the tank was designed to hold at least 20 gallons (75.6 liters). The top of the tank also needed to be below the bottom of the work surface to prevent back flow from the reservoir into the machine. This limited the top of the tank to a height of 41", but the lower the tank, the more gravity fed

drainage could be expected. The high pressure pump and motor required a surrounding frame with dimensions of 36”L x 14”W x10”H (91.44 cm x 35.5 cm x 25.4 cm) to fully enclose them. The frame was built with 2” box tubing, which, when placed on casters, created an overall frame height of 18”. To ensure a solid base for the reservoir tank, the length and width dimensions were copied from the frame dimensions and with these two dimensions set, the third dimension was calculated to be 9.2”. For ease of fabrication, the height dimension was rounded up to 10”, thus ensuring a 20 gallon tank.

### 3.3.8 On-Machine Tank

Because the cavitation occurs between the two interacting streams, it is not necessary to provide a tank to hold a stagnant fluid as is common during CJW peening. However, due to the limited quantity of oil, it is necessary to capture and re-circulate the oil. To capture the oil, the workpiece must be placed in a tank, with the oil draining from the tank back into the reservoir tank. The on-machine tank needed to provide fixturing points to hold the workpiece steady. To accomplish this multiple threaded holes were provided to allow for fixturing points. A pass-through bulkhead fitting was placed along the bottom edge of the tank to provide a drainage point for the oil.

## 3.4 Assembly

The final assembly of the system created a few issues that had to be dealt with in order for the system to operate properly. Because there were no swivel fittings available for the pressure and size used in the system, all the connections were straight direct connections. This required the system to be assembled from the base pumping unit outwards. While straightforward, this requires more than one person to finish the assembly, as multiple parts during the final step must be rotated simultaneously.

Another issue not accounted for during the initial design was the placement of the oil filter prior to the fluid passing into the high pressure pump. As seen in Figure 31, sufficient room was available between the reservoir tank and the high pressure pump. The main issue with the current placement is during filter changes, there is little room to maneuver the tools necessary for the job.

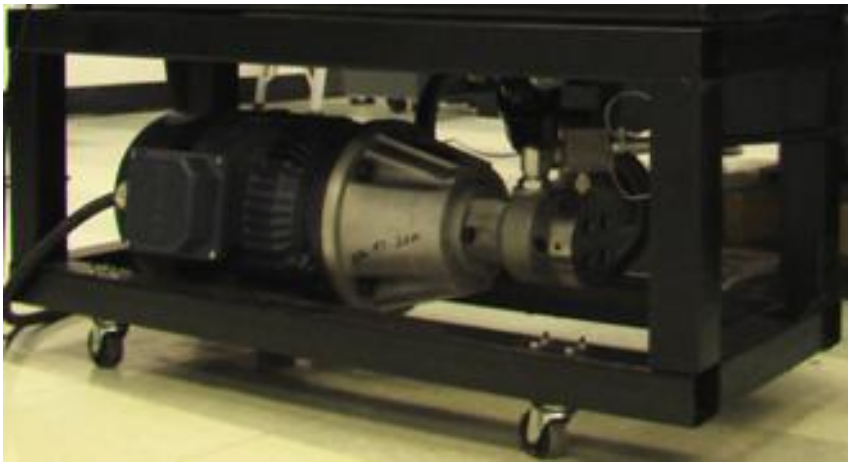

**Figure 31**: High pressure pump under reservoir tank

For the high pressure pump to mate to the motor, a coupling was required. While the coupling used is a standard shaft-shaft coupler, the area around the coupling point was severely limited by the reservoir tank on top and the floor underneath, as seen Figure 31. This created an area that only allowed limited movement of the Allen wrench that was used to tighten the couplers halves onto their respective shafts.

## 3.5 System Limitations

The fully assembled system has a few limitations both with respect to process parameters as well as geometric limitations. Result based limitations will be discussed in the results section, while only the physical system limitations will be discussed here.

At the closest stand-off distance, the spot size is only .030” (0.762 mm). With limited coverage areas, to generate any amount of overlap between consecutive passes, the step size must become smaller, leading to longer processing times.

With the fluid being constantly recirculated, the pumping process generates a lot of heat in the fluid. As the pump and hoses are only rated to 140°F, the system has a limited non-stop operation time span. This limit is approximately 3 hours, after which the system must be shut off for 5 hours to allow the fluid to cool before re-use.

### 3.6 Scalability

In order to create a cavitating jet in air system that is competitive with standard shot peening systems, the process time must decrease dramatically. Chillman studied the effect of the impact pressure on residual stress and determined that increases in upstream pressure did not increase the amount of induced compressive residual stress, but rather decreased the time necessary to reach the saturated level [34]. While the pump in the system presented here is able to provide 15,000 (103 MPa) psi pressure, other pumps are able to reach as high as 60,000 psi (413 MPa), but at a significantly higher cost.

To keep costs down, the pump purchased and used for the experiments had a relatively low flow rate of less than 0.25 gpm (0.945 lpm). This low flow rate resulted in a spot size that was as small as 0.030” (0.762 mm) under certain process parameters. In order to increase the spot size, a higher flow rate pump could be used, once again at a higher cost. Because exposure time is linearly related to the spot size area, doubling the spot size while maintaining pressure would decrease the exposure time by 50%. This increase in spot size is considerably more economical when compared to the alternative of utilizing higher pressure pumps.

Another option for scalability would be to create multiple machines operating in parallel. While each individual spot size and associated pressure would potentially be no different than what was used in the prototype setup, each nozzle would only be covering a fraction of the treated area rather than the entire surface.

## 3.7 Summary

The design of the oil based cavitating jet in air system presented here was influenced by many different requirements and constraints. This chapter presented the requirements and constraints placed on the system, as well as how each were resolved in the design and fabrication. The lack of a commercially available system required each component to be individually selected and then incorporated into the system. Finally, the need to incorporate the system into a standard machining environment was addressed with each design decision, with the final design and system being integrated into the Okuma Millac-44V available in the Precision Machining Research Laboratory.

# 4 Experimental Results

An experimental investigation was conducted to determine the effectiveness of the oil jet cavitation peening in air process on Al 2024-T3 samples. The chapter discusses the entire experimental process including the instrumentation and tooling required, the experimental design and the experimental procedure. The chapter then discusses the measured response variables, which includes averaged values, an analysis of variance, statistically significant trends and results, and explanations for these results and trends.

## 4.1 Experimental Procedure

### 4.1.1 Control Variables

The control variables under consideration follow those presented by others who have done liquid cavitation peening, mainly Soyama [14] and Grinspan [16]. As illustrated in Figure 32, the variables of interest are the traverse speed (mm/s), stand-off distance (mm), and pass-to-pass overlap (%).

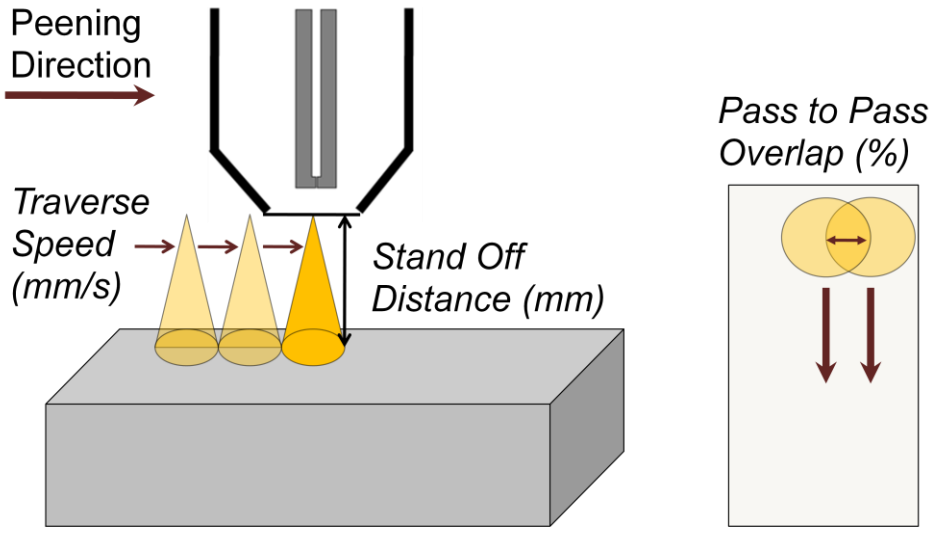


**Figure 32:** Process Variables

#### 4.1.1.1 Traverse Speed

The traverse speed is the speed at which the peening nozzle moves along (or "scans") the workpiece surface. This is held constant during each run and is directly controlled by the stage controller. The traverse speed directly affects the time the workpiece surface is exposed to the cavitation jet. As no prior work has been done with cavitating oil jets in air, a wide range of traverse speeds were selected: 0.5 mm/s, 5 mm/s, and 10 mm/s. These values are based roughly on values reported by Soyama [14] and Grinspan [16] for their respective cavitation peening in submerged liquid systems.

#### 4.1.1.2 Stand-off Distance

As illustrated in Figure 32, the stand-off distance is the distance from the exiting stream measured from the bottom of the combining nozzle to the top of the workpiece. Due to the stream diverging, the further the nozzle is from the workpiece surface, the larger the affected area. Because of this effect, changes in stand-off distance forced changes in the peening path to ensure the appropriate amount of pass-to-pass overlap on the surface. The stand-off distance was held constant during each run and was controlled by the machine tool stage controller. Based on Grinspan's prior work [16], the following values were selected: 5 mm, 15 mm, and 25 mm. Standoff distances closer than 5 mm were not possible as this would have caused a collision between the combining nozzle and the workpiece fixture.

#### 4.1.1.3 Overlap Percentage

Coverage percentage is a measure used in shot peening to determine how much of the workpiece area has been directly impinged by the shot. As shots represent individual discrete events, it was initially necessary to allow for values below 100% as some areas may not have been peened. Values above 100% indicate the same area has been exposed to multiple impacts, which may be desirable depending on the material and stress requirements. For the oil jet cavitation peening in air process, the stream was assumed to

peen 100% of the area it passed over, negating the need for values less than 100%. This assumption was verified utilizing painted strips and measuring pre- and post-process hardness in the paint removed area, as shown in Figure 33.

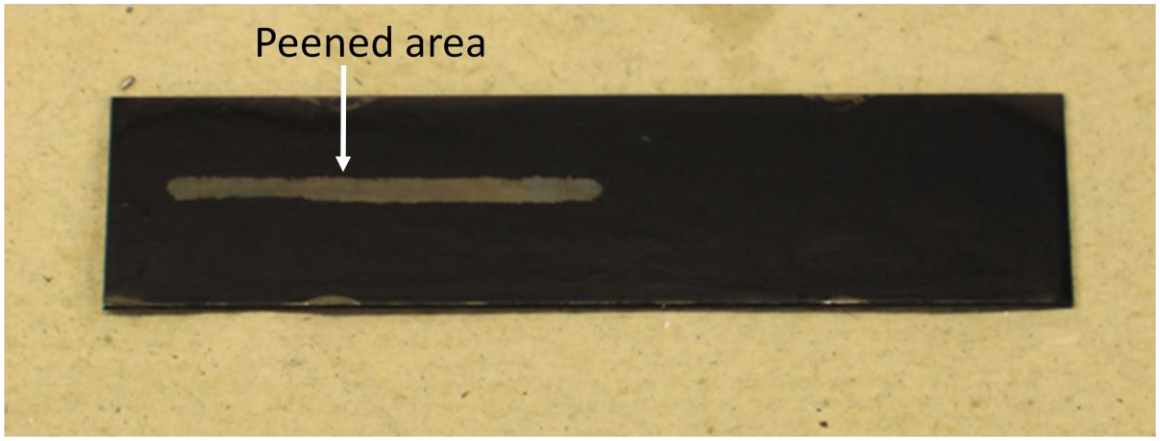


**Figure 33:** Path Peening Verification

Overlap percentage utilizes the coverage percentage definition and sets the base value to be 0% due to the aforementioned verified assumption. As shown in Figure 34a, 0% overlap indicates successive passes have no overlap and no space between the passes.

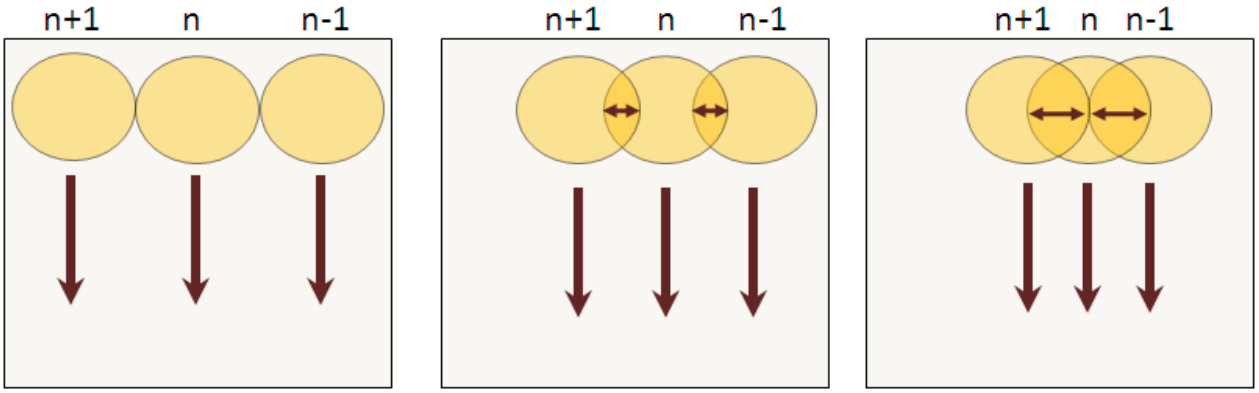


**(a)** **(b)** **(c)**

**Figure 34:** Illustrations of (a) 0% overlap, (b) 50% overlap, and (c) 100% overlap

The entire surface was peened, but successive passes did not affect areas that had previously been peened. Figure 34b illustrates the 50% overlap case which occurs when pass n is set to cover the far left 25% area covered by the previous pass (n-1). The successive pass, n+1, is then set to cover the far left 25% of the peened area covered

during pass n. This results in 50% of the workpiece surface area being peened again. Figure 34c represents 100% overlap which occurs when pass n is set to cover the far left 50% of the area covered by the (n-1) pass. The successive pass, n+1, is then set to cover the far left 50% of the peened area covered during pass n. This results in 100% of the workpiece surface area being peened again. The values selected for the pass-to-pass overlap percentage in this study were as follows: 0%, 50%, and 100%.

### 4.1.2 Response Variables

#### 4.1.2.1 Deflection

Due to the nature of Almen strips, measuring deflection provides a quick but indirect method to determine the residual stress induced in the sample by the peening process. Deflection is commonly used for standard shot peening in determining the process parameters for a given workpiece [42].

As the surface is impacted by the bubbles, the material plastically deforms, creating an area in compression immediately beneath the affected area. This effect, when applied to the entire strip results in a measurable deflection in the almen strip, as illustrated in Figure 35.

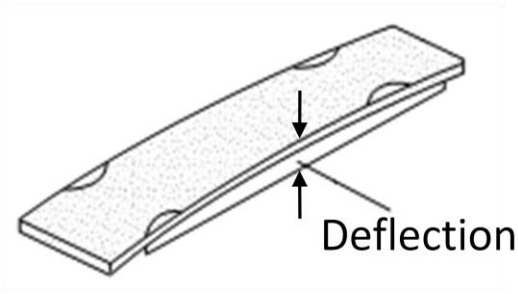


**Figure 35:** Almen Strip Deflection

Basic correlations have been created to relate residual stress to workpiece deflection. Walton [43] utilizes basic strength of materials relationships correlate deflections in

beams with non-uniform residual stresses to deflection. The final correlation between residual stress and deflection is as follows:

$$\sigma = \frac{Etd}{2L^2} \tag{4.1}$$

where E is Young's modulus, t is the thickness of the Almen strip, d is the measured deflection of the Almen strip, and L is the length of the curved surface which is typically estimated to be the length of the Almen strip.

The deflection of the Almen strips was measured using a Brown and Sharpe MicroVal® PFx tooled with a Renishaw TP-ES 5 mm ruby probe and then verified utilizing a low force Starrett 811 Dial Test Indicator, both of which were scanned over the surface to determine the maximum deflection. This was measured and reported in 0.0001" (2.54 μm) increments.

#### 4.1.2.2 Surface Area Roughness

Standard shot peening [44], water jet [45], and oil jet peening [36] have been shown to produce a rougher surface. The surface roughness must be monitored to ensure the part is not overly roughened, thus shortening the fatigue life of the specimen [36]. The surface roughness of the workpieces was measured before and after the peening process in 5 randomly selected areas on the workpiece using the Zygo New View 200 Optical Interferometer. The surface area roughness (Sa) was measured and reported in this research.

#### 4.1.2.3 Acoustic Emission

Cavitation creates a well known acoustic signal that has been studied in turbine applications [46] as well as in pump applications [47]. As the cavitating bubble collapses on the workpiece surface, a shock wave is generated. This shock wave gives off a high frequency acoustic signature that can be measured. The goal in measuring the acoustic

emission was to determine if the chosen combination of peening process parameters resulted in cavitation or not. In addition, it was of interest to determine if the emission frequency and/or magnitude could be utilized to characterize the process *in situ*. The system was instrumented as shown schematically in Figure 36.

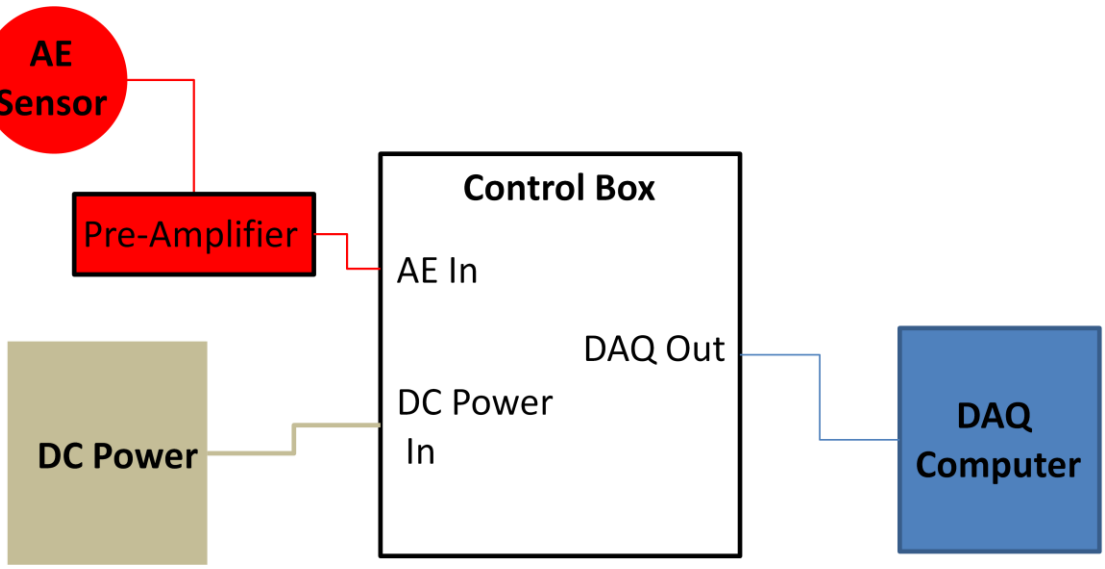


**Figure 36:** Schematic for Acoustic Emission Sensor

The signal was monitored via a Physical Acoustic Corporation Nano-30 AE sensor attached directly to the workpiece, as seen in Figure 37.

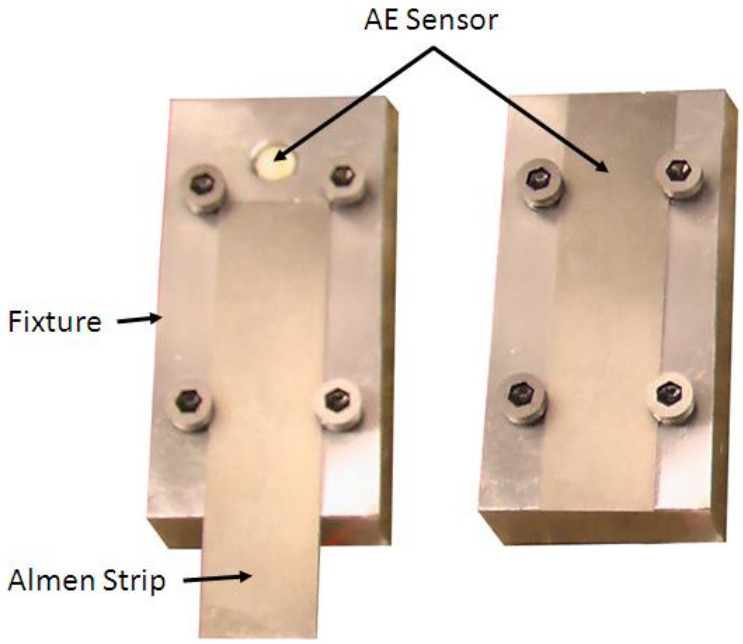


**Figure 37:** Acoustic Emission Sensor Fixture

The cable was then connected to a selectable 0x/20x/40x db gain preamplifier which sends the amplified signal to the control box. From the control box, the signal is read into the data acquisition computer.

4.1.2.4 Micro Hardness

Peening processes tend to work harden the workpiece due to the inhomogeneous plastic deformation caused by the process [44]. Aluminum is especially amenable to work hardening during peening processes and can be strengthened by work hardening [48]. In addition, micro hardness increases have been correlated to increased levels of compressive residual stress [49]. The more popular hardness tests, Brinell, Rockwell, Vickers, etc., all rely on an indenting ball to come into contact with the workpiece surface and then press into the surface under a given load for a specified time duration. Frankel, et al. [49] correlated the load caused by the indenter to a corresponding hoop stress, *h*, and residual stress, *r*, Figure 38 .

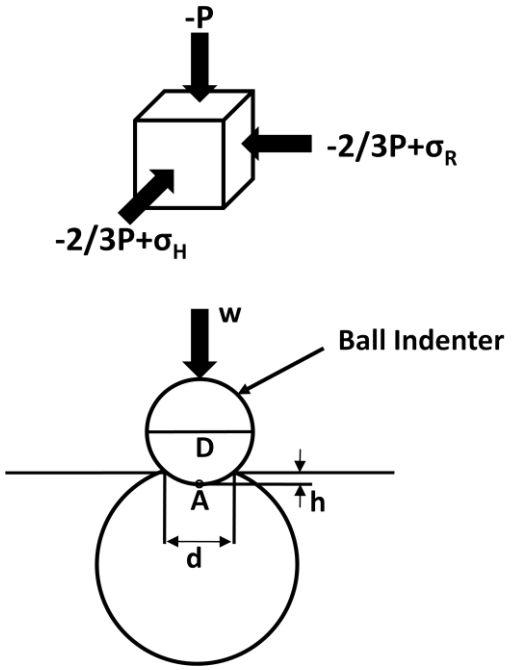


**Figure 38:** Stress relationship to Hardness [49]

While this correlation overestimates the stresses, it does estimate the general residual stress that can be expected. Utilizing this relation, an increase in micro hardness, which in and of itself is a desirable trait, also provides an indication of the residual stress a process induces.

The micro hardness was measured after the peening process in 5 different areas per peened workpiece using the Buehler Micromet 2104 Microhardness Tester and is reported in Vickers Hardness values. The Vickers Hardness number is determined by the ratio *F/A* where *F* is the force applied to the diamond indenter in kilograms-force and *A* is the surface area of the resulting indentation in square millimeters. *A* can be determined by the equation:

$$A = \frac{d^2}{2\sin\left(\frac{136^\circ}{2}\right)} \tag{4.2}$$

where *d* is the average length of the diagonal left by the indenter on the workpiece surface. Knowing the force applied on the indenter, the Vickers Hardness can then be calculated as :

$$HV = \frac{F}{A} \approx \frac{1.8544F}{d^2} \tag{4.3}$$

For the measurements made, the samples were loaded to 2 kg with a 15 second dwell. The indenter used was a standard Vickers 136° square-based pyramid made of diamond. The indent was optically measured and the hardness then calculated.

4.1.2.5 Mass Loss

One of the possible negative side effects of liquid peening processes is erosion of the workpiece surface, which is often attributed to direct impact of the liquid droplet on the

workpiece surface [36]. As seen in Figure 39, the peening process creates a crater with a small rim. At the upper edges of the rim, a crack is often created [14].

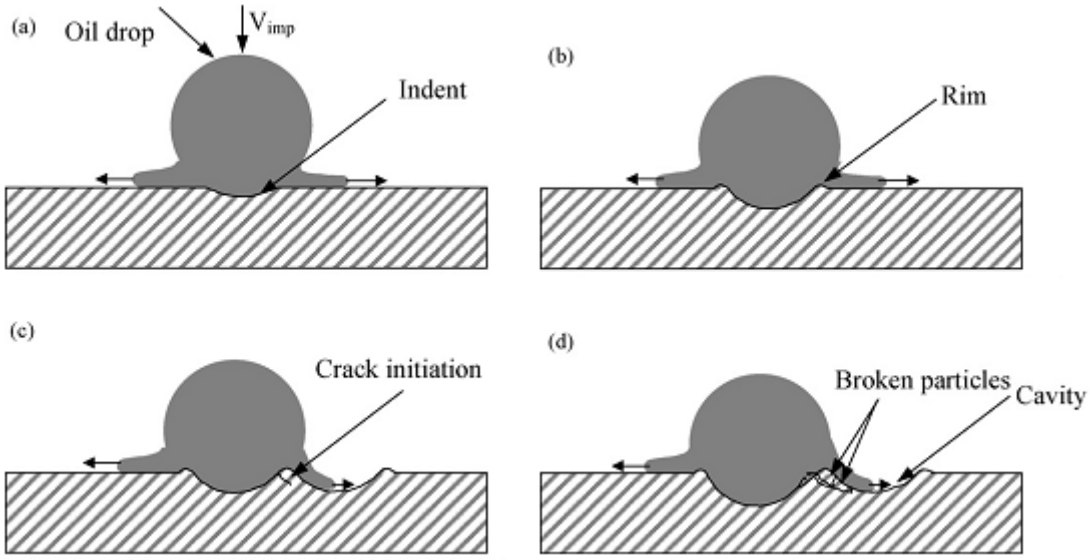


**Figure 39**: Erosion mechanism during liquid peening processes [14]

This rim is then eroded away as the fluid is forced laterally outward [14]. As the erosion process creates small micro-cracks, with too high an erosion rate, fatigue life may be adversely affected. To determine the amount of erosion induced by the process, the mass of the workpiece was measured before and after on a Mettler Toledo XS64 scale and reported in grams and used to determine the resulting mass loss from the workpiece.

#### 4.1.2.6 Residual Stress

Compressive residual stresses are known to increase fatigue life by inhibiting crack growth in the material [50]. Welding, casting, cutting, and processes involving heat or deformation can produce high levels of tensile residual stress, which can decrease the fatigue life. In these cases, relieving the tensile stress by peening can improve the fatigue life substantially. Residual stress is often measured and used to characterize peening processes. In a single point peening model, Figure 40, the area directly beneath the lowest point of the peened indent is in a compressive state. Either side of this point must be in tension to balance the forces. As the surface is peened multiple times, this tensile region

is peened, and the tensile region is pushed further out until the entire region has been peened. Once the entire surface has been peened, the equalizing tensile stresses must necessarily move into the thickness of the workpiece, beneath the compressive residiual stress field. In the case of through-thickness residual stress measurements, a depth is typically reached where the residual stresses transform from compressive to tensile.

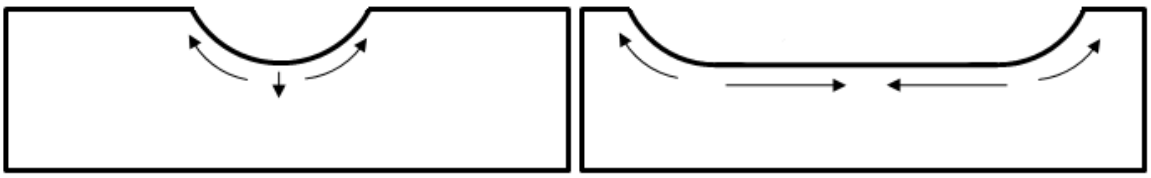

**Figure 40:** Compressive stress field [51]

Soyama [13], Grinspan [7], Daniewicz [45] all utilized x-ray diffraction methods to measure the residual stress in the liquid peened specimen, and this method was also chosen for this study.

X-ray diffraction relies on Bragg's Law which is given by $n\lambda=2d\ sin\theta$, and provides the expected angle for coherent scattering in a single crystal lattice [51]. In Bragg's Law, $n$ is an integer, $\lambda$ is the wavelength of the incident wave, $d$ is the spacing between the atomic planes in the single crystal lattice, and θ is the angle between the incident ray and the scattering planes [51]. The diffraction is best explained by considering a crystalline material exposed to a beam of x-rays approaching and leaving the surface at an angle θ, as illustrated in Figure 41.

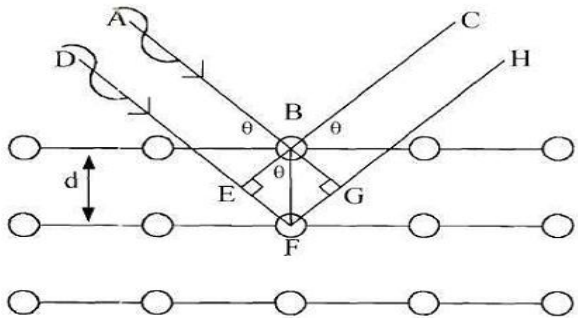


**Figure 41:** Illustration of Diffraction between 2 layers [52]

Initially both lines AB and DE have the same wavelength and will stay in phase if EFG is an integral multiple of the beams wavelength. If EFG is not an integral multiple of the incident beam's wavelength, the lines will then be out of phase, resulting in destructive interference, preventing any diffraction. As a result, only the integral multiples are diffracted [52].

If a compressive stress is present on the top lattice structure, the distance BF will decrease. Utilizing Bragg's law, the Bragg angle increases as a result of this applied stress. This change in the crystal's interplanar spacing is essentially a residual strain, which can then be related to residual stresses utilizing the appropriate constitutive equations of elasticity [51] which will be discussed below.

X-ray diffraction can also be utilized to measure residual stresses on polycrystalline materials. Similar to single crystal measurements, the polycrystalline material is exposed to the x-ray with a known wavelength. Following Bragg's law, the wavelength, $\lambda$, is known, the Bragg angle, $\theta$, is measured, leaving the interplanar spacing, $d$, as the only unknown. As a stress is applied, the interplanar spacing, $d$, changes.

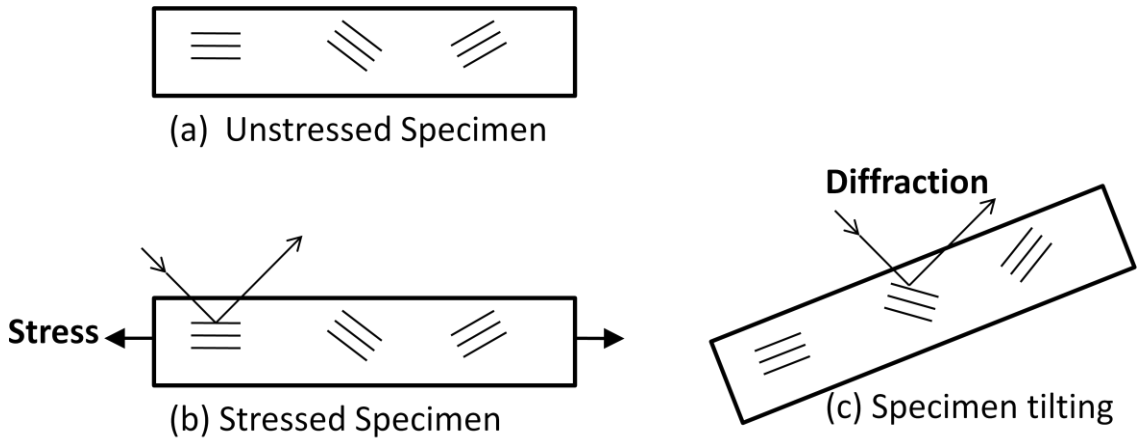


**Figure 42:** Workpiece rotation to capture polycrystalline planes [52]

As all the planes in a polycrystalline sample may not be aligned parallel with the workpiece surface, it becomes necessary to measure across a range of angles. As shown in Figure 42, as the workpiece is titled through various angles, different crystallographic planes are measured, providing a clearer picture of the stress induced in the workpiece.

To measure the residual stress in the oil jet cavitation in air peened specimens, standard powder diffraction techniques were used as outlined by Noyan and Cohen [51]. Figure 43 illustrates the X-Ray Diffraction measurement process geometries. As mentioned above, the sample is tilted at various angles with the x-ray source remaining fixed. The detector then moves through a fixed radius circle centered on the workpiece surface.

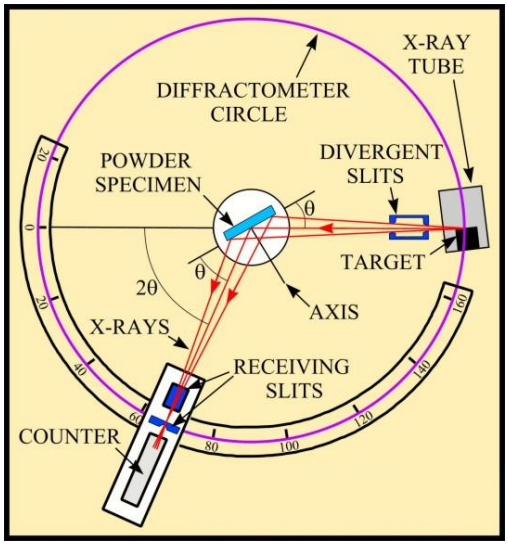


**Figure 43:** Illustration of a Standard XRD Process Geometries [52]

Ideally, the signal peak should be a single sharp line, but due to slight variations in the wavelength of the x-ray source and imperfections in the crystal structure, some widening is observed [51]. The shift in the peak from the expected value to the measured value is then correlated to the residual stress in the specific plane. For the cavitation peened samples, the residual stress was calculated from the shift of the peak angle for aluminum, 38.5˚, which corresponds to the {2 2 2} diffraction plane. The workpiece surface was

rotated through various $\phi$ angles and the corresponding surface longitudinal residual stress, $\sigma_\phi$ was documented, being measured along the workpiece surface. The longitudinal stress is measured along the peening direction of the workpiece surface. The individual stresses, $\sigma_\phi$, were then plotted with a regression line fitted to determine the average surface residual stress, $\sigma_r$, which is reported in the tables and graphs presented later in the chapter.

The residual stress was measured on a Panalytical X-Pert Pro with a 1.8kW Cu x-ray tube. The tube produced Cr Kα radiation with a wavelength of 1.54060 Å. The x-ray was run at a 50% intensity level, which leads to an estimated penetration depth of 7.6 μm in aluminum [51]. The x-ray tube was powered to 40kV at 40mA to ensure a strong clear signal. The X-ray was passed through a long fine focus (LFF) point focus collimator with a 3mm divergence slit at 1° and a 3mm axial mask. The goniometer was centered around the workpiece and operated on a 320 mm radius.

The surface was scanned using 0.02° 2θ increments ranging from 36° to 40°. Count times of 2 seconds were used to allow sufficient collection time and to ensure accurate peak shaping. To decrease the time necessary to measure the samples the scan was run on a continuous basis rather than starting and stopping the collection at each step.

In order to measure the through-thickness residual stress, the peened samples were chemically etched and then measured. Chemical etching is able to gradually remove material without disrupting the residual stress profile of the samples. As only a section of the sample was peened, the remaining material acted as support to prevent the etched sample from deflecting and altering the stress state. Noyan and Cohen [51] indicate this method does to not significantly alter the residual stress state in aluminum as long as the compressive residual stress area is surrounded by sufficient stress neutral material acting to prevent deformation. The sample was placed in a beaker with 10% Sodium Hydroxide,

NaOH. The sample was then removed and measured with a Mitutoyo 293 micrometer in 3 different spots to determine the average thickness of the etched sample.

### 4.1.3 Design of Experiments

In order to capture the effects of the process variables, a fractional factorial design of experiments was conducted. A fractional factorial design only explores a subset of the design space, but when done properly allows for appropriate effects to be calculated.

In fractional factorial designs, some of the effects are confounded and thus cannot be separated from other effects. These confounded effects will end up as a lumped term that, if large enough, may prove to be significant. If the lumped confounded effects are statistically significant, the fractional factorial design is insufficient and more experiments must be performed. However, in this case higher order interactions were assumed to be negligible, resulting in no need for their calculation. This assumption will be shown to be valid in the Results sections below.

The chosen fractional factorial design produces a full factorial across the first two variables, Stand-off Distance (A) and Traverse Speed (B). The third variables factor level, Pass-to-pass Overlap Percentage (C), is constructed from the interaction of the first two variables factor levels. The factor levels for the third variable are computed as C=3-$\text{mod}_3$ (A-B).

**Table 3:** a) DOE with variable levels

| Run | A | B | C |
|---|---|---|---|
| *1* | 0 | 0 | 0 |
| *2* | 0 | 1 | 2 |
| *3* | 0 | 2 | 1 |
| *4* | 1 | 0 | 2 |
| *5* | 1 | 1 | 1 |
| *6* | 1 | 2 | 0 |
| *7* | 2 | 0 | 1 |
| *8* | 2 | 1 | 0 |
| *9* | 2 | 2 | 2 |

b) DOE with variable values

| Run | Stand Off Distance (mm) | Traverse Speed (mm/s) | Pass to Pass Overlap (%) |
|---|---|---|---|
| 1 | 5 | 0.5 | 100 |
| 2 | 5 | 5 | 0 |
| 3 | 5 | 10 | 50 |
| 4 | 15 | 0.5 | 0 |
| 5 | 15 | 5 | 50 |
| 6 | 15 | 10 | 100 |
| 7 | 25 | 0.5 | 50 |
| 8 | 25 | 5 | 100 |
| 9 | 25 | 10 | 0 |

The $\text{mod}_3$ is the modulo-3 operator that finds a number *y* that is less than or equal to *x* and that is evenly divisible by 3. The remainder is then computed between *y* and *x*. An example is as follows: $\text{mod}_3$ (1)=1, $\text{mod}_3$ (2)=2, $\text{mod}_3$ (3)=0, and so forth. The final design is listed below in Table 3a and Table 3b in both the factor level and actual value forms. Each run was performed a total of 3 times to minimize any error or biasing that may have occurred from run to run.

After the initial DOE was conducted, the exposure time was calculated as shown in Table 4. The exposure time represents the total time the workpiece surface is exposed to the cavitating oil jet stream. In peening, the induced residual stress has been shown to be

**Table 4:** Calculated exposure time from DOE

| Run | Standoff Distance (mm) | Traverse Speed (mm/s) | Pass to Pass Overlap (%) | Exposure Time (min) |
|---|---|---|---|---|
| ***1*** | *5* | *0.5* | *100* | 127.0 |
| ***2*** | *5* | *5* | *0* | 6.3 |
| ***3*** | *5* | *10* | *50* | 4.2 |
| ***4*** | *15* | *0.5* | *0* | 20.3 |
| ***5*** | *15* | *5* | *50* | 2.7 |
| ***6*** | *15* | *10* | *100* | 2.0 |
| ***7*** | *25* | *0.5* | *50* | 16.3 |
| ***8*** | *25* | *5* | *100* | 2.4 |
| ***9*** | *25* | *10* | *0* | 0.6 |

influenced by the exposure time [1]. In the cases presented in Table 4, the exposure time is calculated by determining the amount of time required to complete a single pass and then multiplying it by the required number of passes to cover the entire area. With this number calculated, a large disparity was found between run 1 and all other runs.

To avoid excluding a significant portion of the exposure time design space, an additional 3 runs were added. These were selected to fill out the design space with regard to exposure time and are displayed in Table 5.

**Table 5:** Additional runs to fill in exposure time design space

| Run | Standoff Distance (mm) | Traverse Speed (mm/s) | Pass to Pass Overlap (%) | Exposure Time (min) |
|---|---|---|---|---|
| ***10*** | 5 | 0.5 | 50 | 85 |
| ***11*** | 5 | 0.5 | 0 | 63 |
| ***12*** | 5 | 2.5 | 100 | 25.4 |

This led to an additional traverse speed, 2.5 mm/s, that was not included in the initial DOE. This did not adversely affect the ANOVA calculations and could be included in all of the statistical calculations.

## 4.2 Sample Preparation

As the cavitation peening system was initially intended for materials commonly used in the aerospace industry, 2024-T3 aluminum was chosen as the workpiece material. 2024 is commonly used as the skin and frame material for airplanes.

Almen strips were first developed in the 1940's as a result of fatigue failure in early automotive springs [44]. It was discovered that shot peening the springs led to significant increases in the fatigue life, enough to prevent failure during their normal service life. It

became necessary to quantify the peening parameters, specifically the exposure time of the part to the peening process. John Almen developed a thin stress relieved strip that could be placed on critical areas of the spring that would bend when peened.

As shown in Figure 44, when peened, a compressive residual stress is induced on the surface of the workpiece, causing it to deflect. As mentioned in Section 4.1.2.1, the residual stress then corresponds to a measurable deflection of the strip.

The fatigue life of the spring was then tested and correlated to the measured deflection. The strips enabled a quick test to determine how long to peen the parts in order to reach specified fatigue lives. The strip, known as an Almen strip is a stress-relieved strip of 1070 spring steel that must meet the SAE J442 specification or the MIL AMS-S-13165 standard. Both standards provide key characteristics the steel strips must meet, most notably flatness (±0.001", ±0 .0254 mm), hardness (44-50 HRC), overall dimensions (±.001" ±0 .0254 mm), and no residual stress present in the workpiece.

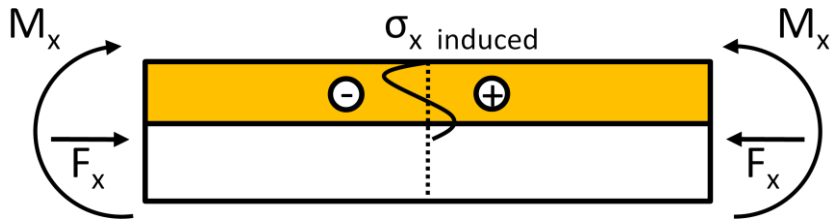


**Figure 44:** Residual stress profile

As shot peening has become more prevalent on aerospace materials, aluminum strips have been developed by the military. 2024T-3 was chosen because it is softer and more sensitive to residual compressive stress compared to 6000 and 7000 series aluminum alloys [53]. For aluminum strips, the only difference in the allowable specs was that the hardness must be between 72 and 78 HRB [53]. The strips utilized in the experiments had an overall thickness of 0.032" (0.8128 mm) and this thin cross section allows them to be sensitive to small changes in peening parameters as will be shown in future sections.

## 4.3 Deflection

### 4.3.1 Deflection Values

The averaged deflection values, listed in Table 6, are the averaged measured deflection on the strips per experiment. The maximum value for deflection occurred near the middle of the sample and was verified by zeroing the CMM or dial indicator after the first measurement was taken and measuring a second time.

**Table 6:** DOE level settings with deflection results

| Run | Standoff Distance (mm) | Traverse Speed (mm/s) | Pass to Pass Overlap (%) | Exposure Time (minutes) | Deflection (.001 in) |
|---|---|---|---|---|---|
| *1* | *5* | *0.5* | *100* | 127.00 | 10.3 (0.26 mm) |
| *2* | *5* | *5* | *0* | 6.35 | 4.6 (0.11 mm) |
| *3* | *5* | *10* | *50* | 4.23 | 1.3 (0.03 mm) |
| *4* | *15* | *0.5* | *0* | 20.31 | 1.2 (0.03 mm) |
| *5* | *15* | *5* | *50* | 2.72 | 1.4 (0.04 mm) |
| *6* | *15* | *10* | *100* | 2.03 | 1.6 (0.04 mm) |
| *7* | *25* | *0.5* | *50* | 16.28 | 0.4 (0.01 mm) |
| *8* | *25* | *5* | *100* | 2.44 | 0.16 (0.0 mm) |
| *9* | *25* | *10* | *0* | 0.61 | 0.13 (0.0 mm) |

The maximum deflection value, 0.013” (0.26 mm), was found during Run 1. Of note in these results is the significant increase in exposure time of run 1, approximately 20 times longer compared to run 2, which yields a deflection value of only approximately 2.5 times that of run 2. While this variation is relatively large in the case of the closest standoff distance, 5 mm, this large a variation is not seen for the other standoff distance settings.

The higher deflections occur at the closest standoff distance of 5 mm. This may be due to the cavitation bubbles collapsing prior to impacting the workpiece surface. Soyama [14] reports an optimal standoff distance exists wherein the fluid stream and the cavitating stream induce the largest compressive residual stress. Utilizing higher deflections to

indicate better process settings, the closest standoff distance, from the data reported in Table 6, provides the best results. The other two parameter settings, traverse speed and pass-to-pass overlap, will be discussed in a subsequent section.

This effect of deflection varying with time has been seen in standard shot peening and is characterized utilizing saturation curves [1]. These curves are generated holding the standoff distance and coverage percentage constant while varying the traverse speed. As this is the initial effort with oil jet cavitation in air peening, no such curves exist.

### 4.3.2 Analysis of Variance

The ANOVA was carried out on the complete (not averaged) deflection data. To determine whether the parameters were statistically significant, a 95% confidence level was chosen. In order to be deemed statistically significant, the parameter setting's P-value must be equal to or lower than 0.05 (5%). If the P-value is indeed below 0.05, the null hypothesis (no relationship between the parameter setting and the response variable) can be deemed false and the parameter is considered to have caused the measured change.

Utilizing a 95% confidence level, standoff distance, traverse speed, and percentage overlap affect a statistically significant change in the amount of deflection induced in the workpiece. As seen in Table 7, all three parameters have P-values below 0.05.

**Table 7:** ANOVA analysis on deflection

| | DF | Adj MS | F | P |
|---|---|---|---|---|
| **Standoff Distance** | 2 | 71.4 | 23.2 | 0.0004 |
| **Traverse Speed** | 3 | 12.6 | 12.6 | 0.0007 |
| **Pass-to-pass Overlap** | 2 | 22.7 | 7.4 | 0.003 |
| **Error** | 28 | 3 | | |
| **Total** | 35 | | | |

Standoff distance in cavitation peening has been found to impact the cavitation intensity the workpiece experiences [14, 16]. Should the standoff distance be too high, the cavitating jet diverges and the workpiece does not experience the necessary cavitation bubble density to induce a compressive residual stress [54]. Conversely, if the standoff distance is too close, the stream will not have had sufficient time to cavitate.

The physical significance of both traverse speed and pass-to-pass overlap can be seen as the cumulative effect of the exposure time of the workpiece to the cavitating stream. As the workpiece experiences more impact events, the compressive residual stress will increase. This increase reaches a material maximum over time and can reach up to approximately 80% of the yield strength of most materials [1].

### 4.3.3 Effect of Control Variables on Deflection

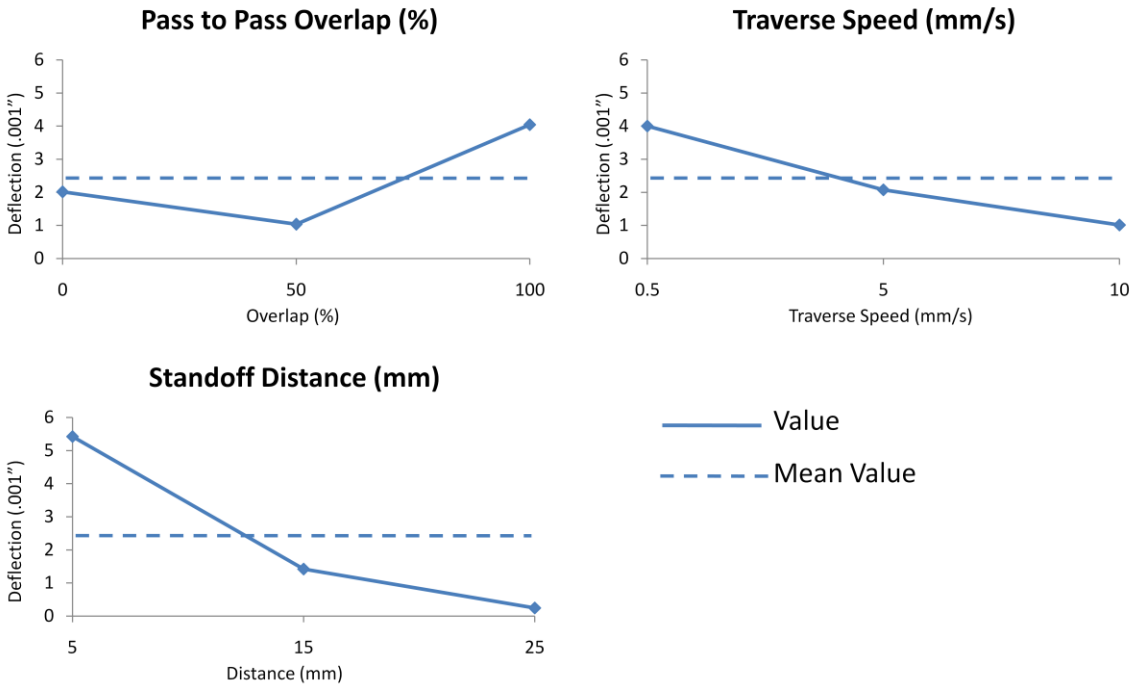


**Figure 45:** Main effects plot for deflection

The slopes of the lines in the main effects plots shown in Figure 45 indicate a strong correlation between the traverse speed and deflection, as well as the standoff distance and

deflection. While little correlation can be seen in the overlap percentage from 0% to 50%, a line with a significant slope can be seen from 50% to 100%.

With all three variables found to be statistically significant, changes in any of the three should lead to changes in the deflection. From the main effects plot it can be seen that to maximize deflection (and in turn maximize compressive residual stress) the traverse speed should be set as slow as possible. In effect this exposes the workpiece to the cavitating stream for a longer period of time, allowing for higher compressive residual stresses to be induced by increasing the number of cavitation implosion events experienced by the surface.

The lower the standoff distance the higher the expected deflection. This can be attributed to a decrease in the cavitation bubble density of the stream as the nozzle is located further from the workpiece. While the cavitation bubbles are being formed, it may the case that they are imploding prior to reaching the workpiece surface when the stand off distance is increased. Cavitation intensity has been shown to have an optimal position in a fluid stream, with intensity decreasing in either direction of this position [54].

The overlap percentage shows relatively little change between 0% and 50% coverage. This may be due to the non-overlapped region dominating the residual stress profile. However, from 50% to 100% a significant slope is seen, and is supported by corresponding deflection values. The results show that the overlap percentage should be driven to 100% as this created the largest change in deflection. Essentially, the higher overlap leads to an increase in total exposure time and similar to what was found for slower traverse speed, leads to a higher deflection.

## 4.4 Surface Roughness

### 4.4.1 Surface Roughness Values

The averaged surface roughness values shown in Table 8, are the averaged measured surface roughness values. Each workpiece was measured five times at randomly selected locations. The values were then averaged for each run, and the three sets of measurement per run were then averaged to create the data shown in Table 8.

**Table 8:** DOE level settings with surface area roughness (Sa) results

| Run | Standoff Distance (mm) | Traverse Speed (mm/s) | Pass to Pass Overlap (%) | Roughness (Sa) µm |
|---|---|---|---|---|
| *1* | *5* | *0.5* | *100* | 0.528 |
| *2* | *5* | *5* | *0* | 0.509 |
| *3* | *5* | *10* | *50* | 0.547 |
| *4* | *15* | *0.5* | *0* | 0.498 |
| *5* | *15* | *5* | *50* | 0.556 |
| *6* | *15* | *10* | *100* | 0.540 |
| *7* | *25* | *0.5* | *50* | 0.543 |
| *8* | *25* | *5* | *100* | 0.550 |
| *9* | *25* | *10* | *0* | 0.585 |

### 4.4.2 Analysis of Variance

The ANOVA was carried out on the complete (not averaged) set of surface roughness data and the results are shown in Table 9. Utilizing a 95% confidence level none of the variables (standoff distance, traverse speed, and percentage overlap) affects a statistically significant change in the surface roughness of the workpiece. According to the adjusted mean squares values, the error also does not account for any changes in the surface roughness.

**Table 9:** ANOVA analysis on surface roughness (Sa)

| | DF | Adj MS | F | P |
|---|---|---|---|---|
| **Standoff Distance** | 2 | 0.004 | 0.76 | 0.479 |
| **Traverse Speed** | 3 | 0.003 | 0.55 | 0.651 |
| **Pass-to-pass Overlap** | 2 | 0.0006 | 0.11 | 0.893 |

| | | |
|---|---|---|
| **Error** | 28 | 0.005 |
| **Total** | 35 | |

### 4.4.3 Effects of Control Variables on Surface Roughness

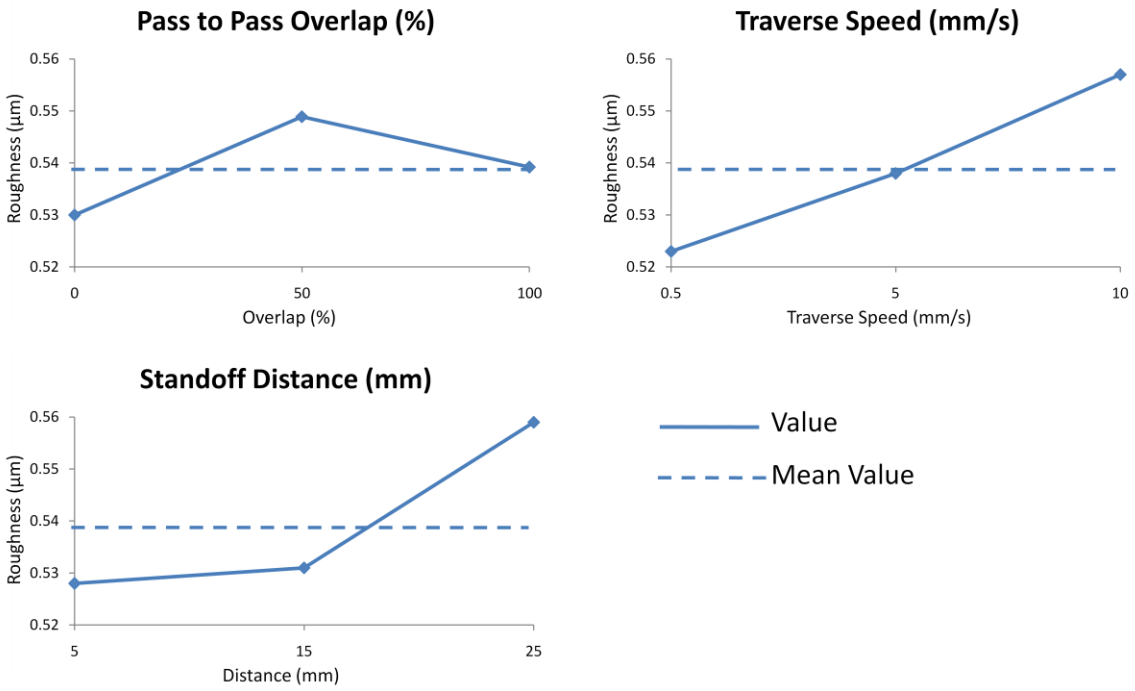


**Figure 46:** Main effects plot for surface area roughness (Sa)

With none of the variables found to be statistically significant, peening samples under any combination of the process parameters studied should not affect the surface roughness. From the main effects plots, Figure 46, there appears to be some interaction between both the traverse speed and mass loss as well as the standoff distance and mass loss. However, the scale for the surface area roughness, Sa, located on the vertical axis of the graphs, is sufficiently small so that any perceived correlation is in fact not statistically significant. It is important to note that the workpieces were not polished before peening as was done in the work performed by Grinspan [36] and Soyama [13]. As mentioned in

Section 4.4.2, the hydraulic oil chosen to minimize mass loss, may have also directly prevented a roughening of the workpiece surface.

## 4.5 Acoustic Emission

### 4.5.1 Frequency

#### 4.5.1.1 Frequency Values

In order to verify that cavitation was indeed occurring in the process, Acoustic Emission measurements were made with the low pressure fluid turned off. The resulting power spectrum, Figure 47, has no dominant spectrum peak or magnitude, especially at frequencies above 200 MHz, which is characteristic of cavitating streams [46, 47].

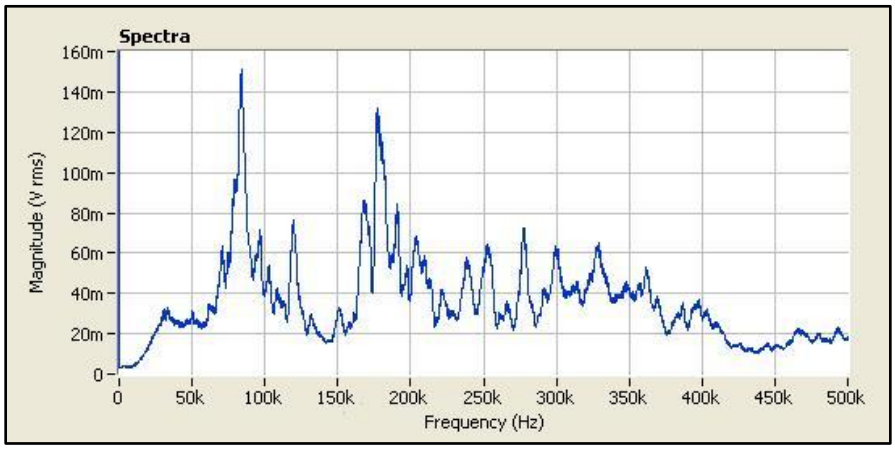


**Figure 47:** Acoustic Emission power spectrum during non-cavitation jet peening

With the low pressure pump turned on, the Acoustic Emission power spectrum was captured, and as shown in Figure 48, a very clear high frequency peak is detected between 250 kHz and 300 kHz.

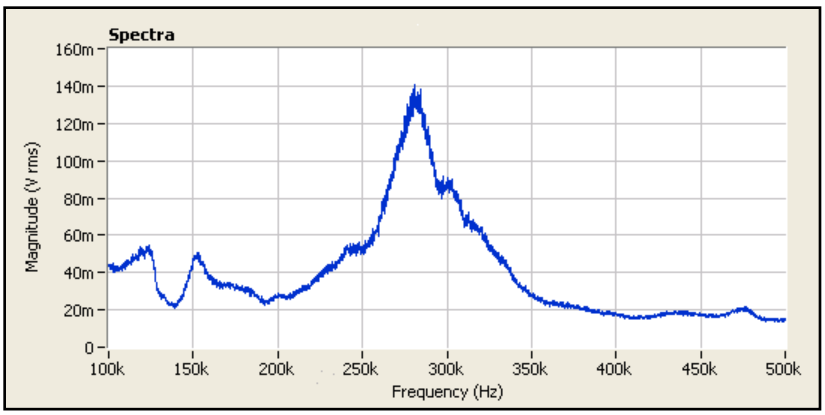


**Figure 48:** Acoustic Emission power spectrum during oil jet cavitation peening in air

The values measured for the maximum frequency were found to lie within the expected values (200 kHz – 1MHz) for cavitation phenomena reported in literature [46, 47].

The averaged acoustic emission frequency values are presented in Table 10. Each workpiece was measured three times during the peening. The values were then averaged for each run, and the three sets of measurements per run were then averaged to create the data presented in the table.

**Table 10:** DOE level settings with acoustic emission frequency results

| Run | Standoff Distance (mm) | Traverse Speed (mm/s) | Pass to Pass Overlap (%) | Frequency (kHz) |
|---|---|---|---|---|
| *1* | *5* | *0.5* | *100* | 281.2 |
| *2* | *5* | *5* | *0* | 279.6 |
| *3* | *5* | *10* | *50* | 285.3 |
| *4* | *15* | *0.5* | *0* | 282.2 |
| *5* | *15* | *5* | *50* | 277.9 |
| *6* | *15* | *10* | *100* | 281.4 |
| *7* | *25* | *0.5* | *50* | 286.8 |
| *8* | *25* | *5* | *100* | 281.4 |
| *9* | *25* | *10* | *0* | 283.9 |

All the values of the measure Acoustic Emission Frequency were found to be similar. As the fluid type and workpiece material never changed, bubble collapsing never created a different AE signature. Literature reports varying values for the bubble collapse

frequency, but this variation is only seen when the workpiece material varies [47]. With this result in mind, the frequency may be better utilized to verify that the workpiece is being impinged upon by a cavitating stream, rather than controlling the process, as was mentioned in section 4.1.2.3.

#### 4.5.1.2 Analysis of Variance

**Table 11:** ANOVA analysis on acoustic emission frequency

| | DF | Adj MS | F | P |
|---|---|---|---|---|
| **Standoff Distance** | 2 | 34.6 | 6.25 | 0.006 |
| **Traverse Speed** | 3 | 24.6 | 4.44 | 0.011 |
| **Pass-to-pass Overlap** | 2 | 2.9 | 0.53 | 0.595 |
| **Error** | 28 | 5.531 | | |
| **Total** | 35 | | | |

The ANOVA was carried out on the complete (not averaged) frequency data and the results are show in Table 11. Utilizing a 95% confidence level, standoff distance and traverse speed were found to be statistically significant.

With only two of the three variables found to be statistically significant, changes to either standoff distance or traverse speed will affect the frequency. However, the pattern of frequency change does not directly correlate to any of the other response variables. The statistical significance in this case is therefore misleading, especially when considering the scale and accuracy of the measurement. The scale is important to note with these measurements. The changes seen (from 1 kHz to 4 kHz) represent a less than 2% change in the measured frequency. Such a small percentage change could also be induced through fixturing, electronic noise, or acoustic noise. While this small percent change is statistically significant, the overall scale of the change and possible sources of error could significantly affect the statistical findings.

#### 4.5.1.3 Effects of Control Variables on Frequency

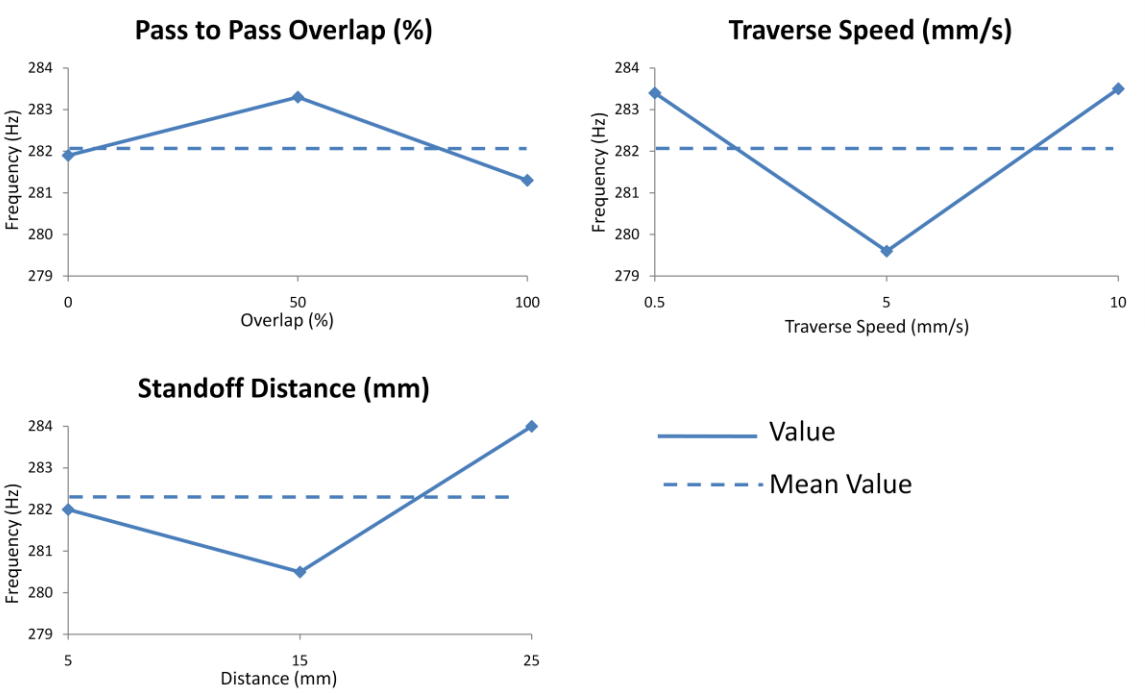


**Figure 49:** Main effects plot for acoustic emission frequency

As seen in the main effects plots in Figure 49, increasing the traverse speed from 0.5 mm/s to 5.0 mm/s decreases the measured frequency. The measured frequency increases as traverse speed increase from 5.0 mm/s to 10 mm/s. This trend is not seen in any of the other measured response variables for traverse speed, preventing any additional correlations between frequency, traverse speed and other measured responses.

The standoff distance, similar to traverse speed, undergoes a decrease in expected frequency response from 5 mm to 15 mm but demonstrates an increase in expected frequency response from 15 mm to 25 mm. This trend is not observed in any of the other measured response variables for standoff distance, preventing any additional correlations between frequency, standoff distance and other measured responses.

The overlap percentage was not found to be statistically significant. As was found in cavitation work previously [46], acoustic emissions were only affected by the distance from the cavitating source and the speed of the source relative to the sensor.

### 4.5.2 Magnitude

#### 4.5.2.1 Magnitude Values

The averaged acoustic emission signal magnitude values are presented in Table 12. Each workpiece was measured three times during the peening process and the three averaged sets per run were then averaged to create the data presented in the table.

**Table 12:** DOE level settings with acoustic emission magnitude results

| Run | Standoff Distance (mm) | Traverse Speed (mm/s) | Pass to Pass Overlap (%) | Magnitude (mV) |
|---|---|---|---|---|
| ***1*** | *5* | *0.5* | *100* | 143.5 |
| ***2*** | *5* | *5* | *0* | 115.3 |
| ***3*** | *5* | *10* | *50* | 90.3 |
| ***4*** | *15* | *0.5* | *0* | 84.2 |
| ***5*** | *15* | *5* | *50* | 66.0 |
| ***6*** | *15* | *10* | *100* | 32.0 |
| ***7*** | *25* | *0.5* | *50* | 7.1 |
| ***8*** | *25* | *5* | *100* | 6.2 |
| ***9*** | *25* | *10* | *0* | 2.9 |

#### 4.5.2.2 Analysis of Variance

The ANOVA was carried out on the complete acoustic emission signal magnitude data and the results are shown in Table 13. Utilizing a 95% confidence level, standoff distance and traverse speed were found to be statistically significant. Overlap was not found to be statistically significant.

**Table 13:** ANOVA analysis on acoustic emission magnitude

| | DF | Adj MS | F | P |
|---|---|---|---|---|
| **Standoff Distance** | 2 | 32477 | 199.71 | 0.0003 |
| **Traverse Speed** | 3 | 2271 | 13.97 | 0.0008 |
| **Pass-to-pass Overlap** | 2 | 175 | 1.08 | 0.354 |
| **Error** | 28 | 163 | | |
| **Total** | 35 | | | |

#### 4.5.2.3 Effects of Control Variables on Magnitude

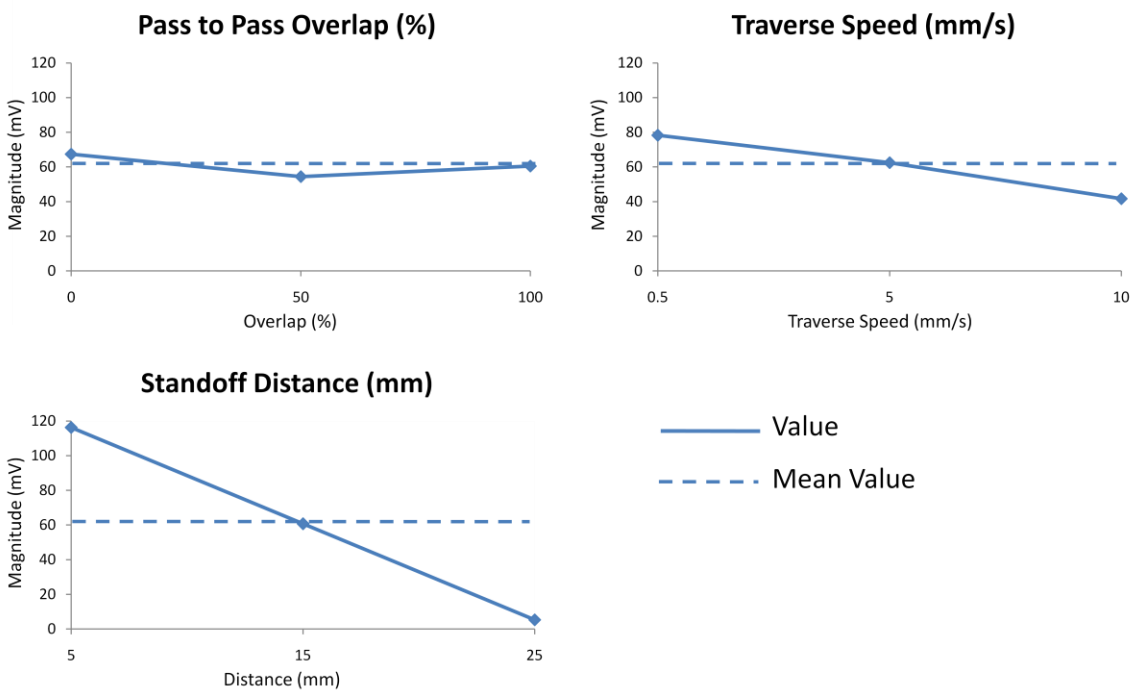


**Figure 50:** Main effects plot for acoustic emission magnitude

The acoustic emission signal magnitude is found to be a much better indicator of the process *in situ* for the two statistically significant parameters, traverse speed and standoff distance. As see in the main effects plot shown in Figure 50, the acoustic emission signal magnitude decreases with increases in traverse speed. Correspondingly, the deflection follows a similar pattern, which would allow for the magnitude to be monitored and the

process parameters to be changed on-line to provide varying peening intensities for different areas on the same part. As seen in Figure 51, the deflection increases with increases in the measured acoustic emission signal magnitude.

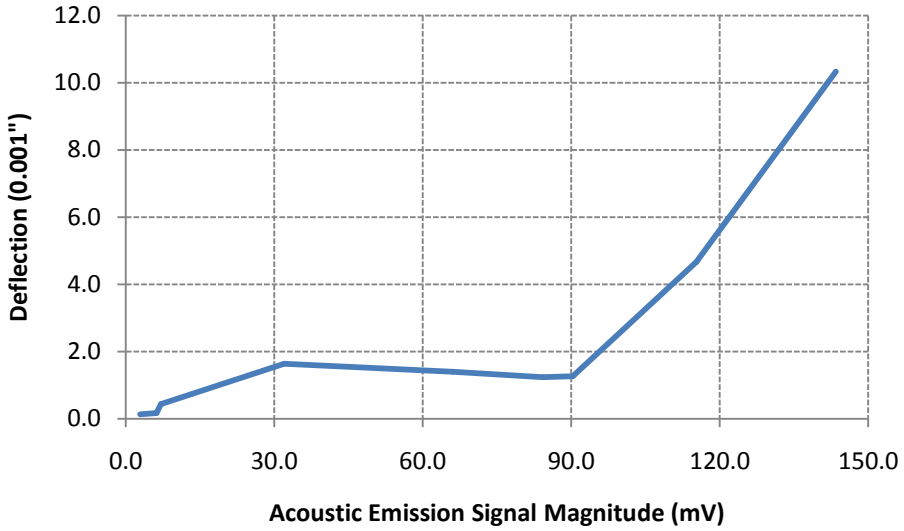


**Figure 51:** Deflection Variation with respect to AE Magnitude

This result is interesting to note, as the workpiece deflects with small values of measured signal magnitude, but then levels off. Upon reaching 90 mV magnitude, the part again begins to deflect rapidly. While based on limited data, this result correlating the Acoustic Emission Signal magnitude with the workpiece deflection (and correspondingly the induced compressive residual stress) may provide a quick method of determining or predicting the peening intensity with its corresponding workpiece deflection.

The acoustic emission signal magnitude is also significantly affected by the standoff distance. The acoustic emission signal magnitude decreases with increases in standoff distance, as shown in the main effects plot (Figure 50). As is the case with the traverse speed, the acoustic emission signal magnitude would be a good indicator to control the standoff distance to achieve specific peening intensities.

As was mentioned in Section 4.1.2.1, standoff distance in cavitation peening has been found to impact the cavitation intensity the workpiece experiences [14, 16]. Should the standoff distance be too high, the cavitating jet diverges and the workpiece does not experience a large amount of impinging cavitating bubbles [54]. Conversely, if the standoff distance is too close, the stream will not have had sufficient time to cavitate. Following this correlation, the acoustic emission signal magnitude appears to be adequate for measuring the intensity of the cavitating stream.

## 4.6 Micro Hardness

### 4.6.1 Micro Hardness Values

The micro hardness was tested 5 times per sample at different locations. The values were then averaged for each sample, and the 3 repeated runs were then averaged to obtain the final averaged micro hardness values presented in Table 14.

**Table 14:** DOE level settings with micro hardness results

| Run | Standoff Distance (mm) | Traverse Speed (mm/s) | Pass to Pass Overlap (%) | Micro hardness (HV) |
|---|---|---|---|---|
| *1* | *5* | *0.5* | *100* | 160.6 |
| *2* | *5* | *5* | *0* | 148.9 |
| *3* | *5* | *10* | *50* | 147.0 |
| *4* | *15* | *0.5* | *0* | 145.0 |
| *5* | *15* | *5* | *50* | 144.7 |
| *6* | *15* | *10* | *100* | 145.3 |
| *7* | *25* | *0.5* | *50* | 145.3 |
| *8* | *25* | *5* | *100* | 143.5 |
| *9* | *25* | *10* | *0* | 144.6 |

### 4.6.2 Analysis of Variance

The ANOVA was carried out on the complete micro hardness data and the results are shown in Table 15. Utilizing a 95% confidence level, the standoff distance, traverse speed and overlap percentage were found to be statistically significant.

**Table 15:** ANOVA analysis on micro hardness

| | DF | Adj MS | F | P |
|---|---|---|---|---|
| **Standoff Distance** | 2 | 160.3 | 18.03 | 0.00002 |
| **Traverse Speed** | 3 | 36.6 | 4.12 | 0.015 |
| **Pass-to-pass Overlap** | 2 | 62.2 | 6.99 | 0.003 |
| **Error** | 28 | 8.9 | | |
| **Total** | 35 | | | |

### 4.6.3 Effects of Control Variables on Micro Hardness

While the traverse speed has a statistically significant effect on the micro hardness, from the main effects plot shown in Figure 52, the main effect is seen from the 0.5 mm/s traverse speed. At the lowest traverse speed, the exposure time of the workpiece to the cavitating stream is the greatest. The cavitating stream then is able to induce more compressive residual stress (to be verified in section 4.8), which following Frankel's work [49] should lead to a higher micro hardness value. While both the 5mm/s and 10 mm/s traverse speeds cause increases in the micro hardness, there is no visible slope change between the two, indicating both would affect similar changes.

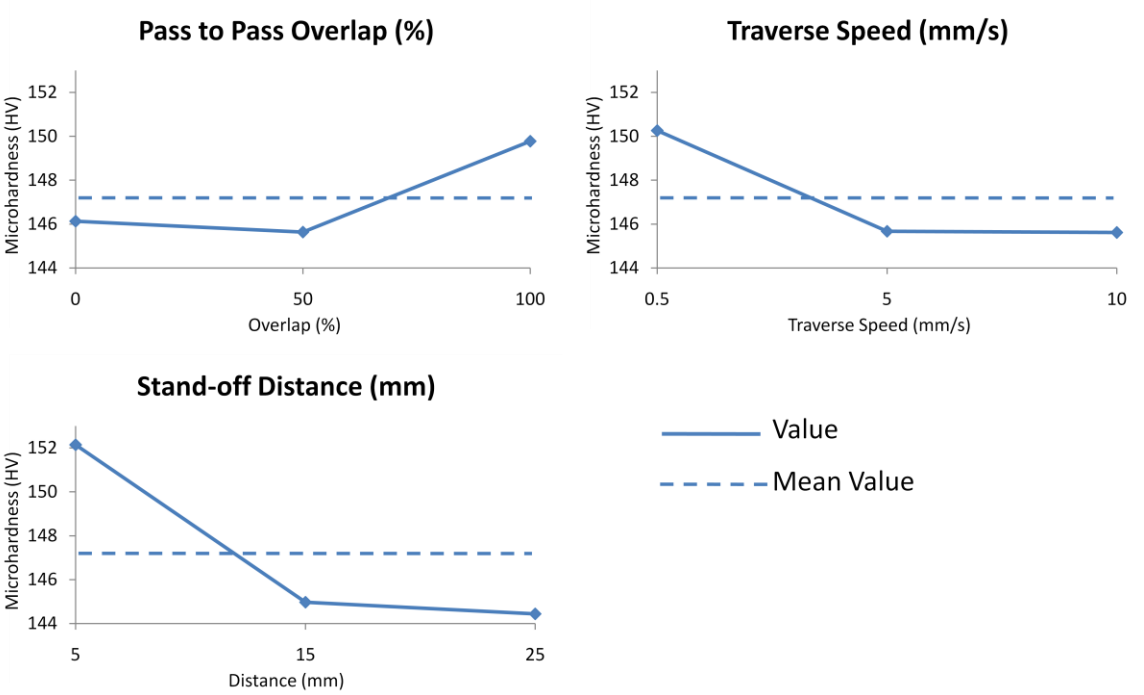


**Figure 52:** Main effects plot for micro hardness

The standoff distance, similar to the traverse speed, creates the largest change in micro hardness at the closer standoff distances. The 5 mm standoff caused the largest increase in micro hardness, with a small difference, less than 1 HV, seen in the increase in micro hardness for 15mm and 25 mm standoffs. The increase seen at the closest standoff distance, 5 mm, is likely due to cavitation intensity being larger than at the other two values. The acoustic emission signal magnitude indicates that at the closest standoff distance, 5 mm, the cavitation intensity is the greatest, and as such, the workpiece is undergoing the largest number of bubble impacts. Similar to the deflection-magnitude graph, Figure 51, the acoustic emission signal magnitude reaches a similar magnitude (~90 mV) before the large increase in micro hardness is measured (Figure 53).

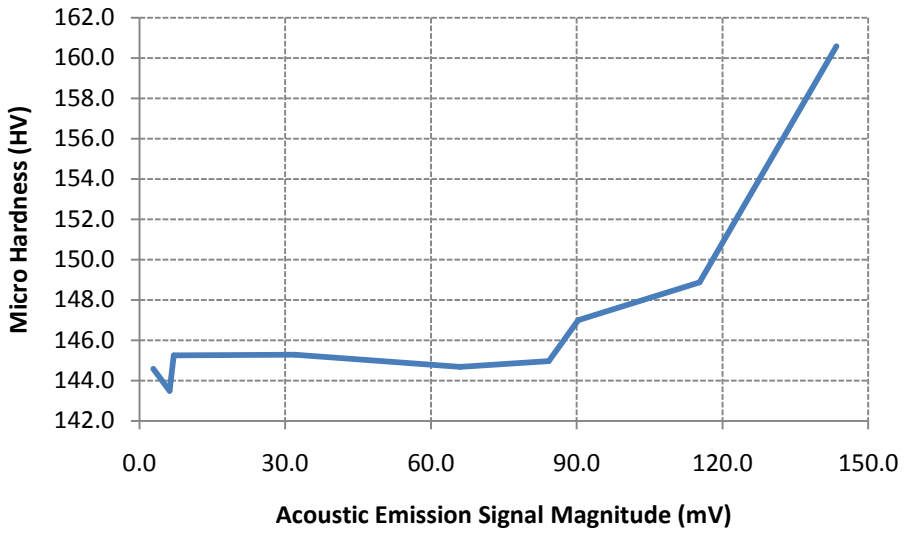


**Figure 53:** Micro Hardness Variation with respect to AE Magnitude

The overlap percentage change between 0% and 50% causes a negligible change in the micro hardness, as illustrated in Figure 52. However, at 100% overlap, there is a large change in the measured micro hardness. This would indicate that to improve the micro hardness, the overlap should be set at 100%.

## 4.7 Mass Loss

### 4.7.1 Mass Loss Values

The mass of the samples was measured before peening and again after peening. The post peening mass was then subtracted from the pre-peening mass to arrive at the total mass loss. Each of the three repeated samples per run condition were then averaged and are reported in Table 16. The measured mass loss values for the oil jet cavitation in air peening system were found to be about 100 times smaller than reported values for water cavitation peening in air [14], 10 times smaller than reported values for water peening [14], and 25% less than water cavitation peening in water [14]. The only system that offers comparable mass loss rates is oil jet peening [36].

**Table 16:** DOE level settings with mass loss results

| Run | Standoff Distance (mm) | Traverse Speed (mm/s) | Pass to Pass Overlap (%) | Mass Loss (mg) |
|---|---|---|---|---|
| *1* | *5* | *0.5* | *100* | 9.97 |
| *2* | *5* | *5* | *0* | 0.60 |
| *3* | *5* | *10* | *50* | 0.47 |
| *4* | *15* | *0.5* | *0* | 0.27 |
| *5* | *15* | *5* | *50* | 0.00 |
| *6* | *15* | *10* | *100* | 0.00 |
| *7* | *25* | *0.5* | *50* | 0.00 |
| *8* | *25* | *5* | *100* | 0.00 |
| *9* | *25* | *10* | *0* | 0.00 |

### 4.7.2 Analysis of Variance

The ANOVA shown in Table 17 was carried out on the complete mass loss data. Utilizing a 95% confidence level, the standoff distance, traverse speed and overlap percentage were found to be statistically significant.

**Table 17:** ANOVA analysis on mass loss

| | DF | Adj MS | F | P |
|---|---|---|---|---|
| **Standoff Distance** | 2 | 34.1 | 10.4 | 0.0002 |
| **Traverse Speed** | 3 | 34.8 | 10.6 | 0.0005 |
| **Pass-to-pass Overlap** | 2 | 38.5 | 11.7 | 0.0004 |
| **Error** | 28 | 3.3 | | |
| **Total** | 35 | | | |

### 4.7.3 Effects of Control Variables on Mass Loss

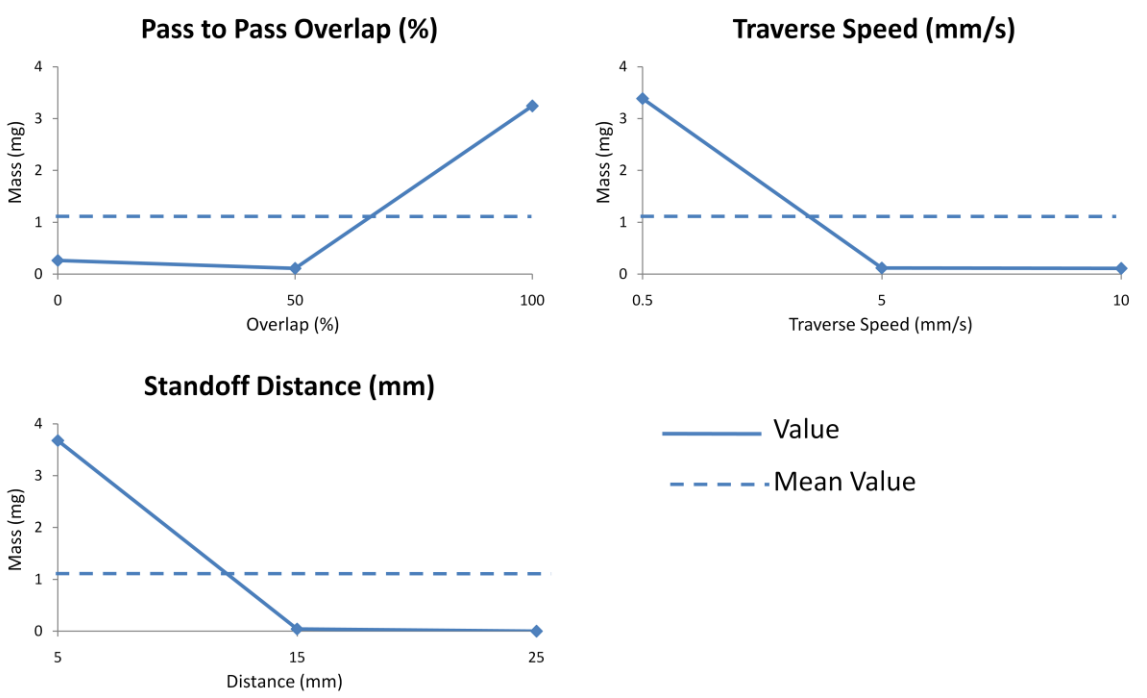


**Figure 54:** Main effects plot for mass loss

The traverse speed created a relatively large mass loss at the lowest traverse speed, 0.5 mm/s. At the higher speeds of 5 mm/s and 10 mm/s, very little mass loss was measured. As indicated by the acoustic emission magnitude levels, at the higher standoff distance less cavitation is seen, causing less mass loss.

The 5 mm standoff distance caused the largest mass loss in the workpiece. This can be related to the intensity of the cavitating stream that is impinging on the surface utilizing the acoustic emission magnitude levels, Figure 55. At the 15 mm standoff distance, negligible mass loss is observed and at 25 mm, no mass loss is observed. This finding indicates that there is insufficient force to produce cavitation bubble collapse at the workpiece surface or there is an insufficient number of cavitation bubble collapse events to cause a measurable mass loss.

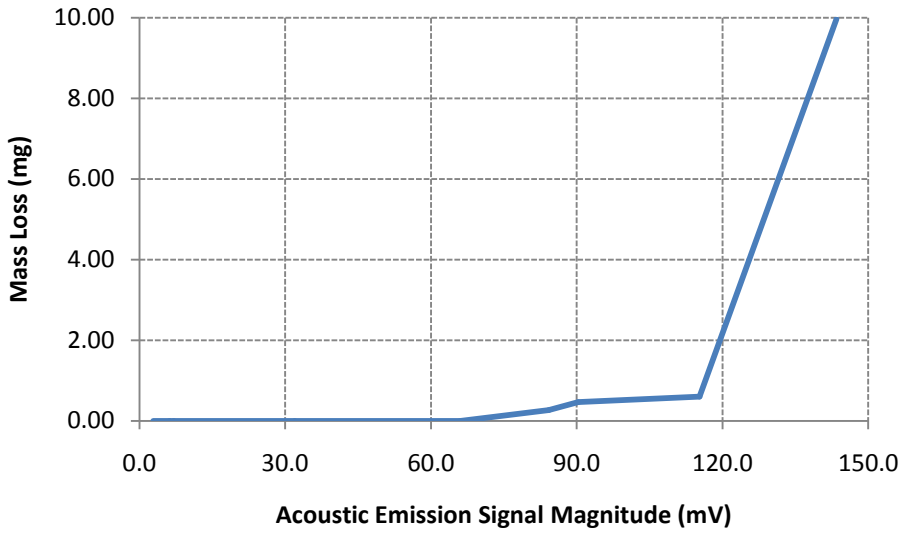


**Figure 55:** Acoustic Emission Signal Magnitudes effects on workpiece mass loss

As discussed in section 4.1.2.5, one of the steps prior to mass loss is a roughening of the surface. This roughened surface develops micro-cracks that, when propagated, result in material erosion. From Section 4.4, the process is shown to cause no statistically significant change in the surface roughness. As mass loss is expected to decrease with the oil [35], it would appear part of this decrease may be due to the lack of surface roughening caused by the fluid.

## 4.8 Residual Stress

### 4.8.1 Residual Stress Values

For the residual stress measurements made using x-ray diffraction, three run numbers were selected and a strip was then peened with the corresponding settings as outlined in Table 18. The run numbers were chosen based on the overall exposure time of the workpiece to the cavitating oil jet. To prevent skewing the results with extremely long exposure times, the runs selected occur over the complete spectrum of exposure times. As shown in Table 19, the selected runs vary from 127 minutes to 0.61 minutes.

**Table 18:** Parameter settings for residual stress testing

| Sample ID | Run # | Stand Off (mm) | Traverse (mm/s) | Overlap (%) |
|---|---|---|---|---|
| *C1* | 1 | 5 | 0.5 | 100 |
| *C5* | 12 | 5 | 2.5 | 100 |
| *C6* | 9 | 25 | 10 | 0 |

**Table 19:** Run number with associated exposure times

| Run # | Time (minutes) |
|---|---|
| 1 | 127.00 |
| 12 | 25.4 |
| 9 | 0.61 |

While the sample is nominally expected to have a zero stress state, residual stress measurements were made on 5 different unpeened samples to determine the unpeened residual stress. The samples were found to have an average of approximately -15 MPa compressive residual stress. Therefore, when performing the actual residual stress measurements on peened samples, once the residual stress values approached this level, the measurements were stopped and considered complete.

### 4.8.2 Comparisons

The through-thickness residual stress measurements were graphed as a function of depth. As seen in Figure 56, all three parameter sets produced a compressive residual stress in the workpiece surface, but the resulting through-thickness values varied.

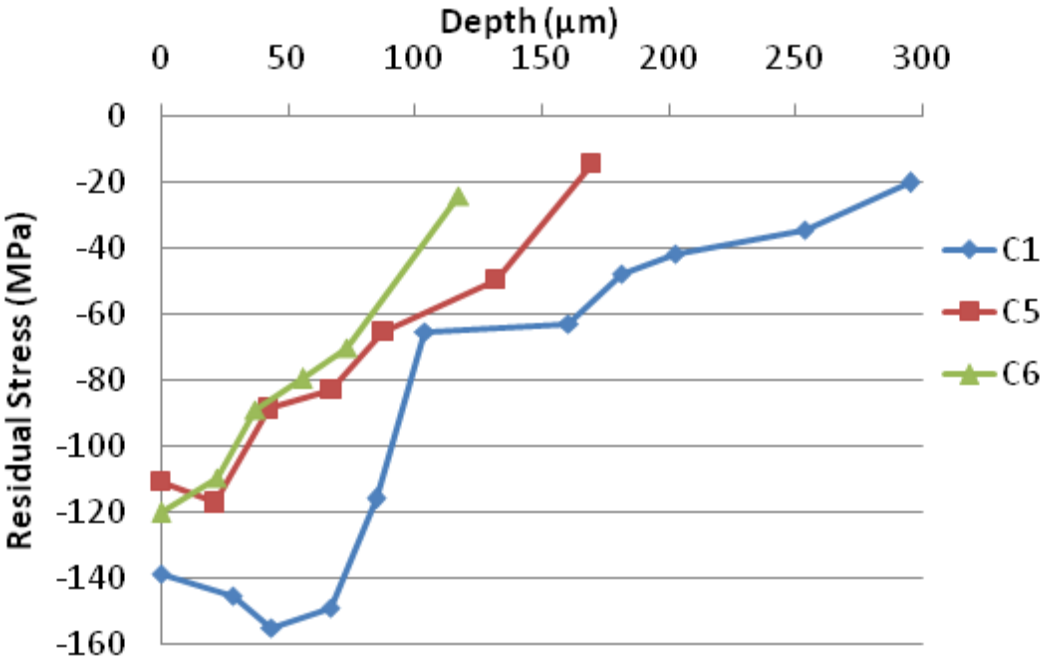


**Figure 56:** Plot of through-thickness residual stress

Sample C1, which was produced with a 5 mm standoff, 0.5 mm/s traverse speed, and 100% overlap resulted in the greatest surface residual stress of -140 MPa. With increasing depth, the sample experienced a maximum value of -155.3 MPa (60% of yield) at a depth of 43 µm.

Sample C5 (5 mm standoff, 2.5 mm/s traverse speed, and 100% overlap) had the lowest surface residual stress at -111 MPa, even though it experienced a much longer exposure time than sample C6. However, the through-thickness results indicate a higher residual stress at all depths, and a marked improvement is seen below 100 µm when compared to sample C6. While sample C5 does not produce the same level of compressive residual stress as sample C1, the total processing time was 20% of the processing time of sample C1 (25 minutes vs 127 minutes).

Sample C6, which was run at 25 mm standoff, 10 mm/s traverse speed, and 100% overlap, resulted in the second highest surface residual stress, but the worst through-thickness profile. While the compressive residual stress diminishes in the first 120 µm, this process required less than 1 minute to complete, compared to 127 minutes for sample C1 and 25 minutes for sample C5. The results for sample C6 are especially promising, even as the worst of the three cases presented, it is still producing compressive residual stresses at depths beyond 100 µm.

## 4.9 Cavitation Verification

In order to verify that cavitation was indeed occurring in the process, Acoustic Emission measurements were made with the low pressure fluid turned off. The resulting power spectrum, Figure 48, has no dominant spectrum peak, especially at frequencies above 200 MHz, which is characteristic of cavitating streams [46, 47]. The test with both high and low pressure streams does however have a clear spectrum peak, at 280 kHz as shown in Figure 47.

An additional test was run following identical parameter settings as Run 1 but without the use of the low pressure pump. This was done to jet peen the part without cavitation to aid in verification of the presence of a cavitation stream.

**Table 20:** Values for cavitation peened and jet peened samples

| *Run* | *Standoff Distance (mm)* | *Traverse Speed (mm/s)* | *Pass to Pass Overlap (%)* | *Deflection (.001 in)* | *Micro hardness (HV)* | |
|---|---|---|---|---|---|---|
| | | | | | *Hardness (HV)* | *% Increase* |
| 1 | 5 | 0.5 | 100 | 10.33 | 160.58 | 18.1% |
| Jet Peened | 5 | 0.5 | 100 | 0.3 | 142.11 | 4.5% |

The peened samples, presented in Table 20, clearly show decreases in both the deflection and microhardness of the sample during standard oil jet peening versus oil cavitation peening. Both the acoustic emission signal and the surface characteristics indicate the stream contains collapsing cavitating bubbles

## 4.10 Summary

This chapter showed how Al 2024-T3 responds to the oil jet cavitation in air peening system. Specifically the results indicate that the process is capable of generating beneficial workpiece properties:

- -155 MPa compressive residual stress
- Compressive residual stresses to 300 μm
- 21% increase in micro hardness
- No significant change in surface area roughness (Sa)
- 1.3 $x10^{-6}$ g/s mass loss rate

The results also indicate promising control capabilities utilizing the acoustic emission magnitude information. Magnitude is compared to the deflection, mass loss, and micro hardness, with strong correlations graphed for all three responses.

Decreases in the traverse speed led to increases in mass loss, surface microhardness, deflection acoustic emission signal magnitude with no effect on the surface roughness. Decreases in the stand-off distance led to increases in mass loss, surface microhardness, deflection, acoustic emission signal magnitude with no effect on the surface roughness. Finally, increases in the pass-to-pass overlap led to increases in mass loss, surface microhardness and deflection with no effect on the acoustic emission signal magnitude and the surface roughness.

The best results of the oil jet cavitation in air process are presented in Table 21 along with other techniques initial published results.

**Table 21:** Process Comparison

| | | Compressive Residual Stress | Surface Roughness | Mass Loss Rate |
|---|---|---|---|---|
| **Laser Peening** | *w/ Ablative Layer* | 200 MPa (40% yield) @100µm - Al 7075 [5] | Unchanged [5] | N/A |
| | *w/o Ablative Layer* | 80 Mpa (37% yield )@ 100 µm - SUS304 [26] | 2 µm peened vs .3µm unpeened (SUS 304) [26] | N/A |
| **Water Peening** | | 50% yield @ 80µm [7,15] | 3 µm peened vs .05 µm unpeened (Ti-6Al-4V) [34] | $8.4*10^{-5}$ g/s [14] |
| **Oil Jet Peening** | | 120 MPa (70% yield) - Al6063 [7] | 1.5 µm peened vs .62 µm unpeened (Al 6063) [36] | $1*10^{-6}$ g/s [36] |
| **Water Cavition Peening** | *In Water* | 50 MPa (15% yield) @ 80µm - JIS SKD61 [13] | .2 µm peened vs .1 µm unpeened (Ti-6Al-4V) [15] | $1.7*10^{-6}$ g/s [14] |
| | *In Air* | 200 MPa (60% yield) @ 80 µm - JIS SKD61 [13] | .1 µm peened vs .06 µm unpeened (SKD61) [13] | $1.7*10^{-4}$ g/s [14] |
| **Oil Cavitation Peening** | *In Oil* | 40% yield [16] | .33 µm peened vs .3 µm unpeened (Al6063) [16] | N/A |
| | *In Air* | -155 MPa (60% yield) -Al2024-T3 | Unchanged | $1.3*10^{-6}$ g/s |

While the values in Table 21 provide a comparison between the different processes, it should be noted the materials utilized vary for each process. The compressive residual stress for the oil jet cavitation in air process is comparable to the oil jet peening and the water cavitation in air peening process results. The surface roughness results are especially promising as the only other process that did not roughen the surface is laser peening with ablative layer. All the other processes roughened the workpiece surface, with water peening roughening the surface 600%.

The mass loss rates measured for the oil jet cavitation in air system were only lower for the oil jet peening and the laser shock peening processes. However, the difference between the oil jet peening mass loss rate and the oil cavitation in air mass loss rate is only 0.3μg/s.

# 5 Conclusions and Recommendations

## 5.1 Conclusions

This research indicates that it is feasible to build and implement an oil jet cavitation peening in air system in a standard machine tool environment. The study also indicates that oil cavitation peening in air produces significant surface modification in 2024-T3 aluminum. All three process parameters, stand-off distance, traverse speed, and pass-to-pass overlap, create statistically significant changes in some or all of the response variables. The research concludes that mechanical surface enhancement via oil cavitation peening in air produces desirable changes in the workpiece surface characteristics as well as through thickness residual stress. Specific relationships between the traverse speed, stand-off distance, and pass-to-pass overlap with the measured response variables are summarized below.

### 5.1.1 Best Process Results

The slowest traverse speed, 0.5 mm/s, closest standoff distance, 5 mm, and the highest pass-to-pass overlap, 100% produced the following best results:

- 166 HV hardness (21% increase)
- 155 MPa compressive residual stress (32 % increase over 2.5 mm/s)
- 0.0103” (0.262 mm) deflection
- Highest mass loss rate of 1.3 µg/s, which is comparable to the best of the liquid jet peening results of ~1 µg/s [36].
- No change in the surface roughness (Sa)

### 5.1.2 Effect of Traverse Speed on Material Characteristics

Changes in traverse speed produced statistically significant results in the following responses: frequency, magnitude, deflection, mass loss, and micro hardness. However, changes in traverse speed produced no statistically significant change in the surface area roughness (Sa).

A decrease in traverse speed leads to the following results:

- Increase in Acoustic Emission magnitude
- Increase in part deflection
- Increase in mass loss
- Increase in micro hardness
- No change in the surface roughness (Sa)
- No change in the Acoustic Emission frequency

The traverse speed creates a statistically significant change in the acoustic emission magnitude. From 0.5 mm/s to 5 mm/s the acoustic emission magnitude reduced by 19%, and from 0.5 mm/s to 10 mm/s the acoustic emission magnitude reduced by 37% . Due to this change, changes in traverse speed and their associated impact on the material characteristics may be monitored through the use of the acoustic emission signal and utilized to predict the workpiece response.

### 5.1.3 Effect of Stand-Off Distance on Material Characteristics

Changes in stand-off distance produced statistically significant results in the following responses: frequency, magnitude, deflection, mass loss, and micro hardness. However, changes in stand-off distance produced no statistically significant change in the surface area roughness (Sa).

A decrease in stand-off distance leads to the following results:

- Increase in Acoustic Emission magnitude
- Increase in part deflection
- Increase in mass loss
- Increase in micro hardness
- No change in the surface roughness (Sa)
- No change in the Acoustic Emission frequency

The stand-off distance creates a statistically significant change in the acoustic emission magnitude. From 5 mm to 15 mm the acoustic emission magnitude reduced by 58%, and from 5 mm to 25 mm the acoustic emission magnitude reduced by 95%. Due to this change, changes in stand-off speed and their associated impact on the material characteristics may be monitored through the use of the acoustic emission signal and utilized to predict the workpiece response.

### 5.1.4 Effect of Pass-to-pass Overlap on Material Characteristics

Changes in stand-off distance produced statistically significant results in the following responses: deflection, mass loss, and micro hardness. Changes in pass-to-pass overlap produced no significant change in acoustic emission frequency, acoustic emission magnitude, and surface area roughness on the aluminum samples.

An increase in pass-to-pass overlap leads to the following results:

- Increase in part deflection
- Increase in mass loss
- Increase in micro hardness
- No change in the surface roughness (Sa)
- No change in the Acoustic Emission frequency

- No change in the Acoustic Emission magnitude

Because the pass-to-pass overlap did not affect a statistically significant change in the acoustic emission response, the acoustic emission response currently cannot be utilized to predict material response due to changes in the pass-to-pass overlap.

## 5.2 Recommendations and Future Work

The research suggests that the oil jet cavitation in air process is capable of producing significant and desirable changes in the surface and mechanical properties of the workpiece. With mass loss rates no worse than 1.3 µg/s, the system erodes comparatively small amount of material. This low mass loss rate allows the system to be run at the closest stand-off distance, 5 mm, with the lowest traverse speed, 0.5 mm/s, with 100% pass-to-pass overlap without producing a large detrimental surface erosion. Of the parameters tested, traverse speed and stand-off distance proved more significant to surface change than the pass-to-pass overlap. Additional research should be done to further expand the explored design space to determine higher level interactions of the setting values. Lastly, as the only material processed was 2024-T3 Aluminum, care should be taken in extrapolating the presented results to other materials as the material properties, most notably Young's Modulus, vary widely between aluminum (~70 GPa) and steels (~200 GPa).

The purpose of the research was to build and then determine the effectiveness of an oil jet cavitation peening in air system. No modeling was done of the surface – bubble interaction. This understanding may possibly aid in future process optimization as well as system design changes. Future work should consider possible changes in nozzle positioning relative to the workpiece surface as this has been shown in prior studies to affect the level of induced compressive residual stress in both shot peening [1,44], and has been mentioned but not studied in liquid jet peening [13,14,38,45].

The acoustic emission signal may be a sufficient indicator of the process. To improve confidence in the utility of the signal, additional tests should be run and the acoustic emission recorded to ensure the trends presented can be utilized for a variety of materials and process settings. As this has not been presented or tested in previous research, the additional testing should provide adequate confidence that acoustic emission information can adequately predict the desired change.

The mechanism for inducing cavitation could be varied and compared to the researched fluid-fluid interaction method. Introducing an upset in the high pressure stream or entraining air are two possible methods that could be utilized to produce cavitation. This may provide varying results from the current method and warrant further investigation.

Finally, the system presented in the research was a proof of concept system, and as such, has many physical limitations. Most notably, the system requires relatively long exposure times for a noticeable change in surface conditions to be made. A larger system should be built to not only verify the scaling assumptions made, but also to test a variety of different emulsions that could not be tested in the high pressure pump that was utilized for experiments presented in this thesis. .

# References


1. Drozda, Tom. “Tool And Manufacturing Engineers Handbook: a Reference Book for Manufacturing Engineers, Managers, And Technicians.” 4th ed., Vol. 3, Dearborn, Mich.: Society of Manufacturing Engineers, 1983.
2. Torres, M., Voorwald, H., “An Evaluation of Shot Peening , Residual Stress and Stress Relaxation of the Fatigue Life of AISI 4340 Steel.” International Journal of Fatigue, Vol. 24, 2002, pp. 877–886.
3. Hammond, D., Meguid, S., “Crack Propagation in the Presence of Shot Peening Residual Stress.” Engineering Fracture Mechanics, Vol. 37, Num. 2, 1990, pp 373 – 387.
4. Montross, C., et al.,” Laser shock processing and its effects on microstructure and properties of metal alloys: a review” International Journal of Fatigue, Vol. 24, 2002, pp. 1021–1036.
5. Grinspan, A., Gnanamoorthy, R., “Surface modification by oil jet peening in Al alloys, AA6063-T6 and AA6061-T4: Residual stress and hardness.” Applied Surface Science, Vol. 253, 2006, pp 989-996.
6. Breuer, D., “Laser and Shot Peening – What is it and what does it accomplish?” Indianapolis Chapter ASM, Indianapolis, IN, Sept 20, 2004.
7. Grinspan, A., Gnanamoorthy, R., “Surface modification by oil jet peening in Al alloys, AA6063-T6 and AA6061-T4: Residual stress and hardness.” Applied Surface Science, Vol. 253, 2006, pp 989-996.
8. Hirano, K., et al., “Improvement of Residual Stress on Material Surface by Water Jet Peening.” Transactions of the 14th International Conference on Structural Mechanics in Reactor Technology, August 1997, pp 361-368.
9. Grinspan, A., Gnanamoorthy, R., “Effect of oil jet peening duration on surface modification and fatigue behavior of medium carbon steel, AISI 1040.” Materials Science and Engineering, Volume 456, 2007, pp 210-217.
10. Kunaporn, S., Ramulu, M., Hashish, M., “Mathematical Modeling of Ultra-High-Pressure Waterjet Peening.” Journal of engineering Materials and Technology, Vol. 127, April 2005, pp 186 – 191.
11. Kunaporn, S., Ramulu, M., Jenkins, M., Hashish, M., “Residual Stress induced by Waterjet Peening: A Finite Element Analysis.” Journal of Pressure Vessel Technology, Vol. 126, August 2004, pp 333-340.
12. Babu, N., Rajesh, N., “Multidroplet Impact Model for Prediction of Residual Stresses in Water Jet Peening of Materials.” Materials and Manufacturing Processes, Vol. 21, 2006, pp 299-409.
13. Soyama, H., “Improvement of fatigue strength by using cavitating jets in air and water,” Journal of Material Science, Volume 42, 2007, pp. 6638-6641.

14. Soyama, H., “Introduction of Compressive Residual Stress Using a Cavitating Jet in Air.” Journal of Engineering Materials and Technology, Vol. 126, January 2004, pp 123 – 128.
15. Soyama, H., Odhiambo, D.,“Introduction of compressive residual stress into titanium alloy Ti6Al4V by cavitation shotless peening .” Journal of the Society of Materials Science, Vol. 53, August 2004, pp 836-840.
16. Grinspan, A., Gnanamoorthy, R., “Effect of Nozzle-Traveling Velocity on Oil Cavitation Jet Peening of Aluminum Alloy, AA 6063-T6.” Journal of Engineering Materials and Technology, Vol. 129, Oct. 2007, pp 609-612.
17. Migala, T., Jacobs, T., “Low Plasticity Burnishing: An Affordable, Effective Means of Surface Enhancement.”
18. Seemikeri, C., Brahmanker, P., Mahagaonkar, S., “Low Plasticity Burnishing: An Innovative Manufacturing Method for Biomedical Applications,” Journal of Manufacturing Science and Engineering, Vol. 130, April 2008.
19. Li, F., et al., “Finite element calculation of residual stress and cold-work hardening induced in Inconel 718 by Low Plasticity Burnishing” Proceeding of the 3rd International Conference on Information and Computing, 2010, pp175 - 178.
20. Prevey, P., “The influence of surface enhancement by low plasticity burnishing on the corrosion fatigue performance of AA7075-T6” International Journal of Fatigue, v 26, n 9, p 975-982, September 2004.
21. Prevey, P., et al, “Improved High Cycle Fatigue Damage Tolerance of Turbine-Engine Components by Low Plasticity Burnishing.” Journal of Engineering for Gas Turbines and Power, Vol. 130, Jan. 2008, pp 012102-1 - 012102-5.
22. Sartkulvanich, P., Altan, T., Ciro, F., “Finite Element Modeling of Hard Roller Burnishing An Analysis on Effects of Process Parameters Upon Surface Finish and Residual Stresses.” Journal of Manufacturing Science and Engineering, Vol. 129, Aug 2007, pp. 705-716.
23. Yu, Z., et al, “Effect of surface treatments on fatigue life of Ti-6-22-22 alloy at room and high temperatures.” Materials Science and Engineering, Vol. 383, 2004, pp 283-288.
24. El-Tayeb, N., Low, K., Brevern, P., “Enhancement of Surface Quality and Tribological Preperties Using Ball Burnishing Process.” Machining Science and Technology, Vol. 12, 2008, pp 234-23.
25. Mordyuk, B., et al, “Characterization of ultrasonically peened and laser-shock peened surface layers of AISI 321 stainless steel.” Surface and Coatings Technology, Vol. 202, 2008, pp 4875-4883.
26. Sano, Y., et al, “Retardation of crack initiation and growth in austenitic stainless steels by laser peening without protective coating.” Materials Science and Engineering, Vol. 417, 2006, pp 334-340.

27. Sano, Y., et al, “Development and Applications of Laer Peening without Coating as a Surface Enhancement Technology.” Proceedings of SPIE Vol. 6343, 2006, pp 634324:1 – 634324:12.
28. Fabro, R., Peyre, P., Berthe, L., Sollier, A., Bartnicki E., “Physics and Applications of Laser Shock Processing Applications.” Proceedings of SPEI Vol. 3888.
29. Tan, Y., Wu, G., Yang, J.M., Pan, T., “Laser Shock Peening on Fatigue Crack Growth Behavior of Aluminum Alloy,” Fatigue Fracture Engineering and Material Sturctures, Vol. 27, 2004, pp. 649 – 656.
30. Luong, H., Hill, M., “The effects of laser peening on high-cycle fatigue in 7085-T7651 aluminum alloy.” Materials Science and Engineering, Vol. A477, 2008, pp 208-216.
31. Yu, Z., et al, “Effect of surface treatments on fatigue life of Ti-6-22-22 alloy at room and high temperatures.” Materials Science and Engineering, Vol. 383, 2004, pp 283-288.
32. Obato, M., et al., “Effect of Laser Peening on Residual Stress and Stress Corrosion Cracking for Type 304 Stainless Steel.” Proceeding of the 7th International Conference on Shot Peening, 1999.
33. Tönshoff, H., “High-Pressure Water Peening – a New Mechanical Surface-Strengthening Process.” Annals of the CIRP, Vol. 46, January 1997, pp 113 – 116.
34. Chillman, A., Ramulu, M., Hashish, M., “Waterjet Peening and Surface Preparation at 600 MPa: a Preliminary Experimental Study.” Journal of Fluids Engineering, Vol. 129, April 2007, pp 485 – 490.
35. Pai, R., Hargreaves, D., “Performance of Environment-Friendly Hydraulic Fluids and Material Wear in Cavitating Conditions.” Wear, Vol. 252, Num. 11-12, Jun 2002, pp 970-978.
36. Grinspan, A., Gnanamoorthy, R., “Surface modification by oil jet peening in Al alloys, AA6063-T6 and AA6061-T4 Part 2: Surface morphology, erosion, and mass loss.” Applied Surface Science, Vol. 253, 2006, pp 997-1005.
37. Singh, G., Grandhi, R., Stargel, D., Langer, K., “Modeling and Optimization of a Laser Shock Peening Process.” Proceedings of 12th AIAA/ISSMP Multidisciplinary Analysis and Optimization Conference, 10-12 September 2008.
38. Han, B., Jub, D., Jia, W., “Influence of water cavitation peening with aeration on fatigue behaviour of SAE1045 steel.” Applied Surface Science, Vol. 253, 2007, pp. 9342–9346.
39. “Millac 44-V Full Specifications”, The Millac Series, Jan 2009, http://www.okuma.com/products/machines/vmc/millac-v_series/millac44v/.
40. “Hydro Safe® ISO VG-68FR”, Hydro Safe Fire Retardant Oils, Jan 2009, http://www.hydrosafe.com/products/isovg68fr.htm.

41. Olsen, J., “A Comparison Between Intensifier and Crank Drive Pumps” OMAX, Jan 2009, http://www.omax.com/pumps_comparison.php.
42. SAE Specification J442, “Procedures for Using Standard Shot Peening Almen Strip.” June 2010.
43. Walton, H., “Deflection Methods to Estimate Residual Stress” ASM International, 2002, pp. 89-98.
44. Moore, Herbert F. “Shot Peening” [2nd ed.] Mishawaka, Ind.: American Wheelabrator & Equipment Corp, 1946.
45. Daniewicz, S., Cummings, S., “Characterization of a Water Peening Process.” Journal of Engineering Materials and Technology, Vol. 121, July 1999, pp 336-340.
46. Rus. T., et al., “An Investigation of the Relationship Between Acoustic Emission, Vibration, Noise, and Cavitation Structures on a Kaplan Turbine.” Journal of Fluids Engineering, Transactions of the ASME, Vol. 129, Number 9, September 2007, pp 1112-1122.
47. Neill, G. D., Reuben, R. L., and Sandford, P. M., 1997, “Detection of Incipient Cavitation in Pumps Using Acoustic Emission,” Proceedings of the Institution of Mechanical Engineers, Part E: Journal of Process Mechanical Engineering, Vol. 211(4), pp 267–277.
48. Smith, William F, and Javad Hashemi. “Foundations of Materials Science And Engineering.” 4th ed. Boston: McGraw-Hill, 2006.
49. Frankel, J., et al., “The Effects of Residual Stresses on Hardness Measurements.” Experimental Mechanics, Vol. 33, Num. 2, Jun 1993, pp 164-168.
50. de los Rios, E.R., et al., “Fatigue crack initiation and propagation on shot-peened surfaces in A316 stainless steel.” International Journal of Fatigue, Vol. 17, Num. 7, Oct 1995, pp 493-499.
51. Noyan, Ismail C, and J. B Cohen. “Residual Stress: Measurement by Diffraction And Interpretation.” New York: Springer-Verlag, 1987.
52. Cullity, B.D., Elements of X-Ray Diffraction, Addison - Wesley, Reading, MA, 1956.
53. U.S.A. Air Force “Manual on Aircraft Paint Stripping.” Chapter 5.
54. Coleman, A., et al., Physics in Medicine and Biology, v 38, n 11, p 1545, Nov 1993.

# Appendix

**Table XXII:** Design of Experiment's Parameter Settings

| Run | Stand Off (mm) | Traverse Speed (mm/s) | Pass to Pass Overlap (%) | Exposure Time (min) |
|---|---|---|---|---|
| 1 | 5 | 0.5 | 100 | 127.00 |
| 2 | 5 | 5 | 0 | 6.35 |
| 3 | 5 | 10 | 50 | 4.23 |
| 4 | 15 | 0.5 | 0 | 20.31 |
| 5 | 15 | 5 | 50 | 2.72 |
| 6 | 15 | 10 | 100 | 2.03 |
| 7 | 25 | 0.5 | 50 | 16.28 |
| 8 | 25 | 5 | 100 | 2.44 |
| 9 | 25 | 10 | 0 | 0.61 |

**Table XXIII:** Almen sample numbers with DOE Run Number

| Almen # | Run | Number |
|---|---|---|
| 2 | 1 | 1 |
| 3 | 1 | 2 |
| 4 | 1 | 3 |
| 5 | 2 | 1 |
| 6 | 2 | 2 |
| 7 | 2 | 3 |
| 8 | 3 | 1 |
| 9 | 3 | 2 |
| 10 | 3 | 3 |
| 11 | 4 | 1 |
| 12 | 4 | 2 |
| 13 | 4 | 3 |
| 14 | 5 | 1 |
| 15 | 5 | 2 |
| 16 | 5 | 3 |
| 17 | 6 | 1 |
| 18 | 6 | 2 |
| 19 | 6 | 3 |
| 20 | 7 | 1 |
| 21 | 7 | 2 |
| 22 | 7 | 3 |
| 23 | 8 | 1 |
| 24 | 8 | 2 |
| 25 | 8 | 3 |
| 26 | 9 | 1 |
| 27 | 9 | 2 |
| 28 | 9 | 3 |
| 32 | 10 | 1 |
| 33 | 10 | 2 |
| 34 | 10 | 3 |
| 38 | 11 | 1 |
| 39 | 11 | 2 |
| 40 | 11 | 3 |
| 41 | 12 | 1 |
| 42 | 12 | 2 |
| 43 | 12 | 3 |

**Table XXIV:** Surface Area Roughness (Sa) Values

| Sample | Trial # | PV | rms | Ra | Size X (mm) | Size Y (mm) |
|---|---|---|---|---|---|---|
| 2 | 1 | 7.031 | 0.588 | 0.469 | 0.7 | 0.53 |
| | 2 | 7.702 | 0.709 | 0.558 | 0.7 | 0.53 |
| | 3 | 7.903 | 0.71 | 0.57 | 0.7 | 0.53 |
| | 4 | 7.317 | 0.573 | 0.453 | 0.7 | 0.53 |
| | 5 | 8.746 | 0.63 | 0.501 | 0.7 | 0.53 |
| 3 | 1 | 13.738 | 0.728 | 0.57 | 0.7 | 0.53 |
| | 2 | 9.735 | 0.711 | 0.549 | 0.7 | 0.53 |
| | 3 | 8.873 | 0.769 | 0.605 | 0.7 | 0.53 |
| | 4 | 14.118 | 0.802 | 0.635 | 0.7 | 0.53 |
| | 5 | 10.291 | 0.692 | 0.562 | 0.7 | 0.53 |
| 4 | 1 | 10.21 | 0.784 | 0.575 | 0.7 | 0.53 |
| | 2 | 8.294 | 0.637 | 0.503 | 0.7 | 0.53 |
| | 3 | 9.583 | 0.575 | 0.457 | 0.7 | 0.53 |
| | 4 | 7.792 | 0.581 | 0.457 | 0.7 | 0.53 |
| | 5 | 9.273 | 0.572 | 0.458 | 0.7 | 0.53 |
| 5 | 1 | 6.757 | 0.697 | 0.552 | 0.7 | 0.53 |
| | 2 | 8.331 | 0.73 | 0.594 | 0.7 | 0.53 |
| | 3 | 6.595 | 0.724 | 0.579 | 0.7 | 0.53 |
| | 4 | 8.541 | 0.747 | 0.595 | 0.7 | 0.53 |
| | 5 | 7.746 | 0.761 | 0.605 | 0.7 | 0.53 |
| 6 | 1 | 6.077 | 0.63 | 0.512 | 0.7 | 0.53 |
| | 2 | 6.828 | 0.607 | 0.468 | 0.7 | 0.53 |
| | 3 | 7.58 | 0.59 | 0.47 | 0.7 | 0.53 |
| | 4 | 5.883 | 0.581 | 0.451 | 0.7 | 0.53 |
| | 5 | 9.209 | 0.514 | 0.405 | 0.7 | 0.53 |
| 7 | 1 | 6.965 | 0.576 | 0.465 | 0.7 | 0.53 |
| | 2 | 5.789 | 0.608 | 0.486 | 0.7 | 0.53 |
| | 3 | 5.977 | 0.578 | 0.464 | 0.7 | 0.53 |
| | 4 | 7.789 | 0.718 | 0.529 | 0.7 | 0.53 |
| | 5 | 8.203 | 0.565 | 0.457 | 0.7 | 0.53 |
| 8 | 1 | 8.78 | 0.692 | 0.55 | 0.7 | 0.53 |
| | 2 | 7.215 | 0.634 | 0.501 | 0.7 | 0.53 |
| | 3 | 7.787 | 0.61 | 0.492 | 0.7 | 0.53 |
| | 4 | 7.91 | 0.636 | 0.504 | 0.7 | 0.53 |
| | 5 | 8.459 | 0.727 | 0.584 | 0.7 | 0.53 |
| 9 | 1 | 7.441 | 0.757 | 0.591 | 0.7 | 0.53 |
| | 2 | 6.997 | 0.722 | 0.584 | 0.7 | 0.53 |
| | 3 | 6.955 | 0.632 | 0.499 | 0.7 | 0.53 |

| | | | | | | |
|---|---|---|---|---|---|---|
| | 4 | 7.159 | 0.793 | 0.628 | 0.7 | 0.53 |
| | 5 | 5.91 | 0.744 | 0.609 | 0.7 | 0.53 |
| 10 | 1 | 7.314 | 0.712 | 0.575 | 0.7 | 0.53 |
| | 2 | 7.389 | 0.617 | 0.502 | 0.7 | 0.53 |
| | 3 | 6.588 | 0.658 | 0.532 | 0.7 | 0.53 |
| | 4 | 8.352 | 0.708 | 0.561 | 0.7 | 0.53 |
| | 5 | 6.591 | 0.622 | 0.49 | 0.7 | 0.53 |
| 11 | 1 | 4.501 | 0.551 | 0.441 | 0.7 | 0.53 |
| | 2 | 7.413 | 0.593 | 0.456 | 0.7 | 0.53 |
| | 3 | 6.854 | 0.543 | 0.439 | 0.7 | 0.53 |
| | 4 | 7.211 | 0.544 | 0.436 | 0.7 | 0.53 |
| | 5 | 5.312 | 0.579 | 0.465 | 0.7 | 0.53 |
| 12 | 1 | 9.058 | 0.646 | 0.509 | 0.7 | 0.53 |
| | 2 | 6.05 | 0.642 | 0.512 | 0.7 | 0.53 |
| | 3 | 6.513 | 0.53 | 0.421 | 0.7 | 0.53 |
| | 4 | 6.891 | 0.651 | 0.525 | 0.7 | 0.53 |
| | 5 | 7.868 | 0.663 | 0.52 | 0.7 | 0.53 |
| 13 | 1 | 8.841 | 0.673 | 0.542 | 0.7 | 0.53 |
| | 2 | 6.547 | 0.652 | 0.514 | 0.7 | 0.53 |
| | 3 | 6.877 | 0.703 | 0.549 | 0.7 | 0.53 |
| | 4 | 6.818 | 0.735 | 0.559 | 0.7 | 0.53 |
| | 5 | 7.152 | 0.725 | 0.576 | 0.7 | 0.53 |
| 14 | 1 | 8.103 | 0.891 | 0.716 | 0.7 | 0.53 |
| | 2 | 6.412 | 0.665 | 0.524 | 0.7 | 0.53 |
| | 3 | 8.104 | 0.649 | 0.508 | 0.7 | 0.53 |
| | 4 | 9.344 | 0.75 | 0.592 | 0.7 | 0.53 |
| | 5 | 11.577 | 0.88 | 0.731 | 0.7 | 0.53 |
| 15 | 1 | 5.286 | 0.671 | 0.541 | 0.7 | 0.53 |
| | 2 | 6.44 | 0.781 | 0.635 | 0.7 | 0.53 |
| | 3 | 7.422 | 0.715 | 0.572 | 0.7 | 0.53 |
| | 4 | 8.517 | 0.711 | 0.574 | 0.7 | 0.53 |
| | 5 | 7.665 | 0.726 | 0.587 | 0.7 | 0.53 |
| 16 | 1 | 7.807 | 0.654 | 0.522 | 0.7 | 0.53 |
| | 2 | 7.344 | 0.58 | 0.445 | 0.7 | 0.53 |
| | 3 | 7.417 | 0.503 | 0.4 | 0.7 | 0.53 |
| | 4 | 7.252 | 0.61 | 0.482 | 0.7 | 0.53 |
| | 5 | 8.098 | 0.663 | 0.518 | 0.7 | 0.53 |
| 17 | 1 | 9.836 | 0.684 | 0.549 | 0.7 | 0.53 |
| | 2 | 7.282 | 0.68 | 0.551 | 0.7 | 0.53 |
| | 3 | 5.597 | 0.711 | 0.551 | 0.7 | 0.53 |
| | 4 | 6.41 | 0.632 | 0.512 | 0.7 | 0.53 |

| | | | | | | |
|---|---|---|---|---|---|---|
| | 5 | 7.18 | 0.66 | 0.521 | 0.7 | 0.53 |
| 18 | 1 | 5.548 | 0.643 | 0.524 | 0.7 | 0.53 |
| | 2 | 6.215 | 0.621 | 0.5 | 0.7 | 0.53 |
| | 3 | 6.772 | 0.58 | 0.476 | 0.7 | 0.53 |
| | 4 | 5.396 | 0.549 | 0.445 | 0.7 | 0.53 |
| | 5 | 6.628 | 0.563 | 0.46 | 0.7 | 0.53 |
| 19 | 1 | 6.589 | 0.64 | 0.526 | 0.7 | 0.53 |
| | 2 | 10.247 | 0.671 | 0.545 | 0.7 | 0.53 |
| | 3 | 9.207 | 0.771 | 0.595 | 0.7 | 0.53 |
| | 4 | 6.1 | 0.875 | 0.685 | 0.7 | 0.53 |
| | 5 | 8.393 | 0.839 | 0.659 | 0.7 | 0.53 |
| 20 | 1 | 8.28 | 0.778 | 0.618 | 0.7 | 0.53 |
| | 2 | 7.17 | 0.886 | 0.715 | 0.7 | 0.53 |
| | 3 | 6.982 | 0.711 | 0.55 | 0.7 | 0.53 |
| | 4 | 7.174 | 0.8 | 0.651 | 0.7 | 0.53 |
| | 5 | 7.048 | 0.64 | 0.499 | 0.7 | 0.53 |
| 21 | 1 | 6.637 | 0.784 | 0.627 | 0.7 | 0.53 |
| | 2 | 7.196 | 0.661 | 0.529 | 0.7 | 0.53 |
| | 3 | 5.884 | 0.581 | 0.473 | 0.7 | 0.53 |
| | 4 | 6.937 | 0.64 | 0.496 | 0.7 | 0.53 |
| | 5 | 6.056 | 0.638 | 0.518 | 0.7 | 0.53 |
| 22 | 1 | 5.673 | 0.648 | 0.533 | 0.7 | 0.53 |
| | 2 | 7.03 | 0.624 | 0.505 | 0.7 | 0.53 |
| | 3 | 7.013 | 0.625 | 0.498 | 0.7 | 0.53 |
| | 4 | 6.459 | 0.647 | 0.501 | 0.7 | 0.53 |
| | 5 | 6.133 | 0.549 | 0.439 | 0.7 | 0.53 |
| 23 | 1 | 6.162 | 0.648 | 0.52 | 0.7 | 0.53 |
| | 2 | 6.14 | 0.809 | 0.66 | 0.7 | 0.53 |
| | 3 | 7.485 | 0.727 | 0.578 | 0.7 | 0.53 |
| | 4 | 5.782 | 0.755 | 0.621 | 0.7 | 0.53 |
| | 5 | 5.906 | 0.6 | 0.492 | 0.7 | 0.53 |
| 24 | 1 | 13.586 | 0.646 | 0.508 | 0.7 | 0.53 |
| | 2 | 7.272 | 0.552 | 0.433 | 0.7 | 0.53 |
| | 3 | 13.385 | 0.607 | 0.484 | 0.7 | 0.53 |
| | 4 | 7.691 | 0.653 | 0.52 | 0.7 | 0.53 |
| | 5 | 8.354 | 0.586 | 0.477 | 0.7 | 0.53 |
| 25 | 1 | 8.761 | 0.766 | 0.629 | 0.7 | 0.53 |
| | 2 | 5.494 | 0.722 | 0.567 | 0.7 | 0.53 |
| | 3 | 9.292 | 0.788 | 0.567 | 0.7 | 0.53 |
| | 4 | 7.386 | 0.702 | 0.573 | 0.7 | 0.53 |
| | 5 | 7.548 | 0.761 | 0.614 | 0.7 | 0.53 |

| | | | | | | |
|---|---|---|---|---|---|---|
| 26 | 1 | 10.222 | 0.629 | 0.503 | 0.7 | 0.53 |
| | 2 | 9.023 | 0.681 | 0.541 | 0.7 | 0.53 |
| | 3 | 9.978 | 0.796 | 0.644 | 0.7 | 0.53 |
| | 4 | 7.721 | 0.714 | 0.547 | 0.7 | 0.53 |
| | 5 | 8.686 | 0.741 | 0.606 | 0.7 | 0.53 |
| 27 | 1 | 7.685 | 0.85 | 0.669 | 0.7 | 0.53 |
| | 2 | 7.994 | 0.812 | 0.651 | 0.7 | 0.53 |
| | 3 | 8.491 | 0.871 | 0.697 | 0.7 | 0.53 |
| | 4 | 8.219 | 0.695 | 0.543 | 0.7 | 0.53 |
| | 5 | 14.033 | 0.825 | 0.62 | 0.7 | 0.53 |
| 28 | 1 | 8.375 | 0.681 | 0.556 | 0.7 | 0.53 |
| | 2 | 7.307 | 0.727 | 0.597 | 0.7 | 0.53 |
| | 3 | 8.304 | 0.678 | 0.553 | 0.7 | 0.53 |
| | 4 | 11.05 | 0.703 | 0.56 | 0.7 | 0.53 |
| | 5 | 10.366 | 0.602 | 0.489 | 0.7 | 0.53 |
| 32 | 1 | 10.008 | 0.789 | 0.64 | 0.7 | 0.53 |
| | 2 | 13.302 | 0.795 | 0.62 | 0.7 | 0.53 |
| | 3 | 13.931 | 0.782 | 0.593 | 0.7 | 0.53 |
| | 4 | 9.258 | 0.703 | 0.536 | 0.7 | 0.53 |
| | 5 | 13.195 | 0.71 | 0.566 | 0.7 | 0.53 |
| 33 | 1 | 8.349 | 0.574 | 0.445 | 0.7 | 0.53 |
| | 2 | 8.766 | 0.793 | 0.648 | 0.7 | 0.53 |
| | 3 | 8.579 | 0.609 | 0.467 | 0.7 | 0.53 |
| | 4 | 7.702 | 0.583 | 0.46 | 0.7 | 0.53 |
| | 5 | 6.68 | 0.539 | 0.434 | 0.7 | 0.53 |
| 34 | 1 | 8.368 | 0.493 | 0.395 | 0.7 | 0.53 |
| | 2 | 8.536 | 0.696 | 0.56 | 0.7 | 0.53 |
| | 3 | 7.667 | 0.54 | 0.43 | 0.7 | 0.53 |
| | 4 | 8.075 | 0.539 | 0.422 | 0.7 | 0.53 |
| | 5 | 9.627 | 0.567 | 0.442 | 0.7 | 0.53 |
| 38 | 1 | 7.127 | 0.622 | 0.49 | 0.7 | 0.53 |
| | 2 | 8.693 | 0.616 | 0.489 | 0.7 | 0.53 |
| | 3 | 8.04 | 0.642 | 0.508 | 0.7 | 0.53 |
| | 4 | 10.301 | 0.706 | 0.535 | 0.7 | 0.53 |
| | 5 | 8.224 | 0.509 | 0.407 | 0.7 | 0.53 |
| 39 | 1 | 9.286 | 0.688 | 0.563 | 0.7 | 0.53 |
| | 2 | 7.221 | 0.625 | 0.507 | 0.7 | 0.53 |
| | 3 | 7.847 | 0.79 | 0.613 | 0.7 | 0.53 |
| | 4 | 9.065 | 0.694 | 0.532 | 0.7 | 0.53 |
| | 5 | 9.331 | 0.62 | 0.474 | 0.7 | 0.53 |
| 40 | 1 | 8.387 | 0.547 | 0.427 | 0.7 | 0.53 |

| | | | | | | |
|---|---|---|---|---|---|---|
| | 2 | 6.196 | 0.573 | 0.445 | 0.7 | 0.53 |
| | 3 | 8.935 | 0.589 | 0.485 | 0.7 | 0.53 |
| | 4 | 12.218 | 0.863 | 0.701 | 0.7 | 0.53 |
| | 5 | 7.613 | 0.659 | 0.527 | 0.7 | 0.53 |
| 41 | 1 | 8.082 | 0.841 | 0.662 | 0.7 | 0.53 |
| | 2 | 10.376 | 0.789 | 0.631 | 0.7 | 0.53 |
| | 3 | 7.592 | 0.68 | 0.552 | 0.7 | 0.53 |
| | 4 | 10.081 | 0.901 | 0.714 | 0.7 | 0.53 |
| | 5 | 7.992 | 0.791 | 0.612 | 0.7 | 0.53 |
| 42 | 1 | 8.839 | 0.555 | 0.438 | 0.7 | 0.53 |
| | 2 | 8.982 | 0.603 | 0.485 | 0.7 | 0.53 |
| | 3 | 6.771 | 0.586 | 0.451 | 0.7 | 0.53 |
| | 4 | 11.377 | 0.564 | 0.462 | 0.7 | 0.53 |
| | 5 | 6.814 | 0.651 | 0.514 | 0.7 | 0.53 |
| 43 | 1 | 8.361 | 0.669 | 0.507 | 0.7 | 0.53 |
| | 2 | 6.93 | 0.65 | 0.522 | 0.7 | 0.53 |
| | 3 | 7.196 | 0.604 | 0.471 | 0.7 | 0.53 |
| | 4 | 7.399 | 0.687 | 0.536 | 0.7 | 0.53 |
| | 5 | 9.238 | 0.698 | 0.548 | 0.7 | 0.53 |

**Table XXV:** Microhardness Values

| Sample | Trial # | D1 (µm) | D2 (µm) | HV |
|---|---|---|---|---|
| A2 | 1 | 145.2 | 145.2 | 175.9 |
| | 2 | 151.7 | 153.2 | 159.6 |
| | 3 | 148.8 | 150.1 | 166.0 |
| | 4 | 151.4 | 153 | 160.1 |
| | 5 | 151.4 | 153.5 | 159.6 |
| A3 | 1 | 158.7 | 155.3 | 150.5 |
| | 2 | 150.6 | 155.1 | 158.7 |
| | 3 | 148.4 | 153.2 | 163.1 |
| | 4 | 154.1 | 154.1 | 156.2 |
| | 5 | 146.5 | 153.3 | 165.1 |
| A4 | 1 | 144.7 | 154.2 | 166.0 |
| | 2 | 157 | 157 | 150.5 |
| | 3 | 152 | 157.3 | 155.1 |
| | 4 | 151.2 | 155.6 | 157.6 |
| | 5 | 147.2 | 152.9 | 164.7 |
| A5 | 1 | 159.2 | 159.2 | 146.3 |
| | 2 | 158.6 | 158.6 | 147.4 |
| | 3 | 157.8 | 157.9 | 148.8 |
| | 4 | 155.9 | 159 | 149.6 |
| | 5 | 160.9 | 159.5 | 144.5 |
| A6 | 1 | 157 | 156.6 | 150.8 |
| | 2 | 160.1 | 154.9 | 149.5 |
| | 3 | 157.6 | 157.6 | 149.3 |
| | 4 | 156.8 | 157 | 150.7 |

| | | | | |
|---|---|---|---|---|
| | 5 | 153.8 | 157.4 | 153.2 |
| A7 | 1 | 154.6 | 158.8 | 151.0 |
| | 2 | 160.1 | 160.8 | 144.1 |
| | 3 | 158.7 | 160.3 | 145.8 |
| | 4 | 157.4 | 157.2 | 149.9 |
| | 5 | 155.6 | 156.8 | 152.0 |
| A8 | 1 | 156.8 | 156.8 | 150.8 |
| | 2 | 152.6 | 155.5 | 156.3 |
| | 3 | 157.8 | 158.4 | 148.4 |
| | 4 | 158.8 | 161.4 | 144.7 |
| | 5 | 156.7 | 161.8 | 146.2 |
| A9 | 1 | 159.3 | 154.8 | 150.4 |
| | 2 | 162.2 | 161.5 | 141.6 |
| | 3 | 159.8 | 158.1 | 146.8 |
| | 4 | 163 | 157.9 | 144.1 |
| | 5 | 157.5 | 162.2 | 145.1 |
| A10 | 1 | 157.5 | 160.3 | 146.9 |
| | 2 | 158 | 158.5 | 148.1 |
| | 3 | 160.4 | 158.9 | 145.5 |
| | 4 | 159.8 | 161.4 | 143.8 |
| | 5 | 156.9 | 161.7 | 146.1 |
| A11 | 1 | 154.6 | 160.9 | 149.0 |
| | 2 | 153.9 | 153.9 | 156.6 |
| | 3 | 157.4 | 163.5 | 144.1 |
| | 4 | 160.2 | 164.2 | 141.0 |
| | 5 | 158.3 | 158.6 | 147.7 |
| A12 | 1 | 161.4 | 160.1 | 143.5 |

| | | | | |
|---|---|---|---|---|
| | 2 | 162.1 | 165.1 | 138.6 |
| | 3 | 158.8 | 161.8 | 144.3 |
| | 4 | 159.2 | 158.5 | 147.0 |
| | 5 | 159.5 | 163.5 | 142.2 |
| A13 | 1 | 153.9 | 164.5 | 146.3 |
| | 2 | 160.4 | 163.7 | 141.2 |
| | 3 | 157.5 | 160.4 | 146.8 |
| | 4 | 161 | 160.6 | 143.4 |
| | 5 | 162.1 | 160.4 | 142.6 |
| A14 | 1 | 158.4 | 163 | 143.6 |
| | 2 | 158 | 156.8 | 149.7 |
| | 3 | 158.3 | 156.8 | 149.4 |
| | 4 | 160.8 | 160.8 | 143.4 |
| | 5 | 158.4 | 160.7 | 145.7 |
| A15 | 1 | 158.7 | 161.4 | 144.8 |
| | 2 | 156.5 | 161.5 | 146.7 |
| | 3 | 158 | 163.9 | 143.2 |
| | 4 | 162.1 | 160.4 | 142.6 |
| | 5 | 159.2 | 160.4 | 145.2 |
| A16 | 1 | 157.3 | 161.7 | 145.8 |
| | 2 | 161 | 162.9 | 141.4 |
| | 3 | 162.3 | 162.7 | 140.4 |
| | 4 | 162.3 | 159.9 | 142.9 |
| | 5 | 158.6 | 161.1 | 145.1 |
| A17 | 1 | 161 | 157.7 | 146.1 |
| | 2 | 159.2 | 155.8 | 149.5 |
| | 3 | 159.7 | 155.2 | 149.6 |

| | | | | |
|---|---|---|---|---|
| | 4 | 158.6 | 164.6 | 142.0 |
| | 5 | 157.3 | 157.3 | 149.9 |
| A18 | 1 | 155.9 | 164.1 | 144.9 |
| | 2 | 159.1 | 163.5 | 142.5 |
| | 3 | 164.8 | 161.3 | 139.5 |
| | 4 | 162.5 | 160.2 | 142.5 |
| | 5 | 160.4 | 161.1 | 143.5 |
| A19 | 1 | 160.4 | 159.6 | 144.9 |
| | 2 | 157.7 | 161.5 | 145.6 |
| | 3 | 154.6 | 162.4 | 147.6 |
| | 4 | 159.9 | 156.6 | 148.1 |
| | 5 | 157.8 | 164.3 | 143.0 |
| A20 | 1 | 162.5 | 158.9 | 143.6 |
| | 2 | 159.4 | 158 | 147.3 |
| | 3 | 159.7 | 161 | 144.2 |
| | 4 | 159.3 | 162.1 | 143.6 |
| | 5 | 159.2 | 160 | 145.6 |
| A21 | 1 | 161.1 | 155.7 | 147.8 |
| | 2 | 153.4 | 162.5 | 148.7 |
| | 3 | 164.9 | 155.5 | 144.5 |
| | 4 | 159 | 165.5 | 140.9 |
| | 5 | 157.7 | 166.3 | 141.3 |
| A22 | 1 | 157.2 | 159.4 | 148.0 |
| | 2 | 158 | 161.3 | 145.5 |
| | 3 | 159.6 | 160.6 | 144.7 |
| | 4 | 158.8 | 156.5 | 149.2 |
| | 5 | 160.1 | 161 | 143.9 |

| | | | | |
|---|---|---|---|---|
| A23 | 1 | 157 | 161.7 | 146.1 |
| | 2 | 159.6 | 160.4 | 144.9 |
| | 3 | 166.5 | 163.4 | 136.3 |
| | 4 | 161.4 | 161.7 | 142.1 |
| | 5 | 160.1 | 160.9 | 144.0 |
| A24 | 1 | 162.9 | 158.5 | 143.6 |
| | 2 | 157.4 | 158.9 | 148.3 |
| | 3 | 161.7 | 162.3 | 141.3 |
| | 4 | 163.2 | 156.8 | 144.9 |
| | 5 | 158 | 162.8 | 144.2 |
| A25 | 1 | 156.1 | 162.4 | 146.2 |
| | 2 | 156.2 | 153.1 | 155.1 |
| | 3 | 159.2 | 171.9 | 135.3 |
| | 4 | 162.1 | 161.2 | 141.9 |
| | 5 | 164.5 | 163.2 | 138.1 |
| A26 | 1 | 160 | 158.4 | 146.3 |
| | 2 | 159.8 | 157.6 | 147.3 |
| | 3 | 158.4 | 158.8 | 147.4 |
| | 4 | 159.4 | 162.3 | 143.3 |
| | 5 | 162.6 | 166.3 | 137.1 |
| A27 | 1 | 161.6 | 157.2 | 146.0 |
| | 2 | 163.4 | 161.1 | 140.9 |
| | 3 | 161.2 | 165.3 | 139.2 |
| | 4 | 156.5 | 160.1 | 148.0 |
| | 5 | 159 | 162.8 | 143.3 |
| A28 | 1 | 158.5 | 158.3 | 147.8 |
| | 2 | 159.6 | 160.4 | 144.9 |

| | | | | |
|---|---|---|---|---|
| | 3 | 162.1 | 162.9 | 140.4 |
| | 4 | 160.4 | 153.9 | 150.2 |
| | 5 | 159.4 | 158.8 | 146.5 |
| 32 | 1 | 152.7 | 154.4 | 157.3 |
| | 2 | 159.6 | 158.6 | 146.5 |
| | 3 | 157 | 148.7 | 158.7 |
| | 4 | 156 | 151.7 | 156.7 |
| | 5 | 157.9 | 156.4 | 150.2 |
| 33 | 1 | 157 | 159.9 | 147.7 |
| | 2 | 164.4 | 163.5 | 138.0 |
| | 3 | 158.8 | 157.8 | 148.0 |
| | 4 | 159.3 | 158.3 | 147.1 |
| | 5 | 155.7 | 159.5 | 149.3 |
| 34 | 1 | 157.8 | 159.8 | 147.1 |
| | 2 | 160.7 | 155.9 | 148.0 |
| | 3 | 153.9 | 158.4 | 152.1 |
| | 4 | 158.6 | 155.5 | 150.4 |
| | 5 | 157.2 | 156.8 | 150.5 |
| 38 | 1 | 156.4 | 159.4 | 148.8 |
| | 2 | 154.4 | 155.4 | 154.6 |
| | 3 | 159.2 | 152.5 | 152.7 |
| | 4 | 155 | 160.3 | 149.2 |
| | 5 | 154.6 | 154.8 | 155.0 |
| 39 | 1 | 161.4 | 156.3 | 147.0 |
| | 2 | 166.1 | 152.8 | 145.9 |
| | 3 | 152.5 | 159.8 | 152.1 |
| | 4 | 155.1 | 155.2 | 154.1 |

| | | | | |
|---|---|---|---|---|
| | 5 | 154.6 | 151.4 | 158.4 |
| 40 | 1 | 151.8 | 160.6 | 152.0 |
| | 2 | 155 | 155.4 | 154.0 |
| | 3 | 155.9 | 153.6 | 154.9 |
| | 4 | 152.7 | 160.7 | 151.0 |
| | 5 | 157.8 | 157.6 | 149.1 |
| 41 | 1 | 155.3 | 154.8 | 154.3 |
| | 2 | 157.8 | 152.8 | 153.8 |
| | 3 | 157.5 | 148.4 | 158.5 |
| | 4 | 154.4 | 150.8 | 159.3 |
| | 5 | 152.1 | 161 | 151.3 |
| 42 | 1 | 154 | 153.8 | 156.6 |
| | 2 | 154.9 | 159.8 | 149.8 |
| | 3 | 158.8 | 162.2 | 144.0 |
| | 4 | 155.5 | 156 | 152.9 |
| | 5 | 153.5 | 155.2 | 155.7 |
| 43 | 1 | 153.8 | 154.8 | 155.8 |
| | 2 | 157.4 | 158.7 | 148.5 |
| | 3 | 154.8 | 156.2 | 153.4 |
| | 4 | 153.7 | 162.3 | 148.6 |
| | 5 | 156.1 | 157.4 | 150.9 |

**Table XXVI:** Residual Stress Values

| **C1** | | **C5** | | **C6** | |
|---|---|---|---|---|---|
| *Depth* | *Residual Stress (Mpa)* | *Depth* | *Residual Stress (Mpa)* | *Depth* | *Residual Stress (Mpa)* |
| 0 | -138.9 | 0 | -111 | 0 | -120.2 |
| 28.7 | -145.7 | 21.59 | -117.3 | 22.225 | -109.5 |
| 43.815 | -155.3 | 42.545 | -88.6 | 37.465 | -89.1 |
| 66.675 | -149.2 | 67.31 | -82.8 | 55.88 | -79.6 |
| 85.09 | -116 | 87.63 | -65.5 | 73.66 | -70 |
| 104.14 | -65.1 | 132.08 | -49.3 | 117.475 | -24 |
| 160.655 | -62.9 | 169.545 | -14.2 | | |
| 181.5 | -47.6 | | | | |
| 202.565 | -41.7 | | | | |
| 253.365 | -34.3 | | | | |
| 295.275 | -20 | | | | |

**Table XXVII:** Acoustic emission data

| | ***Spectra*** | |
|---|---|---|
| **Almen #** | **Frequency (kHz)** | **Magnitude (mV)** |
| 2 | 281.41 | 132.84 |
| 3 | 279.05 | 174.30 |
| 4 | 283.08 | 123.23 |
| 5 | 278.99 | 117.96 |
| 6 | 278.70 | 122.03 |
| 7 | 281.01 | 105.80 |
| 8 | 284.79 | 87.43 |
| 9 | 285.42 | 96.29 |
| 10 | 285.71 | 87.14 |
| 11 | 282.15 | 93.70 |
| 12 | 280.14 | 88.74 |
| 13 | 284.44 | 70.25 |
| 14 | 276.12 | 72.35 |
| 15 | 279.04 | 66.32 |
| 16 | 278.41 | 59.37 |
| 17 | 280.42 | 36.55 |
| 18 | 281.34 | 31.46 |
| 19 | 282.44 | 27.85 |
| 20 | 285.83 | 8.59 |
| 21 | 289.85 | 3.45 |
| 22 | 284.65 | 9.16 |
| 23 | 281.64 | 6.05 |
| 24 | 282.08 | 5.74 |
| 25 | 280.46 | 6.82 |
| 26 | 282.81 | 4.24 |
| 27 | 282.08 | 1.87 |
| 28 | 286.77 | 2.49 |

**Table XXVIII:** Deflection Data

| Almen # | Deflection (.001") |
|---|---|
| 2 | 12 |
| 3 | 10 |
| 4 | 9 |
| 5 | 5 |
| 6 | 5 |
| 7 | 4 |
| 8 | 2 |
| 9 | 1 |
| 10 | 0.8 |
| 11 | 1.5 |
| 12 | 1.1 |
| 13 | 1.1 |
| 14 | 1.6 |
| 15 | 1.2 |
| 16 | 1.4 |
| 17 | 1.7 |
| 18 | 1.4 |
| 19 | 1.8 |
| 20 | 0.5 |
| 21 | 0.5 |
| 22 | 0.3 |
| 23 | 0.2 |
| 24 | 0.1 |
| 25 | 0.2 |
| 26 | 0.2 |
| 27 | 0.1 |
| 28 | 0.1 |
| 32 | 8.5 |
| 33 | 7.8 |
| 34 | 3.8 |
| 38 | 4.5 |
| 39 | 4 |
| 40 | 2.3 |
| 41 | 1.3 |
| 42 | 1 |
| 43 | 0.8 |

Table XXIX: Mass Loss Data

| Almen # | Initial Mass (g) | Final Mass (g) | Mass Loss (mg) |
|---|---|---|---|
| 2 | 3.2224 | 3.2131 | 9.3 |
| 3 | 3.2125 | 3.2016 | 10.9 |
| 4 | 3.2166 | 3.2069 | 9.7 |
| 5 | 3.2183 | 3.218 | 0.3 |
| 6 | 3.2237 | 3.2231 | 0.6 |
| 7 | 3.2424 | 3.2415 | 0.9 |
| 8 | 3.2246 | 3.2242 | 0.4 |
| 9 | 3.2518 | 3.2513 | 0.5 |
| 10 | 3.1999 | 3.1994 | 0.5 |
| 11 | 3.2188 | 3.2186 | 0.2 |
| 12 | 3.2165 | 3.2161 | 0.4 |
| 13 | 3.2173 | 3.2171 | 0.2 |
| 14 | 3.2287 | 3.2287 | 0 |
| 15 | 3.2045 | 3.2045 | 0 |
| 16 | 3.2089 | 3.2089 | 0 |
| 17 | 3.2434 | 3.2435 | 0 |
| 18 | 3.2333 | 3.2332 | 0.1 |
| 19 | 3.2045 | 3.2045 | 0 |
| 20 | 3.2045 | 3.2334 | 0 |
| 21 | 3.2126 | 3.2126 | 0 |
| 22 | 3.2036 | 3.2038 | 0 |
| 23 | 3.2146 | 3.2146 | 0 |
| 24 | 3.2125 | 3.2125 | 0 |
| 25 | 3.2175 | 3.2175 | 0 |
| 26 | 3.2374 | 3.2374 | 0 |
| 27 | 3.2397 | 3.2397 | 0 |
| 28 | 3.2213 | 3.2213 | 0 |
| 32 | 3.2401 | 3.2353 | 4.8 |
| 33 | 3.2032 | 3.1995 | 3.7 |
| 34 | 3.2299 | 3.2252 | 4.7 |
| 38 | 3.2111 | 3.2107 | 0.4 |
| 39 | 3.2227 | 3.2217 | 1 |
| 40 | 3.2149 | 3.2143 | 0.6 |
| 41 | 3.2181 | 3.2177 | 0.4 |
| 42 | 3.2226 | 3.2219 | 0.7 |
| 43 | 3.2339 | 3.2336 | 0.3 |